

Ana Rita Londral
Pedro Encarna  o *Editors*

Advances in Neurotechnology, Electronics and Informatics

Revised Selected Papers from the 2nd
International Congress on Neurotechnology,
Electronics and Informatics (NEUROTECHNIX
2014), October 25–26, Rome, Italy

Biosystems & Biorobotics

Volume 12

Series editor

Eugenio Guglielmelli, Campus Bio-Medico University of Rome, Rome, Italy
e-mail: e.guglielmelli@unicampus.it

Editorial Board

Dino Accoto, Campus Bio-Medico University of Rome, Rome, Italy
Sunil Agrawal, University of Delaware, Newark, DE, USA
Fabio Babiloni, Sapienza University of Rome, Rome, Italy
Jose M. Carmena, University of California, Berkeley, CA, USA
Maria Chiara Carrozza, Scuola Superiore Sant'Anna, Pisa, Italy
Paolo Dario, Scuola Superiore Sant'Anna, Pisa, Italy
Arturo Forner-Cordero, University of São Paulo, São Paulo, Brazil
Masakatsu G. Fujie, Waseda University, Tokyo, Japan
Nicolas Garcia, Miguel Hernández University of Elche, Elche, Spain
Neville Hogan, Massachusetts Institute of Technology, Cambridge, MA, USA
Hermano Igo Krebs, Massachusetts Institute of Technology, Cambridge, MA, USA
Dirk Lefeber, Universiteit Brussel, Brussels, Belgium
Rui Loureiro, Middlesex University, London, UK
Marko Munih, University of Ljubljana, Ljubljana, Slovenia
Paolo M. Rossini, University Cattolica del Sacro Cuore, Rome, Italy
Atsuo Takanishi, Waseda University, Tokyo, Japan
Russell H. Taylor, The Johns Hopkins University, Baltimore, MA, USA
David A. Weitz, Harvard University, Cambridge, MA, USA
Loredana Zollo, Campus Bio-Medico University of Rome, Rome, Italy

Aims & Scope

Biosystems & Biorobotics publishes the latest research developments in three main areas: 1) understanding biological systems from a bioengineering point of view, i.e. the study of biosystems by exploiting engineering methods and tools to unveil their functioning principles and unrivalled performance; 2) design and development of biologically inspired machines and systems to be used for different purposes and in a variety of application contexts. The series welcomes contributions on novel design approaches, methods and tools as well as case studies on specific bioinspired systems; 3) design and developments of nano-, micro-, macrodevices and systems for biomedical applications, i.e. technologies that can improve modern healthcare and welfare by enabling novel solutions for prevention, diagnosis, surgery, prosthetics, rehabilitation and independent living.

On one side, the series focuses on recent methods and technologies which allow multiscale, multi-physics, high-resolution analysis and modeling of biological systems. A special emphasis on this side is given to the use of mechatronic and robotic systems as a tool for basic research in biology. On the other side, the series authoritatively reports on current theoretical and experimental challenges and developments related to the “biomechatronic” design of novel biorobotic machines. A special emphasis on this side is given to human-machine interaction and interfacing, and also to the ethical and social implications of this emerging research area, as key challenges for the acceptability and sustainability of biorobotics technology.

The main target of the series are engineers interested in biology and medicine, and specifically bioengineers and bioroboticists. Volume published in the series comprise monographs, edited volumes, lecture notes, as well as selected conference proceedings and PhD theses. The series also publishes books purposely devoted to support education in bioengineering, biomedical engineering, biomechatronics and biorobotics at graduate and post-graduate levels.

About the Cover

The cover of the book series Biosystems & Biorobotics features a robotic hand prosthesis. This looks like a natural hand and is ready to be implanted on a human amputee to help them recover their physical capabilities. This picture was chosen to represent a variety of concepts and disciplines: from the understanding of biological systems to biomechatronics, bioinspiration and biomimetics; and from the concept of human-robot and human-machine interaction to the use of robots and, more generally, of engineering techniques for biological research and in healthcare. The picture also points to the social impact of bioengineering research and to its potential for improving human health and the quality of life of all individuals, including those with special needs. The picture was taken during the LIFEHAND experimental trials run at Università Campus Bio-Medico of Rome (Italy) in 2008. The LIFEHAND project tested the ability of an amputee patient to control the Cyberhand, a robotic prosthesis developed at Scuola Superiore Sant'Anna in Pisa (Italy), using the tf-LIFE electrodes developed at the Fraunhofer Institute for Biomedical Engineering (IBMT, Germany), which were implanted in the patient's arm. The implanted tf-LIFE electrodes were shown to enable bidirectional communication (from brain to hand and vice versa) between the brain and the Cyberhand. As a result, the patient was able to control complex movements of the prosthesis, while receiving sensory feedback in the form of direct neurostimulation. For more information please visit <http://www.biorobotics.it> or contact the Series Editor.

Ana Rita Londral · Pedro Encarnaçāo
Editors

Advances in Neurotechnology, Electronics and Informatics

Revised Selected Papers from the 2nd
International Congress on Neurotechnology,
Electronics and Informatics
(NEUROTECHNIX 2014), October 25–26,
Rome, Italy



Editors

Ana Rita Londral
Faculdade de Medicina
Universidade de Lisboa
Lisbon
Portugal

Pedro Encarnaçāo
Universidade Católica Portuguesa
Lisbon
Portugal

ISSN 2195-3562

Biosystems & Biorobotics

ISBN 978-3-319-26240-6

DOI 10.1007/978-3-319-26242-0

ISSN 2195-3570 (electronic)

ISBN 978-3-319-26242-0 (eBook)

Library of Congress Control Number: 2015954344

Springer Cham Heidelberg New York Dordrecht London

© Springer International Publishing Switzerland 2016

This work is subject to copyright. All rights are reserved by the Publisher, whether the whole or part of the material is concerned, specifically the rights of translation, reprinting, reuse of illustrations, recitation, broadcasting, reproduction on microfilms or in any other physical way, and transmission or information storage and retrieval, electronic adaptation, computer software, or by similar or dissimilar methodology now known or hereafter developed.

The use of general descriptive names, registered names, trademarks, service marks, etc. in this publication does not imply, even in the absence of a specific statement, that such names are exempt from the relevant protective laws and regulations and therefore free for general use.

The publisher, the authors and the editors are safe to assume that the advice and information in this book are believed to be true and accurate at the date of publication. Neither the publisher nor the authors or the editors give a warranty, express or implied, with respect to the material contained herein or for any errors or omissions that may have been made.

Printed on acid-free paper

Springer International Publishing AG Switzerland is part of Springer Science+Business Media
(www.springer.com)

Preface

The present book includes extended and revised versions of a set of selected papers from the Second International Congress on Neurotechnology, Electronics and Informatics (NEUROTECHNIX 2014), held in Rome, Italy from October 25 to 26, 2014.

The purpose of the International Congress on Neurotechnology, Electronics and Informatics is to bring together researchers and practitioners in order to exchange ideas and develop synergies highlighting new advancements of neurotechnology, either in general or regarding a particular case, application, or pathology.

NEUROTECHNIX 2014 was sponsored by INSTICC (Institute for Systems and Technologies of Information, Control and Communication), held in cooperation with MedinRes—Medical Information and Research, Nansen Neuroscience Network, Sociedade Portuguesa de Neurologia (SPN), Associação Portuguesa de EEG e Neurofisiologia Clínica (APEEGNC), Neurotech Network, Societa Italiana de Neurologia (SIN), World Federation for NeuroRehabilitation (WFNR) and the International Neural Network Society (INNS), and in collaboration with The Marketplace for Research Antibodies.

The congress received submissions from 19 countries, in all continents. To evaluate each submission, a double-blind paper review was performed by the program committee, whose members are highly qualified researchers in the NEUROTECHNIX topic areas.

NEUROTECHNIX's program included panels, special sessions, and five invited talks delivered by internationally distinguished speakers: Constantin A. Rothkopf (Technical University Darmstadt, Germany), Danil Prokhorov (Toyota Tech Center, United States), Eugenio Guglielmelli (Università Campus Bio-Medico, Italy); Febo Cincotti (Sapienza University of Rome, Italy), and Hermano Igo Krebs (Massachusetts Institute of Technology, United States).

We would like to thank the authors, whose research and development efforts are recorded here for future generations.

April 2015

Ana Rita Londral
Pedro Encarnaçāo

Organization

Congress Co-chairs

Ana Rita Londral, Universidade de Lisboa, Portugal
Pedro Encarnaçāo, Universidade Católica Portuguesa, Portugal

Area Co-chairs

Aldo Faisal, Imperial College London, UK
Hermano Igo Krebs, Massachusetts Institute of Technology, USA
Vivian K. Mushahwar, University of Alberta, Canada
Antonio Pedotti, Politecnico di Milano, Italy

Organizing Committee

Helder Coelhas, INSTICC, Portugal
Lucia Gomes, INSTICC, Portugal
Ana Guerreiro, INSTICC, Portugal
André Lista, INSTICC, Portugal
Andreia Moita, INSTICC, Portugal
Vitor Pedrosa, INSTICC, Portugal
Cláudia Pinto, INSTICC, Portugal
Susana Ribeiro, INSTICC, Portugal
Sara Santiago, INSTICC, Portugal
Mara Silva, INSTICC, Portugal
José Varela, INSTICC, Portugal
Pedro Varela, INSTICC, Portugal

Program Committee

- Amr Abdel-Dayem, Laurentian University, Canada
Gregor Adriany, University of Minnesota, USA
Lyuba Alboul, Sheffield Hallam University, UK
Pedro Almeida, University of Lisbon, Portugal
Jesús B. Alonso, Universidad de Las Palmas de Gran Canaria, Spain
Alexandre Andrade, Faculdade de Ciências da Universidade de Lisboa, Portugal
Jose M. Azorin, Miguel Hernandez University, Spain
Reneta Barneva, State University of New York, USA
Ammar Belatreche, University of Ulster, UK
Martin Bogdan, Universität Leipzig, Germany
Mamede de Carvalho, Institute of Physiology, Faculty of Medicine-University of Lisbon, Portugal
Amitava Chatterjee, Jadavpur University, India
Albert C.S. Chung, The Hong Kong University of Science and Technology, Hong Kong
Krzysztof Cios, Virginia Commonwealth University, USA
Emmanuel Conchon, University of Toulouse, IRIT/ISIS, France
Jose Luis Contreras-Vidal, University of Houston, USA
Jimmy T. Efird, East Carolina Heart Institute, USA
Gary Egan, Monash University, Australia
Mark J. Embrechts, Rensselaer Polytechnic Institute, USA
Hugo Ferreira, Faculdade de Ciências da Universidade de Lisboa, Portugal
Patrícia Figueiredo, Instituto Superior Técnico, Portugal
Alexander Fingelkurts, BM-Science—Brain & Mind Technologies Research Centre, Finland
Andrew Fingelkurts, BM-Science—Brain & Mind Technologies Research Centre, Finland
Anselmo Frizera, UFES, Brazil
Petia Georgieva, University of Aveiro, Portugal
Michele Giugliano, University of Antwerp, Belgium
Rodrigo Capobiano Guido, University of São Paulo, Brazil
Chung Y. Hsu, China Medical University, Taiwan
Xavier Intes, Rensselaer Polytechnic Institute, USA
Pasi Karjalainen, University of Eastern Finland, Finland
Jonghwa Kim, University of Augsburg, Germany
Constantine Kotropoulos, Aristotle University of Thessaloniki, Greece
Hermano Igo Krebs, Massachusetts Institute of Technology, USA
Ondrej Krejcar, University of Hradec Kralove, Czech Republic
Narayanan Krishnamurthi, Arizona State University, USA
Martin Lauterbach, Hospital da Luz, Portugal
Seung-Hoon Lee, Seoul National University, Korea, Republic of
Christos Loizou, Intercollege, Cyprus

- Nuno Matela, Faculdade de Ciências da Universidade de Lisboa, Portugal
Alessandro de Mauro, Vicomtech-IK4, Spain
Paulo Mendes, University of Minho, Portugal
Claudio Moraga, University of Dortmund, Germany
António J.R. Neves, University of Aveiro, Portugal
Susana Novais, Carnegie Mellon University, USA
Haluk Ogmən, University of Houston, USA
Joao Papa, UNESP—Universidade Estadual Paulista, Brazil
George Perry, University of Texas at San Antonio, USA
Victor Pikov, Huntington Medical Research Institutes, USA
Armando J. Pinho, University of Aveiro, Portugal
Susana Pinto, Institute of Molecular Medicine—Faculty of Medicine, University of Lisbon, Portugal
Gabriel Pires, Institute for Systems and Robotics—Coimbra/Polytechnic Institute of Tomar, Portugal
Hemerson Pistori, Dom Bosco Catholic University, Brazil
Mirjana Popovic, University of Belgrade, Serbia
Ales Prochazka, Institute of Chemical Technology, Czech Republic
Rafael Raya, Spanish National Council for Science Research, Spain
Robert Riener, ETH Zürich, Switzerland
Wim L.C. Rutten, University of Twente, The Netherlands
Ricardo Salvador, Faculdade de Ciências da Universidade de Lisboa, Portugal
Despina Sanoudou, Medical School, University of Athens, Greece
André Saúde, Federal University of Lavras, Brazil
Mohamad Sawan, Ecole Polytechnique de Montreal, Canada
Friedhelm Schwenker, University of Ulm, Germany
Mário Forjaz Secca, CEFITEC, Departamento de Fisica, FCT/UNL, Portugal
Tapiro Seppänen, University of Oulu, Finland
Fiorella Sgallari, University of Bologna, Italy
Miguel Tavares da Silva, Instituto Superior Técnico, Portugal
Armando J. Sousa, Faculdade de Engenharia da Universidade do Porto, Portugal
Sundaram Suresh, Nanyang Technological University, Singapore
João Manuel R.S. Tavares, FEUP—Faculdade de Engenharia da Universidade do Porto, Portugal
Carlos M. Travieso, University of Las Palmas de Gran Canaria, Spain
Nicola Vitiello, Scuola Superiore Sant'Anna, Italy
Dezhong Yao, University of Electronic Science and Technology of China, China
Zeyun Yu, University of Wisconsin at Milwaukee, USA
Günther Zeck, NMI at the University Tübingen, Germany
Chun Zhang, Tsinghua University, China

Auxiliary Reviewers

Camilo Cortes, Vicomtech-IK4 Research Alliance, Spain
Enrique Hortal, Miguel Hernández University, Spain

Invited Speakers

Febo Cincotti, Sapienza University of Rome, Italy
Eugenio Guglielmelli, Università Campus Bio-Medico, Italy
Constantin A. Rothkopf, Technical University Darmstadt, Germany
Danil Prokhorov, Toyota Tech Center, USA
Hermano Igo Krebs, Massachusetts Institute of Technology, USA

Contents

From Biological to Numerical Experiments in Systemic Neuroscience: A Simulation Platform	1
Nicolas Denoyelle, Maxime Carrere, Florian Pouget, Thierry Viéville and Frédéric Alexandre	
Physically-Based Simulation and Web Visualization of <i>C. elegans</i> Behavioural Experiments	19
Andoni Mujika, Gorka Epelde, Peter Leškovský and David Oyarzun	
<i>Si elegans</i>: Modeling the <i>C. elegans</i> Nervous System Using High Performance FPGAS	31
Pedro Machado, John Wade and T.M. McGinnity	
Probabilistic Tractography Using Particle Filtering and Clustered Directional Data	47
Adelino R. Ferreira da Silva	
Post-stroke Robotic Upper-Limb Telerehabilitation Using Serious Games to Increase Patient Motivation: First Results from ArmAssist System Clinical Trial	63
Cristina Rodríguez-de-Pablo, Maša Popović, Andrej Savić, Joel C. Perry, Aitor Beloso, Tijana Dimkić Tomić and Thierry Keller	
Comparison of Electro-Optical Strategies for Mimicking <i>C. elegans</i> Network Interconnectivity in Hardware	79
Lorenzo Ferrara, Alexey Petrushin, Carlo Liberale, Dara Brannick, Brian Connolly, Pat Mitchell and Axel Blau	
Supervised EEG Ocular Artefact Correction Through Eye-Tracking	99
P. Rente Lourenço, W.W. Abbott and A. Aldo Faisal	

An fMRI-Compatible System for 3DOF Motion Tracking of Objects in Haptic Motor Control Studies	115
M. Rodríguez, A. Sylaidi and A.A. Faisal	
Comparing Methods for Decoding Movement Trajectory from ECoG in Chronic Stroke Patients	125
Martin Spüler, Florian Grimm, Alireza Gharabaghi, Martin Bogdan and Wolfgang Rosenstiel	
Detection of Gait Initiation Through a ERD-Based Brain-Computer Interface	141
E. Hortal, D. Planelles, E. Iáñez, A. Costa, A. Úbeda and J.M. Azorín	
Author Index	151

From Biological to Numerical Experiments in Systemic Neuroscience: A Simulation Platform

Nicolas Denoyelle, Maxime Carrere, Florian Pouget, Thierry Viéville and Frédéric Alexandre

Abstract Studying and modeling the brain as a whole is a real challenge. For such systemic models (in contrast to models of one brain area or aspect), there is a real need for new tools designed to perform complex numerical experiments, beyond usual tools distributed in the computer science and neuroscience communities. Here, we describe an effective solution, freely available on line and already in use, to validate such models of the brain functions. We explain why this is the best choice, as a complement to robotic setup, and what are the general requirements for such a benchmarking platform. In this experimental setup, the brainy-bot implementing the model to study is embedded in a simplified but realistic controlled environment. From visual, tactile and olfactory input, to body, arm and eye motor command, in addition to vital interoceptive cues, complex survival behaviors can be experimented. We also discuss here algorithmic high-level cognitive modules, making the job of building biologically plausible bots easier. The key point is to possibly alternate the use of symbolic representation and of complementary and usual neural coding. As a consequence, algorithmic principles have to be considered at higher abstract level, beyond a given data representation, which is an interesting challenge.

Keywords Simulation · Computational neuroscience · Virtual reality

N. Denoyelle · M. Carrere · F. Pouget · T. Viéville (✉) · F. Alexandre
Inria Bordeaux Sud-Ouest, 200 Avenue de la Vieille Tour, 33405, Talence, France
e-mail: Thierry.Vieville@inria.fr

F. Alexandre
e-mail: Frederic.Alexandre@inria.fr

N. Denoyelle · M. Carrere · F. Pouget · F. Alexandre
LaBRI, Institut Polytechnique de Bordeaux, CNRS, UMR 5800,
Université de Bordeaux, Talence, France

M. Carrere · F. Alexandre
Institut des Maladies Neurodégénératives, CNRS, UMR 5293,
Université de Bordeaux, Bordeaux, France

1 Introduction

Computational neuroscience is often presented as a way to better understand the complex relations between structures and functions in the brain. Particularly, these relations are complex because they are not symmetrical: one structure participates to several functions and functions are distributed among many structures. This is an important limitation against developing a model of a structure in isolation, which is often the case in computational neuroscience. This is not sufficient to emulate one behavioral function, but participates only to studying some of its properties, with the risk of neglecting the key influence of another structure on this function. Consequently, for modeling studies interested in integrative and behavioral neuroscience and in the emulation of behavioral functions, this analysis is a plea for designing brain models including many brain structures. In addition, in the framework of studying behavioral functions, the brain must also be considered as a complex system in interaction with the body and the environment. Two important consequences can be drawn. The first consequence is related to the model itself. Additional modules must be considered, to allow for the sensation and processing of signals from the environment (exteroception) and also from the body (interoception). Designing such a network of brain structures and modules at the interface with the outer and inner world includes not only understanding how each subsystem (visual, motor, emotional, etc.) works but also how these subsystems interact as a whole, to yield emerging behaviors, i.e. effects that result from interactions between subsystems. The second consequence is related to the use of this complex system. Studying and validating functional models of brain structures at a macroscopic behavioral scale cannot be performed with restrained artificial static paradigms but requires experiments in complex environments, with realistic sensory-motor tasks to be performed, including high-level interactive behaviors (e.g. survival strategy in the presence of prey/predators) and long-term protocols (since both statistical studies and biologically-plausible learning mechanisms require long epochs). Such paradigms are to be related to biological experiments conducted on animals. These statements are not only characterizing brain models working in interaction with their environment, they also give strong requirements on the tools that must be designed to simulate these models and to experiment them.

Designing such tools is also an excellent way to address at the same time the two main objectives of such brain models at the macroscopic scale. One hand, they are intended to serve neuroscientists as a new platform of experimentation, on which they can apply their classical protocols of observation and analysis of animals at the behavioral as well as electrophysiological levels. It is consequently important that neuroscientists can observe the inner activity of the models, as they use to do for example with electrodes (but we can imagine that this observation in digital models might be more easy than in the real brain). It is also important that they can define classical behavioral protocols like they do in animals (e.g. fear conditioning) in order to observe the resulting behavior and the corresponding brain activation. Defining such protocols implies that the structure of the external world (e.g., maze,

food magazine) as well as its intrinsic rules (e.g. tone followed by an electric shock) should be easy to design.

On the other hand, these tools are also intended to serve computer scientists as a way to design artificial autonomous systems, driven by brain models. In this case, it is important for the supposed properties of the models (e.g., capacity to learn, robustness to noise or changing rules) to be assessed by rigorous evaluation procedures, as it is defined for example in the domain of machine learning. In this case also an easy access must be proposed both to the inner circuitry of the models and to the specification of the external world.

With in mind this double goal of offering convenient tools to both scientific communities, we report in this paper the specifications that we have elaborated and present the corresponding software platform that we call VirtualEnaction. We also introduce the case study of a behavioral function presently under study in our team, pavlovian conditioning, as an illustration of the use of VirtualEnaction. Before that, some more words must be said to justify the need for such a platform.

2 Problem Position

Concerning the nature of such a simulator, real robotic systems are often used and answer particularly well to the second requirement about a realistic environment. However, building viable robotic systems and making them evolve in realistic environments (e.g. natural sites) for long periods of time (e.g. several days) is just too expensive in term of cost and manpower in many circumstances and particularly during early phases of development. Furthermore, the goal of such simulation is not only to make a demo, but also, and more importantly, to study and quantify the behavior of functional models of the brain. As a consequence we not only need a complex, long-term, realistic experimental setup, but we also need a controllable and measurable setup where stimuli can be tuned and responses can be measured. In fact, real environment complexity and parameters are intrinsically difficult when not impossible to control. This is the reason why we propose to use a digital simulator implementing realistic survival and other biological scenarios.

A step further, available macroscopic models of brain functions are not designed for “performance” but to properly implement phenomenological concepts that have been investigated in some cognitive or behavioral framework. They would therefore have “no chance” in a real world. Note that recent computer science mechanisms designed without any constraint regarding biological plausibility but only towards final performances are nowadays probably more efficient but that are not relevant regarding the brain behavior explanation.

As a consequence we also need a setup which can provide a “simplified environment”, for systemic models of the brain at the state of the art not to fail immediately. We must also take into account the fact that (i) such models are rather slow to simulate (unless huge computer power is available), and that (ii) they are

not supposed to focus on precise issues regarding low-level sensory input or motor output but on integrated cognitive functions and the resulting behaviors.

This, in addition to technical constraints, yields three key characteristics:

1. No real-time but a look-and-move paradigm: The main restriction we propose is to have the simulator running at a “slower” time (i.e. using several seconds to simulate one real-time second) and also to consider discrete time sampling. This seems obvious as far as digital simulation is concerned, but in terms of underlying framework, this has several consequences (e.g., giving up the possibility for a human observer to interact with the simulation, restraining to clock-based (and not event-based) dynamical models, etc.) [1].
2. No real robotic control but only motor command: Since in the nervous system motor control seems to be a hierarchical system with high-level motor commands, while their closed loop execution is delegated to the peripheral motor system [2], we may accept to only simulate gesture and displacement at a rather symbolic level such as “stand-up” or “turn 90° rightward”. This indeed cancels the possibility to study sharp phenomena of motor interactions with the environment but allows us to concentrate on high-level control such as action selection mechanism and motor planning.
3. Complex but not necessarily natural visual environment: The third main restriction we propose to accept is to consider a complex visual environment (with visual textures, several objects in motion, etc.) but not to invest in the simulation of a realistic natural scene simulation. The reason of this choice is that natural image vision is an issue already well studied [3]. The general conclusion is that biological visual systems are tuned to natural image statistics, decomposed by the early visual front-end in such a way that higher-level visual input only relates on cues orthogonal (in a wide sense) to natural image statistics. In other words, the job regarding this aspect is done by early-vision layers and we may consider more stylistic visual cues at a higher-level. Depending on the study, we may also wish to work on either a pixelic or a symbolic representation of the visual scene. See [4] for details of how the early-visual system implements such dual representation.

3 System Description

We consider that a “brainy-bot”, i.e. the implementation of a global model of the brain functionalities, interacts with its environment with the simple goal of surviving. Our objective is to simulate the sensory-motor interactions of this bot with respect to its environment. Examples of such surroundings are shown in Fig. 1.

Survival is precisely defined as maintaining vital variable values in correct ranges, as formalized in, e.g., [5]. In our context, health, food, water, energy, and



Fig. 1 Two examples of digital experimental environments for systemic neuroscience. *Left* A minimal environment corresponding to a standard maze reinforcement learning task (*source* one of our virtual enactment built). *Right* A complex environment in which survival capabilities are to be checked (*source* landscape encountered when playing with the standard game)

oxygen are the vital state variables. The bot has access to these values. These variables decrease or increase with time since the bot body is supposed to consume the related resource depending on its activity, or change in the presence of an external event (e.g. energy during a predator attack), and restore resources. Restoring resources is obtained either by ingesting items or taking rest (i.e., when making the choice of stopping an action, with the benefit of vital resource increase and the drawback of not acting on the environment, this might be a short-term policy choice if vital variables are low and is a middle-term policy choice otherwise).

The environment structure is very simple and made of “blocks”. Each object in this environment (including the floor, relief,..) is a collection of blocks. Each block is defined by its 3D position, orientation and size, roughness, hardness, temperature, and color. Some blocks correspond to eatable or drinkable resources. Other entities correspond to objects that interact with the bot (e.g. predators that attack the bot or lava to avoid). At this level, survival corresponds to avoid or kill the predators and find resources to eat or drink.

The bot anatomy is functionally made of a body, an arm and a head/eye. It carries a bag with objects found in its environment. The body can move at a given speed and in a given direction, and also rotate at each step to a given angle. It can also jump up to a given relative height, or knee down to take a rest. The head/eye can gaze in a given yaw/pitch direction. The arm can perform predefined symbolic gestures: take an object in hand out of its bag, put the object in hand into its bag, either drop or throw the object in hand, ingest the block in hand (food or water), grasp the object in front of him. The arm can also attack (quantified by a force value and with or without an object in hand) the object in front of him. This is the complete description of the bot motor command output in the present context.

The bot sensory input corresponds to cues related to the blocks which are around it. The touch cues allow the bot to estimate the roughness, hardness and temperature

```
#include "BotAPI.hpp"
using botplug::BotAPI;

class Bot : public BotAPI {
private:
void initBot();
bool stopCondition() const;

protected:
int brainDo();

float getHandRoughness () const
float getHandHardness () const
float getHealth () const
float getFood () const

void setBodyTranslation (float speed, float dir)
void setBodyRotation (float horizontal)
void setHeadMove (float vertical, float horizontal)
void setIngest (bool ingest)
void setAttack (float t_arm)
```

Fig. 2 *Left* The software interface is trivial: each implementation of a brainy-bot provides an initialization routine `initBot()` and a stop function `stopCondition()`, while at each time-step the `brainDo()` method is called. *Right* All status, input and output functionalities are available via a simple API. For instance, hand or vital input, body and head displacement, gestures of resource injection and attack against predator are shown

of the object in hand. The olfactory cues allow to estimate the smell type and intensity of objects close to it (computed by integrating average values over the blocks characteristics). At the bot level, pixelic vision provides an image of the visual field view (i.e., calculating the blocks texture and color projection on the virtual retina). Finally, the proprioceptive cues correspond to gaze direction estimation.

In order to quantify the bot behavior, the interface provides an additional access to the bot absolute position and orientation in space. Symbolic vision is also available, as a list of blocks visible in its visual field, with an access to the block characteristics.

An adaptation of the <https://minecraft.net/minecraftminecraft> open game software yields the proper answer to this wish-list and the so called <http://virtualenaction.gforge.inria.frvirtualenaction> is an open-source free-license implementation of these specifications. Each user buys a end-user low-cost https://account.mojang.com/documents/minecraft_eulamojang license (<20\$) for <https://minecraft.net/minecraftminecraft>, while <http://virtualenaction.gforge.inria.frvirtualenaction> is free of use under a http://www.cecill.info/licences/Licence_CeCILL-C_V1-en.txt CeCILL-C license. Fully-documented scripts facilitate the installation of the software bundle under Linux OS. The bot is implemented in either C/C++, or possibly in Python (via an existing <http://www.swig.orgswigwrapper>) or other computer languages. It uses a http://virtualenaction.gforge.inria.fr/VEDoxygen/html/da/d5b/classbotplug_1_1BotAPI.html simple API, as described in Fig. 2. Furthermore, in order to both observe in slow-down real-time the bot behavior and interact with the digital experiment, a graphic user interface is available as described in Fig. 4. The simple architecture of the platform is schematized in Fig. 3.

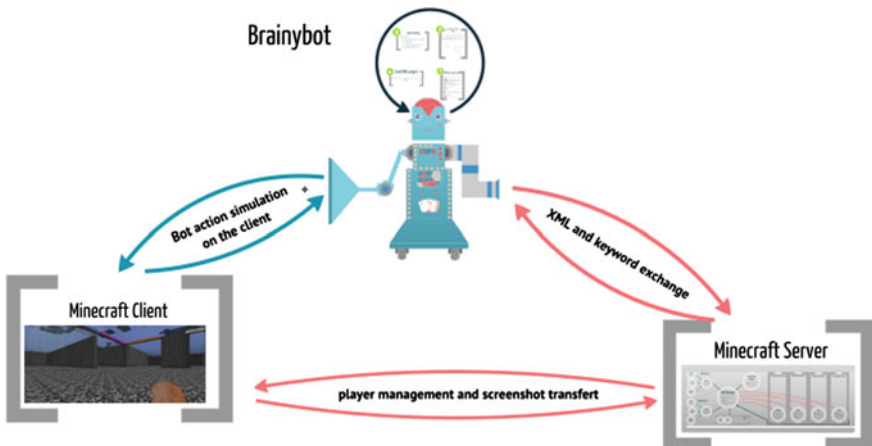


Fig. 3 The platform architecture. At the user level, only the notion of (i) game server where the environment and its mobile objects interactions are computed, (ii) game client where the game-play is rendered and (iii) brainy-bot where the brain model simulation is issued have to be taken into account

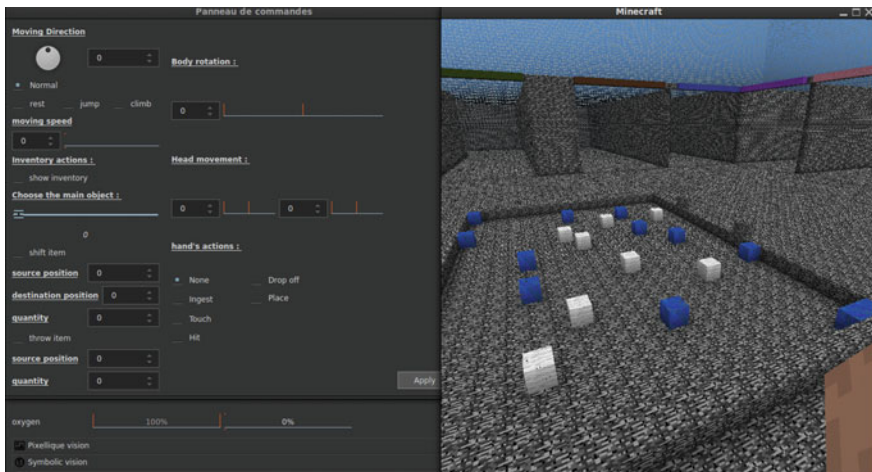


Fig. 4 The software's graphic user interface. In order to observe and control the experiment, a view of the bot vision, status, input and output is available via interactive panels. It is also possible to "cheat" by controlling these variables values, in order to debug an experiment and understand in details what happens in such a complex system interaction

4 Brainy-Bot Generic Functionality

Even when restraining to functional modeling, it is not possible to simulate all sub-systems of the brain at the same level of details. We thus must represent parts of the system with efficient models, but without biologically plausible models. A few sets of generic functionalities are to be proposed to this end. Let us discuss three of them.

1. Associative Memory: Any system has not only to take into account the present input and output in order to generate a proper behavior, but also to store and recall past information. Information is however never exactly the same and similar pieces of information (i.e., being almost equal up to a given threshold) have to be considered as a unique item. Such a memory must not only store and retrieve information, but also define a notion of indistinguishable information.

In our context this has a special meaning: the input/output information corresponds to a hierarchical logical-structure,¹ mixing quantitative and qualitative information,² and using³ structures like *set* or *sequence*, in addition to *tuples* as containers. More precisely:

```

@action: {
    life: { stop: @bool },
    body: { translation: { speed: @percent, direction: @degree }, orientation: , rest: @bool },
    head: { vertical: @percent, horizontal: @percent },
    attack: { strength: @percent },
    jump: { height: @percent },
    gesture: { touch: @bool, ingest: @bool, throw: @bool, climb: @bool },
    hand: { put: { slot: @index }, get: { slot: @index }, count: @count }
},
@sensation: {
    location: { position: @position, orientation: { yaw: @degree, pitch: @degree } },
    vital: { health: @percent, food: @percent, water: @percent, oxygen: @percent, energy: @percent },
    vision: { blocks: [ @block* ], entities: [ @block* ] },
    touch: { blocks: [ @block* ], entities: [ @block* ] },
    hand: { roughness: @percent, hardness: @percent, item: @item },
    olfaction: { intensity: @percent, toxicity: @percent, friendliness: @percent, edibleness: @percent },
    inventory: [ @item* ]
},
@block: {
    id: @index,
    position: @position, roughness: @percent, hardness: @percent, temperature: @percent, color: @color
},
@item: {
    id: @index, count: @count, slot: @index
},
@position: {
    x: @real, y: @real, z: @real
}

```

Notion of divergence. As a consequence, it is not obvious to define a “distance” between such state values (i.e. the whole input/output data structure). But this is required to decide if they are distinguishable or not. Our claim is that the correct

¹Such a structure is of common use in computer science: It corresponds to, e.g., a XML logical-structure, or the JSON syntax underlying data model.

²The following scalar values are used: *bool* for an either true or false Boolean value, *percent* for a proportion value between 0 and 1, *degree* for an angle in degree, *index* stands for a non-negative integer index, *count* stands for a non-negative integer count value, *color* stands for a RGB color value, *real* stands for an unbounded decimal value.

³Sets are unordered lists without repetition, Sequences are sequential lists, and t-uples map strings, or names, to their corresponding value.

notion is the notion of *premetric*⁴ or *divergence* (see Footnote 4), for two state values s_1 and s_2 :

$$d(s_1, s_2) \geq 0 \quad \text{and} \quad d(s_1, s_2) = 0 \Leftrightarrow s_1 = s_2$$

as being the weakest concept that allows to state that two values are distinguishable if and only if $d(s_1, s_2) \geq \varepsilon > 0$, for some threshold ε . It appears that all pre metrics we need are always symmetric (i.e., it is a semi-metric (see Footnote 4)). In our context, the divergence corresponds to a Euclidean distance for a position, angular distance for an orientation, while the divergence between two tuples is simply defined as the weighted sum between each tuple values divergence, for a given set of weights, while the divergence with respect to a undefined value must be defined for this definition to be coherent. At this stage, divergence computation is linear with respect to the state structure size. The introduction of dissimilarity computation of tuples is the cause of being in the context of a semi-metric and not a complete metric with the triangle inequality verified.

A step further, we need pairing (see Footnote 4) divergence between two unsorted sequences (i.e., it corresponds to the classical “stable marriage problem” (see Footnote 4)). This tool is required to define how two sets of blocks (e.g., for symbolic vision input) match, in order, e.g., to recognize a visual object. This pairing is not a distance in the general case.

We also need to define an edit distance (a generalization of the Levenshtein (see Footnote 4) distance, called the Victor-Purpura (see Footnote 4) metric) to define how two temporal sequences match.

Both pairing and edit divergence can be implemented as algorithms quadratic with respect to the set or sequence size.

Let us also mention that informing the bot about its absolute position and orientation or about symbolic information of the scene, as it is the case, is a way to shortcut its localization and sensory modules and provide integrated cognitive information, without considering the related computational issues.

With this set of tools, the mechanism of associative memory of state values is entirely specified, and it must be pointed out that since the space of states has no special structure the algorithms allowing to retrieve a value in the memory (namely the closest value whose divergence with respect to the input value is minimal), or insert a new value (if not already in the memory in an indistinguishable form), or delete it, can not have less than a complexity of $O(\text{memory-size})$, since hash-coding is not compatible with retrieving a similar value.

2. State Categorization: A generic key cognitive feature is the capability to “extract” symbolic information from a bundle of quantitative or qualitative values. During a supervised learning phase prototypes of state values with the corresponding known category are registered. Then, for an incoming state the most plausible category is calculated. Such mechanism includes sensory events detection

⁴Definition available on <https://en.wikipedia.org>.

(e.g., detect the presence of predator from sensory cues), object labeling (e.g., an element as a resource to ingest): Such examples are qualitative values. A biologically plausible support vector machine mechanism is available to this end, with versatile uses [6]. This also includes quantitative values (e.g., associate a reward to a given sensation or action), and support vector machines also include the capability to categorize using a floating point value.

In our case, the issue is the following: If a simple nearest neighbor mechanism (i.e., the category of an incoming state value is set (or interpolated) using the category of the nearest neighbor (or neighbors)) is used, then the notion of divergence introduced before is sufficient. However, such a mechanism is known as being the worst in term of generalization (i.e., inferring correctly the category for incoming state value not corresponding to the prototypes) and robustness (i.e., providing reliable results even if some spurious prototypes).

Notion of gradient. In order to introduce a better mechanism of categorization that will optimize a criterion, we need to define the notion of *gradient*, i.e., small variation of a given state value. One impediment is the fact that some variables are discrete variables. In the present case, `index` and `count` are not to be optimized, thus remain fixed. Boolean variables `bool` however correspond to effective choices or meaningful information, and must be taken into account. As a consequence, we would have to deal with the combinatory complexity of discrete values optimization, known as NP-hard. To overcome this caveat, we simply propose to embed each $b = \text{bool}$ value in bounded $v = [0, 1]$ value, with the obvious correspondence:

$$v = \begin{cases} 1 & \text{if } b \text{ then 1 else 0;} \\ b & b > 0.5 \end{cases}$$

with these specification choices, given a state s we can define a small variation ∂s as small variations of all quantitative scalar values (namely `real`, `color`, `degree`, `percent` and `bool` represented by a $[0, 1]$ value). Given a state criterion, i.e., a real value function of the state, we can optimize this criterion with respect to quantitative values. This construction implicitly maps a state to a N-dimensional real space of the different quantitative variables. This is not exactly an Euclidean space since real value like color or angle lies in some non-Euclidean metric spaces, but usual differential methods can be used.

Following the method in [6] that simply requires optimization with respect to the prototypes state value (and contrary to the original SVM algorithm that proceed in a dual space, which we can not define here since we do not have a concrete metric) we thus can improve the raw nearest neighbor mechanism, by eliminating or merging useless prototypes, and modifying prototypes values to maximize the margin between classes. It must be understood that this method will not (i) perform qualitative optimization (e.g., will not find that we must add or delete a block to represent an object) and (ii) is sub-optimal since we reuse a well-founded method in a context where not all assumptions are verified.

3. Gesture Interpolation: At a functional level a “behavior” (i.e., a complex gesture) can be specified as finding a path from an initial state (e.g., being hungry while food is known to be present elsewhere) to a final state (e.g., having the food

ingested) taking constraints into account (e.g., avoiding or moving aside obstacles on the way). Generic specification of such problem and universal algorithms to solve them exist, in relation with harmonic control which is a biologically plausible framework (i.e., with fully distributed computation based on diffusion mechanism) [7]. This also corresponds to the fact that, in the motor cortex, a motor command is represented by its final state or “end point”, while the trajectory generation to attain this final state is generated elsewhere.

In order to define such a mechanism we simply need the notion of state divergence and state gradient introduced previously. Obstacle to avoid is simply defined by constraints (e.g. real value function of the state that must remain, say, positive). The goal is attained when the divergence to the final state is below the indistinguishability threshold. The algorithm proposed in [7] builds harmonic potential, here in the real space on which the state quantitative variables are mapped. It requires the operation of projection (of a state onto a constraint) to define a repulsive point, and such algorithm reduces to an optimization problem, implementable thanks to our different design choices.

Though we present the simplest aspect of this class of methods, harmonic control is easily linked to optimal control [8], in link with reinforcement learning considering a non-finite realistic state-space [9].

As a conclusion, this section has analyzed to which extent some powerful generic machine learning techniques can be reused in this context and adapted to the symbolic hierarchical data structure defining the bot input and output. The two main ideas are to use a weaker notion of distance and accept adaptation mechanism of the state restrained to quantitative values. Further developing the link with machine-learning algorithms applied on such data structure in order to define high level algorithmic ersatz of cognitive functions is a perspective of this work.

5 Neuroscience Application

Let us now discuss how this setup constitutes a step towards integrative neuroscience digital experimentation.

First of all, let us compare this project with complementary connected projects. The <http://www.animatlab.comAnimatLab> is a software platform allowing to simulate embodiment (bio-mechanical simulation of a body) allowing to investigate the relation between brain and body [10]. Furthermore, it proposes a neural network architecture for the implementation of cognitive functions. On the contrary, the present framework has a rather limited description of the embodiment, but a much larger set of possible interactions with the environment. A step further, not only artificial neural network models are usable in VirtualEnaction, whereas the interface with any existing neuroscience simulation tool (e.g., python based neural simulators, see [11, 12]) is straightforward. This feature is essential, since we must simulate the system at different modeling scales, as developed now. The <http://www.openrobots.org/morseMorse> is a generic simulator for academic robotics, with

realistic 3D simulation of small to large environments, allowing complete integration with any simulation tools. It outperforms concurrent systems like <http://www.cyberbotics.com/overviewWebot>. The interest of VirtualEnaction with respect to Morse is twofold: Since we target integrative cognitive tasks of survival which is exactly what happens with the Minecraft environment, using this specialized product is far simpler and somehow more demonstrative. In terms of performances, as being less sophisticated (using a simplified 3D rendering, while Morse has all 3D capabilities) and being agnostic in terms of programming languages (i.e., allowing fast C/C++ implementation of user modules, whereas Morse is limited to Python scripts) the VirtualEnaction platform is a priori expected to be more efficient in terms of CPU usage. However, with a larger human power all what has been developed within VirtualEnaction could have been developed in Morse.

The main application regarding neuroscience is to test *cognitive computational models* in realistic conditions. Very simply, a behavioral experiment is performed on an animal model or on humans, usually with a training phase, the measurement phase and the data analysis. In order to formalize the obtained result a computational model is proposed that explains the data, and may also have prediction regarding other falsifiable future experiments. The present software and methodological tool allow us to propose to enhance this very general paradigm in the following directions:

- Test the model prediction for several others experimental conditions or model parameter ranges: The idea is to reproduce the experimental setup in this virtual environment (e.g., a delayed reward task, an exploration paradigm) and connect the computational model to this paradigm. As for usual computational modeling, the chosen biological measurements (e.g. neural activity, task success performance) are simulated when running the model. Such model is indeed expected to reproduce qualitatively the ground truth, for a given set of parameters values. A step further, it is very important to numerically verify what happens when modifying any quantitative or qualitative parameter value. If the numerical sensibility is so strong that the results cannot be reproduced for some tiny parameter variation, the model is meaningless because biological values make sense as a numerical range, not a single number. If the numerical sensibility is so weak that any parameter value produces the expected result, this parameter is meaningless and a simpler model very likely explains the same data set. The key-point here is that such predictive verification is not only going to be possible, given a fixed data set, but for any data set obtained during virtual environment simulations. In other words, the computational model variants are going to be always tested *in situ*. With no practical bounds on the experimental variants (e.g., number of trials, sensory input precision, task complexity).
- Design new experimental paradigms to confront the computational model to falsifiable conditions: Building an experiment considering an animal model, training the animals for weeks, restarting from the beginning if it appears that there is an unexpected trap (e.g., the task is too simple or unfeasible, or does not allow to discriminate between two concurrent models) may be a huge work.

Starting to design the experiment in a virtual environment completely changes the method: the hypothesized computational model is first tested in silico (i.e., neither in vivo, nor in vitro, but in a software environment) and only confronted to the biological reality in a second stage. The work plan is inverted with respect to usual neuroscience studies, but in computational engineering (e.g., designing new airplanes) this is exactly the way it goes until a few decades. It is however not new in neuroscience, at the scale of mesoscopic brain map study (see e.g., [13] or [11]). The key point here is that such approach is now possible at the behavioral level, considering sensory-motor interactions with a simple or complex environment. Such process also obviously yields a parsimonious use of animal models. A step further, it lays down the challenge of performing realistic experiment with a computational model of the brain behavior and not only considering toy situations where the plausibility of the model can not be checked.

6 Case Study: Pavlovian Conditioning

The degree of equivalence between simulation outcome and neuroscience experimental results is a key issue. This is the reason why we have chosen a software platform where usual behavioral neuroscience experiments can be reproduced “as a whole”. Such classical experiments include pavlovian and operant conditioning, spatial navigation with tasks involving the focus of attention and multi-sensory integration and other high level cognitive functions involving working memory and planning. The main brain structures involved in such tasks are the thalamus and posterior cortex for sensory processing, the basal ganglia system for selection of action and decision, the hippocampus for episodic memory and the prefrontal cortex for the temporal organization of behavior. Depending on the task, other more specialized structures like the amygdala, cerebellum, superior colliculus, hypothalamus and others may also be considered. These tasks are often related to fundamental survival programs (nourishment, reproduction, integrity of the body) and are organized towards goals, defined from the environment (acquiring appetitive goals or avoiding noxious ones) or from the body (satisfying internal needs), which endows them with a strong behavioral ecological anchoring.

As an illustration, we introduce pavlovian conditioning, presently studied in our team, including the integration of related computational models in VirtualEnaction. Pavlovian conditioning is a fundamental learning capability, allowing to identify aversive and appetitive events in the environment and also exploited in many complex tasks. This learning relies on the ability of animals to automatically detect biologically significant stimuli (also called US, unconditional stimuli) and to trigger corresponding reflexes. Pavlovian learning occurs when a neutral stimulus (conditioned stimulus, CS) reliably predicts the occurrence of the US. After acquisition, the CS presented alone will also trigger a response and allows the animal to

anticipate the nature of the US to come. For example, in the case of fear conditioning [14], the US can be an electric shock automatically triggering freezing. Subsequently to the pairing of the US with a CS like the auditory perception of a tone, the CS alone will evoke freezing. It will also allow the animal to anticipate the nature of the US and prepare more adapted behavior like an escape, depending on the nature of the task and the environment.

Fear conditioning has been extensively studied because in its basic forms, it involves a rather simple and well known cerebral circuit, associated to accessible stimuli in the environment. The amygdala is the key structure for the acquisition and expression of fear conditioning [15]. Its lateral nucleus receives extero and interoceptive information from the thalamus and the sensory cortex and is reported to perform the acquisition of CS-US associations and to activate its central nucleus, a motor structure responsible for the expression of pavlovian responses.

This simple associative learning has also been studied because beyond its simple expression, it demonstrates non trivial characteristics. For example, the CS can be more complex than a simple tone, because it includes a temporal structure (delays) or specific spatial characteristics like the context of learning (the room in which conditioning occurs) or the composition of several stimuli (compound stimuli). In this case, the sensory cortex is not able to supply the information in an adapted configuration and the hippocampus has been shown to be necessary for the acquisition of this CS-US association, through its projections to the basal nucleus of the amygdala [16]. The involvement of the hippocampus is not really surprising here, since this structure is known for its role in episodic learning, another kind of associative learning of arbitrary relations between features including spatial and temporal contexts [17].

Learning CS-US association can also become more complex when the association is not deterministic but can vary in time. This can be due to stochasticity (the association is probabilistic) and also to changes in the rules of our dynamic and changing world, as it is observed in the case of extinction [14]. Experiments in neuroscience have shown that when a predicted US no longer occurs, this does not correspond to the removal of the learned CS-US association but to its temporary inhibition by the medial prefrontal cortex, learning history of performance in behavior. Particularly, this means that, in the case of renewal (the old rule becomes valid again), reacquisition of the CS-US association is immediate because it was not forgotten but only inhibited.

Pavlovian conditioning is also studied for its impact, at a systemic level, on other kinds of learning in the brain. Without going too deep in details, it can be mentioned that successes and errors of US prediction have also a deep impact on episodic learning in the hippocampus and on perceptive category learning in the sensory cortex and also in operant conditioning. It must be also underlined that stimuli learned by the pavlovian procedure are often re-used as goals in operant conditioning.

This short overview of pavlovian conditioning was only meant to indicate that behavioral sequences related to this kind of learning can be studied at different levels of complexity, which is the case in neuroscience, depending on the context of

the experiment. Accordingly, our VirtualEnaction platform must adapt to these contexts. In its simplest form, the environment includes simple sensory CS and US and the body must express stereotyped avoidance or attraction movements. In this case, our brainy-bot integrates a model of the amygdala as we can find in the literature or as we developed in the team. In more complex cases, we might for example take into account the spatial context in which the CS is perceived, which requires to integrate a functionality like episodic memory. In this case, we can integrate a generic functionality of symbolic information manipulation as described in Sect. 4 or a more advanced neuronal model of the hippocampus, depending on the aspects that are to be more deeply studied in relation to biological experiments. The principle would be the same for integrating a model of the medial prefrontal cortex or a simple statistical analysis of the recent history of received and predicted US, in case of an experiment related to an extinction procedure.

In addition to the design of the system adapted to the task under study, another critical step is about the design of the scenarios to be tested. Here, scenario stands for the description of the environment (stimuli and their perceptual dimensions, contexts like a cage or a maze), of the laws ruling this environment (which stimulus is a US and triggers an unconditional response; which stimulus is a CS and how reliably it predicts the US; and other physical laws of the environment like objects that can be moved) and of the precise timing of sequence of events (defining protocols implementing acquisition, extinction and renewal procedures). In its most basic form, such a design is generally thought to fit biological experiments and will be used for the purpose of comparison with behavioral performances as well as with patterns of neuronal population activation and learning. In a more advanced form, this system could be also exploited on the side of computer science, either in terms of performance of learning, to be evaluated in a machine learning perspective, or in terms of autonomous agent, to be evaluated with regard to the range of available behaviors and to the pertinence of their selection. Implementing not only pavlovian conditioning but also operant conditioning is a strong prerequisite for this latter perspective, as the authors are presently considering.

7 Discussion

In this paper, we have presented the platform VirtualEnaction, for implementing brain models and their bodily and external environment. Beyond the description of the functionalities of the platform, we have also explained why it was corresponding to a need in the behavioral and computational neuroscience community. We have illustrated these elements with a case study related to an important class of learning, from a behavioral point of view. Indeed, let us mention that this platform has already been used for preliminary digital experiments about Pavlovian conditioning [18] involving the functional modeling of the amygdala and hippocampus, decision making mechanisms in link with reinforcing signals yielded by aversive or

appetitive stimuli and internal computation [19], plus a student work of the AGREL connectionist categorization model here confronted to a realistic environment [20].

Building one “brainy-bot” is a rather huge task and requires several high-level cognitive functionalities. However, though systemic neuroscience requires to study the system as a whole, it does not imply that each functionality has to be studied at the same level of details. Several blocks may be considered as black-boxes interacting with the part of the system to be extensively studied. This is the reason why the present platform is not limited to a survival environment, but comes also with middleware (presently in development) related to the basic cognitive functionality involved in such paradigms [21]. Some modules will thus be implemented according to a rough description, e.g., via an algorithmic ersatz. The nervous sub-system under study on the reverse, is going to be implemented at a very fine scale (neural network mesoscopic models or even spiking neural networks).

The key features of this digital experimentation platform include the capability to perform experiments involving both long-term continuous time paradigms or short-term decision tasks with a few time-steps. It also allows us to consider either symbolic motor command or sensory input (e.g., ingest or not food, detect the presence of a stimulus) or quantitative gestures and complex trajectory generation (e.g., find resources in an unknown environment). A key point is to be able to mimic and repeat at will experiments performed in neuroscience laboratory on animals. Here, the obtained computational models are not only going to “fit the data” but to be explored far beyond, yielding the possibility to study long-term adaptation, statistical robustness, etc. Not only one instance of a bot can be checked, but several parallel experiments can be run in order to explore different parameter ranges, or compare alternative models.

Beyond these basic features, the input and output can be easily manipulated in order to enlarge the experimental setup. Up to now, the main aspect is “input or output degradation”, i.e. adding noise. Originally, bot perception and action are performed without any added noise or random mistake. Depending on the experiment to be conducted, it is obvious (i.e. inserting a few lines of code between the platform and the bot), either to reduce variables precision range (e.g., add noise to the pixelic image) or to randomly draw the fact that a gesture may succeed or fail (e.g., introduce spurious command).

A step further, as already implemented as plugins, since all environment elements are available (not to the bot, but to the experiment software), it would be possible to design other cues, or more generally other interactions with the environment. However, in collaboration with neuroscience experimentalists, we have carefully selected what seems useful to explore biological systemic models, and avoided to provide a too general tool that does anything.

It would also be instructive to better understand to which extent such bio-inspired architectures actually required to control a biological system could enhance artificial control rules commonly applied in robotics or game engines. This is a challenging issue, beyond the present study, but an interesting perspective of the present work.

Acknowledgments Huge thanks to Nicolas Rougier for precious advice.

References

1. Taouali, W., Viéville, T., Rougier, N.P., Alexandre, F.: No clock to rule them all. *J. Physiol. Paris* **105**, 83–90 (2011)
2. Uithol, S., van Rooij, I., Bekkering, H., Haselager, P.: Hierarchies in action and motor control. *J. Cogn. Neurosci.* **24**, 1077–1086 (2012)
3. Hyvärinen, A.: Natural image statistics a probabilistic approach to early computational vision. Hardcover (2009)
4. Teftef, E., Escobar, M.J., Astudillo, A., Carvajal, C., Cessac, B., Palacios, A., Viéville, T., Alexandre, F.: Modeling non-standard retinal in/out function using computer vision variational methods. *Rapport de recherche RR-8217, INRIA* (2013)
5. Friston, K.: A free energy principle for biological systems. *Entropy* **14**, 2100–2121 (2012)
6. Viéville, T., Crahay, S.: Using an hebbian learning rule for multi-class SVM classifiers. *J. Comput. Neurosci.* (2004)
7. Viéville, T., Vadot, C.: An improved biologically plausible trajectory generator. *Technical Report 4539-2, INRIA* (2006)
8. Connolly, C.I., Grupen, R.A.: The applications of harmonic functions to robotic. *J. Robot. Syst.* **10**, 931–946 (1993)
9. Todorov, E.: Optimality principles in sensorimotor control. *Nat. Neurosci.* **7** (2004)
10. Cofer, D., Cymbalyuk, G., Reid, J., Zhu, Y., Heitler, W.J., Edwards, D.H.: AnimatLab: a 3D graphics environment for neuromechanical simulations. *J. Neurosci. Methods* **187**, 280–288 (2010)
11. Brette, R., Rudolph, M., Carnevale, T., Hines, M., Beeman, D., Bower, J.M., Diesmann, M., Morrison, A., Goodman, P.H., Harris, F.C., Zirpe, M., Natschläger, T., Pecevski, D., Ermentrout, B., Djurfeldt, M., Lansner, A., Rochel, O., Vieville, T., Muller, E., Davison, A.P., El Boustani, S., Destexhe, A.: Simulation of networks of spiking neurons: a review of tools and strategies. *J. Comput. Neurosci.* **23**, 349–398 (2007)
12. Davison, A.P., Brüderle, D., Eppler, J., Kremkow, J., Muller, E., Pecevski, D., Perrinet, L., Yger, P.: PyNN: A Common interface for neuronal network simulators. *Frontiers Neuroinform.* **2** (2008)
13. Chemla, S., Chavane, F., Vieville, T., Kornprobst, P.: Biophysical cortical column model for optical signal analysis. *BMC Neurosci.* **8**, P140 (2007)
14. Herry, C., Ciocchi, S., Senn, V., Demmou, L., Muller, C., Luthi, A.: Switching on and off fear by distinct neuronal circuits. *Nature* **454**, 600–606 (2008)
15. LeDoux, J.: The amygdala. *Curr. Biol.* **17**, R868–R874 (2007)
16. Eichenbaum, H., Sauvage, M., Fortin, N., Komorowski, R., Lipton, P.: Towards a functional organization of episodic memory in the medial temporal lobe. *Neurosci. Biobehav. Rev.* **36**, 1597–1608 (2012)
17. Rolls, E.T.: A computational theory of episodic memory formation in the hippocampus. *Behav. Brain Res.* **215**, 180–196 (2010)
18. Gorojovsky, R., Alexandre, F.: Models of Hippocampus for pavlovian learning. *Rapport de recherche RR-8377, INRIA* (2013)
19. Beati, T., Carrere, M., Alexandre, F.: Which reinforcing signals in autonomous systems? In: *Third International Symposium on Biology of Decision Making*, Paris, France (2013)
20. Carrere, M., Alexandre, F.: Émergence de catégories par interaction entre systèmes d'apprentissage. In: Preux, P., Tommasi, M. (eds.) *Conférence Francophone sur l'Apprentissage Automatique (CAP)*. Lille, France (2013)
21. Denoyelle, N., Pouget, F., Viéville, T., Alexandre, F.: VirtualEnaction: A platform for systemic neuroscience simulation. In: *International Congress on Neurotechnology, Electronics and Informatics*, Rome, Italy (2014)

Physically-Based Simulation and Web Visualization of *C. elegans* Behavioural Experiments

Andoni Mujika, Gorka Epelde, Peter Leškovský and David Oyarzun

Abstract This paper presents the work done in the framework of the *Si elegans* project to develop the physics engine for the simulation of the roundworm *Caenorhabditis elegans* and the interfaces to define and visualize behavioural experiments of the worm. The physically-based simulation of the locomotion of the worm is guided by a biomechanical model, based on anatomically matched biphasic springs. The simulation is presented via an experiment visualization web, using a 3D motion reproduction obtained through animation bones. This web also displays information about the activation in muscles and neurons, on additional information panels. Finally, an experiment definition portal has been developed where, by means of a timeline, the user can easily design complex experimental assays.

Keywords WebGL visualization · Physically-based simulation · *Caenorhabditis elegans*

1 Introduction

Caenorhabditis elegans (*C. elegans*) is one of the best known organisms in the world [1], widely used for different biological or medical assays. This is because, on the one hand, *C. elegans* is very useful for genetic studies, considering that its genome is completely known and is up to 35 % similar to the human one.

A. Mujika (✉) · G. Epelde · P. Leškovský · D. Oyarzun
Vicomtech-IK4, Mikeletegi Pasealekua, 57, 20009 Donostia-San Sebastian, Spain
e-mail: amujika@vicomtech.org

G. Epelde
e-mail: gepelde@vicomtech.org

P. Leškovský
e-mail: pleskovsky@vicomtech.org

D. Oyarzun
e-mail: doyarzun@vicomtech.org

The functions of most of its genes are known and its manipulation for chemical and genetic tests is relatively easy. On the other hand, the relative simplicity of its neuronal system (the hermaphrodite *C. elegans* has 302 neurons) permits to study how its nervous system works. Moreover, it shows a rich behavioural repertoire (e.g. locomotion, feeding and even certain social behaviours).

All these aspects make *C. elegans* a perfect organism for study in the way of understanding how the neural processing in more complex organisms, such as our organism, work. Nevertheless, even if the connectivity of the 302 neurons is known, the knowledge of the scientific community does not explain all the behaviours generated by its nervous system.

The *Si elegans* project aims to emulate the neuronal system of *C. elegans* and show the behaviour that emerges from this emulation in a virtual environment in three dimensions. This way, it will provide the scientific community with an alternative and complementary tool to the laboratory experiments. The specifics of the *Si elegans* project are the hardware-based emulation of the neural network and the parallelism of the neuron to neuron communication.

In the following section, we will introduce the *Si elegans* platform. In Sect. 2 we review the state of the art on the *C. elegans* locomotion simulation. Sections 3, 4 and 5 describe all the aspects regarding physical simulation of the worm and its web visualization (and interaction). Finally, Sect. 6 draws conclusions and discusses the future work.

1.1 The *Si elegans* Platform

The *Si elegans* platform is conceptually composed of two main blocks responsible for the emulation of *C. elegans* and a third block responsible for making the platform available for public use (see Fig. 1).

The first block (identified as Neural hardware design level in Fig. 1) is a hardware-based computation framework that emulates the neural system of the nematode in real time. The nervous system of *C. elegans* is being replicated on a field-programmable gate array (FPGA) hardware architecture. Each of the neurons is represented in a unique FPGA and will be configured and parameterised by the user. This configuration will be carried out via the third block (identified as the platform for public use in Fig. 1). Regarding the inter-neuron connectivity, we focus on true reproduction of the parallel information flow between neurons; implementing the inter-neuron connectome using optical off-chip interconnects. Intensity-tunable laser diode emitters will be triggered by the FPGA neuron modules and the light will be distributed through micro optical light elements to specific pixels of light-receptive arrays.

The second block (identified as Software integration level in Fig. 1) provides the tools to convert the high level neuronal system's configuration (provided by the end-users through the third block) to the configuration required by the neural

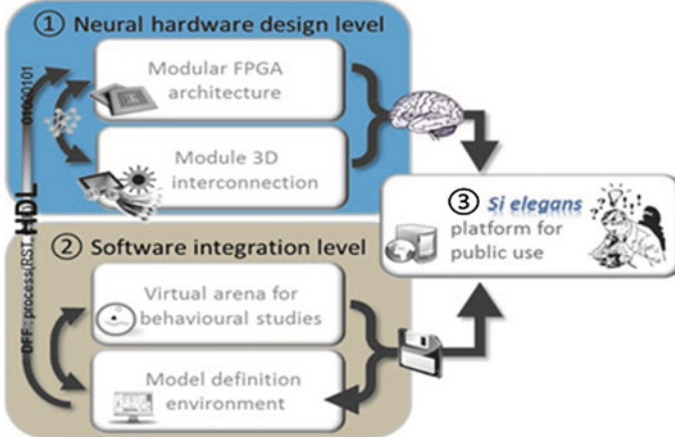


Fig. 1 The *Si elegans* conceptual platform

hardware implementation. It also has a virtual arena that simulates the physics of the worm and its environment.

The third block (identified as *Si elegans* platform for public use in Fig. 1) is responsible for providing the end-users with a web interface to define the neuronal system's configuration and the behavioural experiment, as well as for visualizing the results of the experiment. The user will (i) set all the necessary parameters for defining an experiment (e.g. position of the worm or temperature at different positions of the environment), (ii) watch the resulting motion of the virtual nematode, (iii) monitor the activity of the neuron network, (iv) define new neuronal models, and neuronal network configurations, and (v) share neuron models, experiment configurations and results with the scientific community.

This paper details the solution adopted for the physics-simulation of the worm (identified as the virtual arena for behavioural studies) and the approach of making such simulation available to the end-user (identified as *Si elegans* platform for public use in Fig. 1). Additionally, we will describe the web-based public access part used to define and monitor all the aspects related to the behavioural experiment.

2 Related Work

The pioneering work on the physics simulation of the *C. elegans* was done by Niebur and Erdős [2], in the early nineties. They designed a two-dimensional worm with muscles represented by straight segments. Different forces were applied to the muscles in order to make the body move in a way similar to the real worm.

Thereafter, most models that have been presented [3–5] adopted similar musculo-skeletal anatomy of the worm and force systems that actuate on the worm

and contribute to the generation of the worm's typical motion: internal pressure of the worm, elasticity of the cuticle ("skin" of the worm), muscle forces and environmental forces.

Considering a 2D simulation of locomotion, Boyle et al. [6] developed one of the most realistic models that is suitable for different environments such as water, gelatine or agar. They suggest that the environment does not affect the muscle function because all the different behaviours of the worm, observable in different environments, emerge from the same model. The authors presented a neuronal model that makes the worm adapt to the environment with minimal sensory input.

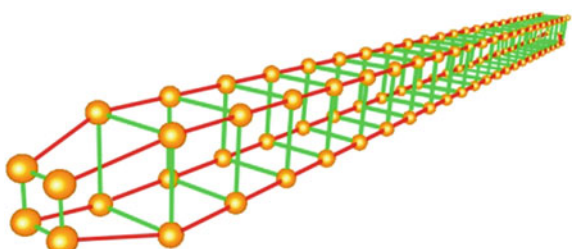
In recent years, 3D simulations of the physics of the worm have appeared. They aim to obtain a more realistic representation of the worm, allowing for moves in the vertical axis. The model presented by Mailler et al. [7], uses a limited neural model and a worm made of 25 rigid cylindrical sections, which is very similar to those described above, but implemented for physics in three dimensions.

The main active project in the field of simulation of *C. elegans*, the OpenWorm Project [8], is also working with 3D simulation of the physics of the worm. It uses Predictive-Corrective Incompressible Smoothed Particle Hydrodynamics (PCI-SPH) [9] to model the behaviour of all the particles that take part in the simulation (including fluids). The realism they want to achieve is very high, although at the moment the performance is too slow for running in a closed-loop with a hardware-based emulation of the neural system and achieve a close to real-time performance (*Si elegans* project's objective).

3 Physical Model

The hermaphrodite *C. elegans* has 95 muscles [10], divided in 4 quadrants of 24 muscles, except for the ventral left quadrant which has 23 muscles. Although a more realistic structure is being developed, our first prototype has 96 symmetrically distributed muscles, as most of the state of art works do. Figure 2 shows the structure constructed to simulate the worm. In each row (quadrant), there are 24 red segments that represent the muscles. These are connected between the quadrants by rings compound of 4 green segments. The first and the last ring are smaller in order to obtain a more similar shape to the shape of the worm.

Fig. 2 Structure of our virtual *C. elegans*



The basis of our model is a classical mass-spring model, but in this case biphasic springs have been used. A biphasic spring is a linear spring that changes its spring constant at a certain length. This way, we stop the spring from elongating more than desired. The formulas describing the kinematics of the biphasic spring are as follows:

$$f_s = -k_s(L_c - L_r) \left(\frac{\vec{p}_2 - \vec{p}_1}{\| \vec{p}_2 - \vec{p}_1 \|} \right)$$

$$f_d = -k_d(\vec{v}_2 - \vec{v}_1) \cdot \left(\frac{\vec{p}_2 - \vec{p}_1}{\| \vec{p}_2 - \vec{p}_1 \|} \right) \left(\frac{\vec{p}_2 - \vec{p}_1}{\| \vec{p}_2 - \vec{p}_1 \|} \right)$$

where f_s and f_d are the spring and damping forces, respectively, that will be applied to the end-points of the springs (in opposite direction), k_s is the variable spring stiffness dependent on the elongation of the current spring, k_d is the damping constant (not depending on the length of the spring), L_c is the current and L_r is the rest length the spring, p_1 and p_2 are the end-points of the spring and v_1 and v_2 are the velocities of the points p_1 and p_2 , respectively.

In order to generate the locomotion of the worm, these springs need to be activated, i.e. they must contract and relax without any external force. For that, a modulating parameter is inserted in the first equation which is modified directly by the motor neurons associated to the corresponding muscle spring. In the case of the rings that maintain the shape of the body, they are springs with higher stiffness and do not activate themselves.

The physical model must define the forces that will be applied to the virtual worm within the simulated environment in order to obtain a coherent locomotion of the whole worm. The forces implemented in our physical model are:

- Muscle contraction: implemented by active springs.
- Cuticle elasticity: implemented by passive springs.
- Gravitation force.
- Internal pressure: as gravity would collapse the spring structure, internal forces are simulated. We use a force field that models behaviour similar to a cube made out of silicon, similar to the one described in [11]. The body of the worm is divided into a grid of hexahedra, supposed to behave isotropically, and then a linear Finite Element Method (FEM) is used to simulate the internal forces, as opposition to the collapsing tendency of the spring structure.
- Friction: is the crucial force which ensures that the worm will move forwards. In our model it is based on Signorini's law and Coulomb's friction law. In the simulation loop, the positions of the mass-points defining the worm are computed taking into account collisions with the floor. Then, based on the considered physical laws, a Non-linear Complementary Problem is obtained and solved for with numerical strategies. Finally, the previous position is corrected in order to encounter for the computed contact forces.

- Other collisions: (e.g. with obstacles) are detected and the resultant forces are applied to the nematode.
- User-defined mechanosensory interaction: for example, the user will be able to touch the worm with a laboratory instrument at a certain time of the simulation. Furthermore, experiments with changes in temperature or chemical substances will be implemented.

All the physics simulation is run using the Simulation Open Framework Architecture (SOFA) [12]. This tool facilitates the creation of complex environments using a wide range of components (solvers, objects, collision detection algorithms, etc.). In our case, these components have been used:

- A Constraint Solver implementing the Non-linear Complementarity Problem formulation described above.
- An Euler Implicit Solver for Ordinary Differential Equations.
- A Conjugate Gradient Linear Solver for systems of linear equations.
- Bounding box hierarchies and a simple triangle/point intersection algorithm for collision detection.

4 Visualization

This section presents how the simulation of the locomotion of *C. elegans* is converted from the simulation calculated in the physics engine to the visualization displayed to the user in a web browser. Since most users of the *Si elegans* framework will be scientists, they might be interested in observing either only the general behaviour of the worm or in analysing the behaviour of a specific neuron or a muscle, and more specifically they would prefer to have access to the values of its inner parameters at each time and not only its position in the simulated environment. Thus, the positions of the whole spring structure are not transferred to the web client.

Only the minimum required information is transferred to the web and there, a realistic 3D reproduction of the nematode (see Fig. 3) is generated according to the simulation computed in the physics engine. To render the 3D environment without any plug-in installation, the Three.js library [13], that makes use of WebGL [14], has been used.

As shown in Fig. 3, the degree of transparency of the skin of the animal can be changed in order to make the neurons visible. In the next stages of the project, these reproductions of neurons and muscles will be used to show additional information about them, e.g. the use of different colours to represent different degrees of excitation of a neuron.

To synchronize the motion of the 3D reproduction in the web with the worm in the physics engine, animation bones have been set along the body of the virtual worm (see Fig. 4). The triangle mesh that represents the body of the worm is



Fig. 3 3D reproduction of *C. elegans*, showing its 302 neurons

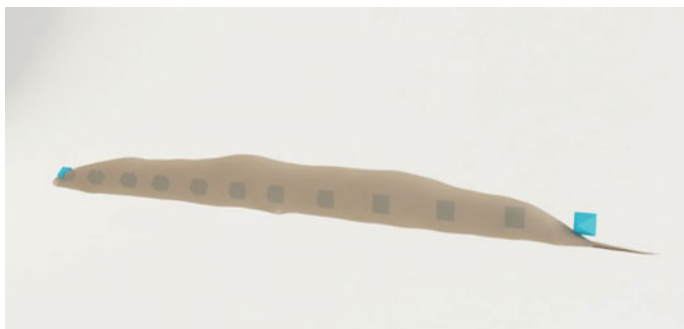


Fig. 4 Animation bones of the worm

attached to these bones, and thus the mesh moves accordingly to the transformations of the bones. The bones are transformed according to the following formula:

$$q_i = \frac{p_{vl,2i} + p_{cr,2i+1}}{2} \quad i = 0, \dots, 11$$

where q_i is the position of the animation bone in the web site; $p_{vl,j}$ is the j th mass point in the ventral, left row and $p_{cr,j}$ is the j th mass point in the dorsal, right row of the server side worm.

5 Web Interaction

The *Si elegans* web portal will be used to define all the aspects of the *Si elegans* emulation system (neuron models, connectivity, behavioural experiments...) and to visualize the results obtained from the system. In this section, we describe the interfaces developed for the definition of the behavioural experiment and the visualization of its simulation results.

5.1 Defining the Experiment

The experiment definition web portal of *Si elegans* will have three main windows: the experiment definition window, the properties window and the 3D visualization window. Figure 5 shows these three parts of the web-page.

A timeline editor (at the bottom of the web-page) is the interface that controls the experiment creation. All the events that will happen during the assay are placed in the timeline, marked with a colour specific to the given type of event. This way, the configuration of the experiment is clearly recognized, at a glance.

In the properties windows, all the properties of the selected event are shown (on the right side of the website). For instance, in a temperature gradient experiment,

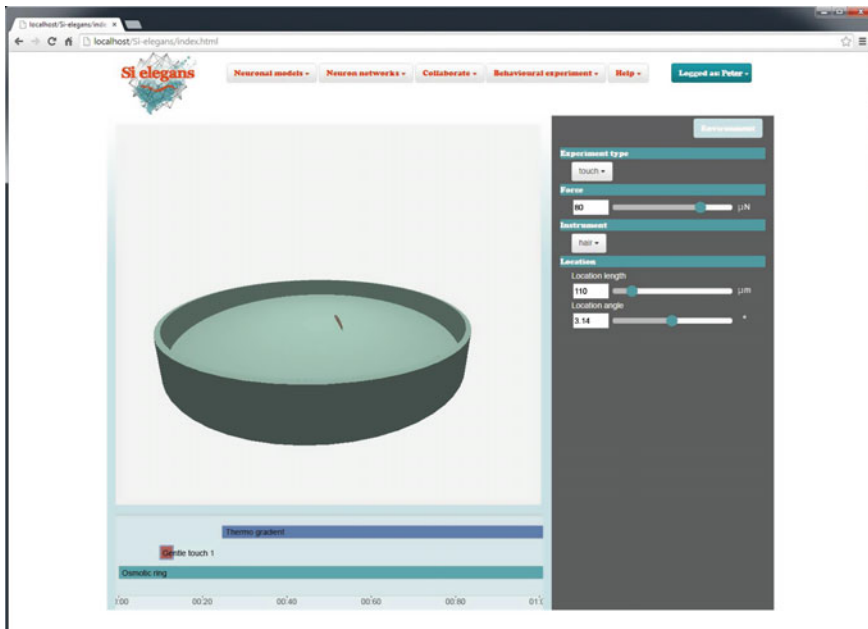


Fig. 5 Experiment definition web-page

the user will set where the heat source will be placed, which temperature it will have and at which moment of the experiment it will be activated.

Besides, in the properties window, the parameters of the environment can be defined: shape of the plate, environmental substance (water, air, silicon, etc.), the initial position and the orientation of the animal, obstacles, etc.

Finally, the 3D visualization window (in the middle) shows the initial configuration of the experiment (without animating anything). This window can be used to insert obstacles in the plate, to choose the place where the toxin drop will be released during the experiment, or to choose at which part of the body the worm will be touched, either by clicking on the 3D plate or on the 3D reproduction of the worm, to mark the desired location.

5.2 Observing and Analysing the Results

The web-page for the visualization of the results of the defined experiment consists of three windows: the selection window, the timeline window and the 3D graphics visualization window. The appearance of this web-page is shown in Fig. 6.

The selection window (at the right side of the web-page) is a grid of squares representing all the neurons and muscles that have been selected to retrieve data.

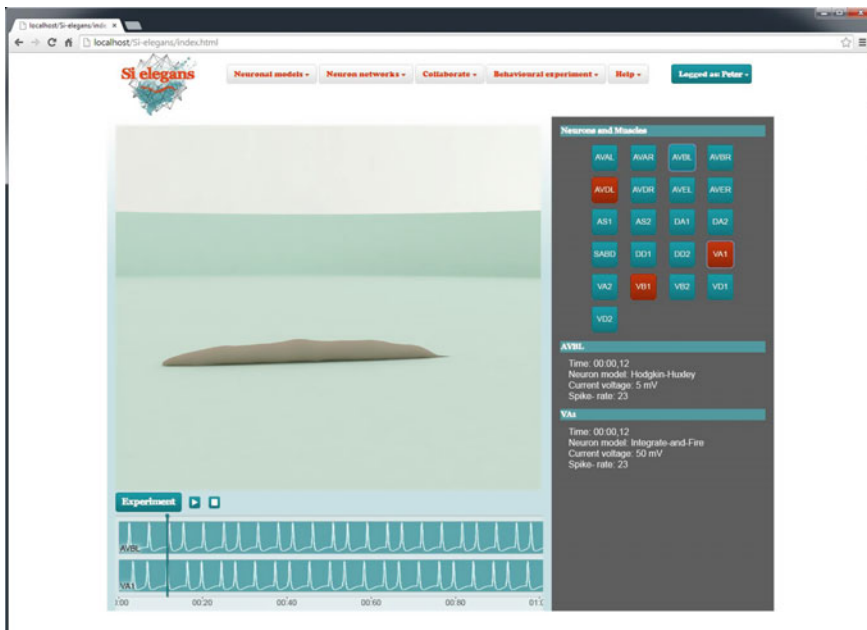


Fig. 6 Visualization web-page

The colour of the squares represents the voltage of each neuron; a spike of a neuron is represented with red colour. This way, the user can know what is happening in all the neurons and muscles he is interested, at a glance.

Furthermore, the user can explore the behaviour of a specific neuron in more detail by clicking one cell of the grid. In the timeline window (at the bottom of the page), a graph representing the voltage of those selected neurons will appear aligned with the experiment timeline and in the selection window, additional information, such as the neuron model that has been chosen for that neuron, is shown.

The timeline window is also used to control the timing of the simulation or to show the previously defined experiment and all the parameters (temperature, chemical concentration...) that take part in the assay. Thus, the user can check how each different stimulus influences the function of the neurons.

The 3D graphics window (in the middle) is where the behaviour of the worm will be displayed, as calculated by the physics engine and transformed for web representation using the animation bones technique, as described in previous sections. Similar to the experiment definition tool, the user will be able to explore the area with the mouse. At this moment, internal parts of the worm are shown, but they are not interactive. In further stages of the project, the 3D window will be used to select cells of the worm or to show advanced/additional information.

6 Conclusions and Future Work

We have described the tools that allow users to define, simulate and follow experiments with the *C. elegans* nematode in the frame of the *Si elegans* project.

Firstly, we have presented the physically-based simulation of the locomotion of the worm. For that, we have created a structure made of biphasic springs, modelling the basic anatomy and the muscular system of the worm. The muscles contract themselves following the signals that come from the neurons. Currently, a simplification that models four equal muscular quadrants has been used. Nevertheless, in further stages of the project, the muscular structure will be changed to make it more similar to the one of the real *C. elegans*.

After the simulation, the movements of the muscles are transformed to a realistic 3D visualisation of the animal, applying the animation bones technique. The visualization web will help the user to understand what is going on in the physiology of the nematode. At the moment, the information about the muscles and the neurons is displayed on information panels, but in the future, the 3D reproduction will be used to show this information.

Finally, we developed a web portal that uses a timeline to design the experiment that will be simulated by the *Si elegans* platform. The user will be able to easily design assays as complex as desired. The challenge of this part of the project will be to implement more types of possible biological assays and allow the user to specify the corresponding experiment details in a user-friendly way.

Acknowledgments The *Si elegans* project is funded by the 7th Framework Programme (FP7) of the European Union under FET Proactive, call ICT-2011.9.11: Neuro-BioInspired Systems (NBIS).

References

1. Altun, Z., Hall, D.: Introduction. In: WormAtlas (2009)
2. Niebur, E., Erdos, P.: Theory of the locomotion of nematodes. *Biophys. J.* **60**, 1132–1146 (1991)
3. Suzuki, M., Goto, T., Tsuji, T., Ohtake, H.: A dynamic body model of the nematode *C. elegans* with neural oscillators. *J. Robot. Mechatron.* **17**(3), 318–326 (2005)
4. Bryden, A., Cohen, N.: Neural control of caenorhabditis *elegans* forward locomotion: the role of sensory feedback. *Biol. Cybern.* **98**(4), 339–351 (2008)
5. Voegtlind, T.: Clones: a closed-loop simulation framework for body, muscles and neurons. *BMC Neurosci.* **12**(1) (2011)
6. Boyle, J.H., Berri, S., Cohen, N.: Gait modulation in *C. elegans*: an integrated neuromechanical model. *Front. Comput. Neurosci.* **6**(10) (2012)
7. Mailler, R., Avery, J., Graves, J., Willy, N.: A biologically accurate 3D model of the locomotion of caenorhabditis *elegans*. In: Proceedings of the 2010 International Conference on Biosciences (BIOSCIENCESWORLD'10), pp. 84–90 (2010)
8. Vella, M., Palyanov, A., Khayrulin, S.: Integration of predictive-corrective incompressible SPH and Hodgkin-Huxley based models in the OpenWorm in silico model of *C. elegans*. *BMC Neurosci.* 8 July 2013, 14 (Suppl 1):P209 (2013). doi:[10.1186/1471-2202-14-S1-P209](https://doi.org/10.1186/1471-2202-14-S1-P209)
9. Solenthaler, B., Pajarola, R.: Predictive Corrective Incompressible SPH. *ACM Trans. Graph.* **28**(3), 1–6 (2009)
10. Altun, Z.F., Hall, D.H.: Muscle system, somatic muscle. In: WormAtlas (2009)
11. Nesme, M., Marchal, M., Promayon, E., Chabanas, M., Payan, Y., Faure, F.: Physically realistic interactive simulation for biological soft tissues. *Recent Res. Dev. Biomech.* **2**, 1–22 (2005)
12. Allard, J., Cotin, S., Faure, F., Bensoussan, P.-J., Poyer, F., Duriez, C., Delingette, H., Grisoni L.: SOFA—an open source framework for medical simulation. In: Medicine Meets Virtual Reality (MMVR'15), pp. 13–18 (2007)
13. Three.js: <http://threejs.org/> (2014). Accessed Oct 2015
14. WebGL: <http://www.khronos.org/webgl/> (2014). Accessed Oct 2015

Si elegans: Modeling the C. elegans Nematode Nervous System Using High Performance FPGAs

Pedro Machado, John Wade and T.M. McGinnity

Abstract The mammalian nervous system is very efficient at processing, integrating and making sense of different sensory information from the outside world. When compared to the processing speed of modern computers the mammalian nervous system is very slow but is compensated for by the dense parallel nature of the brain. Understanding and harnessing the computational power of such systems has long been the goal of computational neuroscientists. However, elucidating the most basic cognitive behaviour has been difficult due to the vast complexity of such a system. Through understanding and emulating simpler nervous systems, such as the *C. elegans* nematode, it is hoped that new insights into nervous system behaviour can be achieved. The *Si elegans* EU FP7 project aims to develop a Hardware Neural Network (HNN) to accurately replicate the *C. elegans* nervous system which has been widely studied in recent years and there now exists a vast wealth of knowledge about its nervous function and connectivity. To fully replicate the *C. elegans* nervous system requires powerful computing technologies, based on parallel processing, for real-time computation and therefore will use Field Programmable Gate Arrays (FPGAs) to achieve this. The project will also deliver an open-access framework via a Web Portal to neuroscientists, biologists, clinicians and engineers and will enable a global network of scientists to gain a better understanding of neural function. In this paper an overview of the complete hardware system required to fully realise *Si elegans* is presented along with an early small scale implementation of the hardware system.

P. Machado (✉) · T.M. McGinnity

Computational Intelligence Laboratory, School of Science and Technology,

Nottingham Trent University, Nottingham, UK

e-mail: pedro.baptistamachado@ntu.ac.uk

T.M. McGinnity

e-mail: martin.mcginnity@ntu.ac.uk; tm.mcginnity@ulster.ac.uk

J. Wade · T.M. McGinnity

Intelligent Systems Research Centre (ISRC), University of Ulster,

Magee Campus, Derry, UK

e-mail: jj.wade@ulster.ac.uk

Keywords *Si elegans* • Field programmable gate array (FPGA) • Hardware neural network (HNN) • *C. elegans* • Wireless networks • Zigbee

1 Introduction

The *Si elegans* project aims to develop a high performance computational system for accurate emulation of the *C. elegans* worm's nervous system behaviour. The objective is to achieve a better understanding of biological signal processing in the *C. elegans* worm, and by doing so translate such knowledge into improved understanding of how the human brain processes information, in both a healthy and diseased state. Such knowledge will advance our understanding of human cognitive processing and lead to major advances in computational architectures.

A replication of the *C. elegans* biological system requires powerful computing technologies, based on parallel processing, for real-time computation. To achieve this, *Si elegans* will use Field Programmable Gate Arrays (FPGAs), due to their advanced programmable features that allow reconfigurability, emulation of biological plasticity, high performance parallel processing and relatively low price per programmable logic element.

FPGA devices consist of a substantial amount of uncommitted hardware resources, which can be reprogrammed after manufacture. Basically any circuit implemented on an FPGA can be seen as a hardware simulation of a corresponding hard-wired circuit. Furthermore, FPGA-based circuits have the following characteristics: reprogrammable, mainly parallel, low power consumption and easy to integrate. Because of these characteristics, FPGAs have evolved substantially in recent years, making FPGAs extremely powerful computational devices. Modern FPGAs have increased speed, lower power consumption, Intellectual Property (IP) blocks for Digital Signal Processing (DSP), increased built-in memory and large numbers of I/Os. These features are fundamental in allowing *Si elegans* to achieve a unique emulation framework where users can perform their complex neural simulations.

To mimic the parallel computational power of a nervous system, the *Si elegans* project will harness the large number of FPGA Inputs/Outputs (I/Os) to keep neural communications completely parallel. Therefore the connections between FPGAs can be made through a wired or a wireless connection. In this paper possible synaptic connectivity solutions based on wired connections and ZigBee mesh wireless connections are explored.

In Sect. 2 a brief review of current wireless network (WN) technology is presented and is followed by a background review of Hardware Neural Networks using FPGAs in Sect. 3. An overview of the *Si elegans* hardware framework is described in Sect. 4. The *Si elegans* project is currently at an early stage and in Sect. 4 a small scale prototype of the *Si elegans* project is described and some preliminary results are presented in Sect. 5. Finally, Sect. 6 draws conclusion to the paper and describes future work.

2 Wireless Networks

In this section we focus briefly on wireless network technologies, specifically, wireless local area networks (WLANs) IEEE 802.11, and wireless personal area networks (WPANs) IEEE 802.15. Due to the evolution of distributed computation, medicine, robotics, defence, aerospace technology, automation and other demanding applications new requirements related to speed, costs, power consumption and range have arisen. Wireless Mesh Networks (WMNs) are specified by IEEE 802.11 s and IEEE 802.15.5 standards. WLAN and WPAN try to implement the majority of these requirements making the selection of the right wireless network technology very complex. Several surveys have been made comparing different WLAN and WPAN types, highlighting the positive and negative aspects of each [1–4]. From these surveys the most relevant WN can be seen in Table 1.

In our small scale system 17 wireless devices are required (see Sect. 5 for further details). The ultra-wideband (UWB) and the Bluetooth WN were not considered as they only support up to 8 nodes. The selection between Wi-Fi and Zigbee devices relies on the data rate, price per device, transmission speed and connectivity protocol. The two candidates were the WiFly (WiFi protocol) wireless module by Rovers Networks and the XBee (Zigbee protocol) series 2 by Digi. Both devices have Universal Asynchronous Receiver-Transmitter (UART)-to-wireless bridges that facilitate data transmission with abstraction from the wireless layer. The XBee module was selected because an XBee network configuration is much simpler than WiFly and the price of each XBee modules is almost half of the price of each WiFly modules.

Table 1 Comparison of bluetooth, UWB, zigbee and Wi-Fi networks [2, 4]

	Bluetooth	UWB	Zigbee	Wi-Fi
IEEE spec	802.15.1	802.15.3a	802.15.4	802.11a/b/g
Frequency band	2.4 GHz	3.1–10.6 GHz	868/915 MHZ; 2.4 GHz	2.4 GHz; 5 GHz
Nominal TX power	0–10 dBm	−41.3 dBm/MHz	−25 to 0 dBm	15–20 dBm
Max signal rate	1 Mbps	110 Mbps	250 Kbps	54 Mbps
Number of cell nodes	8	8	>65000	2007
Indoor range	10 m	10 m	100 m	100 m

3 FPGA Neural Network Background

Hardware neural networks (HNNs) take advantage of the truly parallel and distributed processing capabilities of a biological nervous system. Over the last 2 decades FPGAs have been used for many intelligent applications, including the emulation of neural processing, but also in pattern recognition and robotics [5].

Most HNN implementations to date emulate multiple-neurons on a single FPGA device [6–9]. However, some implementations of a single neuron per FPGA device exist [10, 11]. Similar to these approaches, it is proposed that the *Si elegans* system utilise a single FPGA per neuron topology allowing for greater biophysically realistic neuron and synaptic descriptions. *Si elegans* is different from previous single FPGA per neuron systems in that users can select neuron models from a neuron model library and freely parameterise these models. All library models are represented in VHDL format and currently consists of 2 simple neuron models, namely the Integrate and Fire (IF) given by [12]:

$$I(t) = C_m \frac{dv}{dt} \quad (1)$$

and the LIF given by [12]:

$$\tau_m \frac{dv}{dt} = -v(t) + R_m I(t) \quad (2)$$

where v is the membrane potential, R_m is the membrane resistance, $I(t)$ is the sum of all synaptic currents at time t , C_m is the membrane capacitance and τ_m is the membrane time constant. Ongoing work is focused on VHDL translations of more biophysical realistic neural models such as the Hodgkin and Huxley Model [13], FitzHugh-Nagumo Model [14, 15], Morris-Lecar Model [16] and the Izhikevich Model [17].

3.1 *Si elegans* Overview

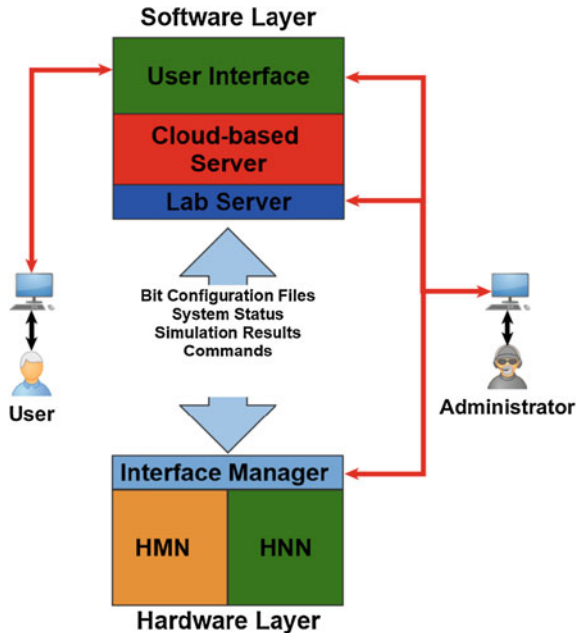
The *Si elegans* project commenced in April 2013 and is thus currently at an early developmental stage. In this section an overview of the full *Si elegans* framework is presented.

The project aims to develop a powerful framework capable of performing realistic simulations of the *C. elegans* nervous system. An overview of the full *Si elegans* framework architecture is depicted in Fig. 1.

Users are assumed to include neuroscientists, biologists, computational intelligence and intelligent systems researchers interested in studying the *C. elegans*' BNS.

It is anticipated that users connect to *Si elegans* platform via a Web Portal using a variety of computational devices. Users can activate *Si elegans* using the User

Fig. 1 *Si elegans* framework architecture



Interface (UI). The UI provides an advanced graphical Hardware Neuron Network (HNN) and Hardware Muscle Network (HMN) definition environment where users can define simulations using predefined neural models/parameters or create their own and then run their simulation on the dedicated hardware.

The UI will also provide a dynamic environment (Virtual Arena) both for emulating the worm's physical sensory input interactions with the world, and for observing the resulting behaviour of the nematode in a 3D cinematic virtual environment.

The main aim of the work presented in this paper is related to the development of the hardware layer, which is composed of 330 tightly coupled FPGA boards, arranged in a set of conventional racks. These correspond to the *C.elegans* 302 neurons and 95 muscles. The focus of the paper is an exploration of non-wired connectivity schemes, in this case a wireless network based synaptic connectivity scheme.

4 Small Scale *Si elegans* HNN

In this section a small scale prototype system composed of 16 neuron FPGAs and one.

Interface Manager (IM) FPGA is implemented for concept validation. All FPGAs are Terasic Altera-based DE4 boards.

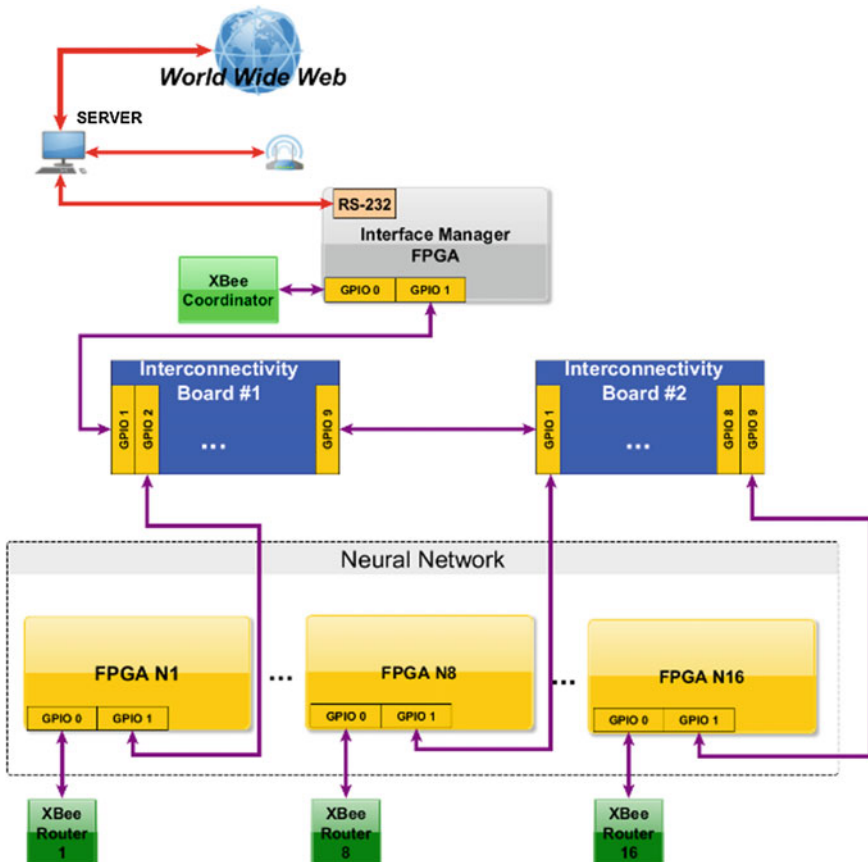


Fig. 2 16 HNN architecture

An XBee module was installed on each of the 17 FPGAs via custom built XBee shields connected to one of the two 40-pin general purpose inputs outputs (GPIO). The second 40-pin GPIO was used to interconnect the 17 FPGAs using a specifically designed interconnect board to provide wired synaptic connections. These latter wired connections allow for a comparison between the two connection schemes and are not used during XBee simulations.

The Interface Manager (IM) is connected to a Server through an RS-232 cable that is used to receive simulation parameters from the Server and to send the simulation results back to the Server. Figure 2 represents the 16 HNN architecture.

4.1 Hardware Layer

The hardware layer of the small scale 16 HNN is composed of:

- **Interface Manager (IM):** this programs the neuron FPGAs and ensures that all the neurons are on the same biological clock cycle. Collates the simulation results and sends back to the Server.
- **Server:** sends simulation parameters, receives and visualizes simulation results;
- **Hardware Neural Network (HNN):** performs computations;
- **XBee Modules:** transmits/receives spikes across the Zigbee mesh network (ZMN).
- **Interconnectivity Board:** wired interconnectivity of neurons and interface manager for comparison with the wireless connectivity scheme.

Interface Manager: The IM shares 5 channels that are used to exchange data and for synchronization with the neuron FPGAs. Each channel is used to transmit/receive the following data type:

- Biological Clock Pulse (BCP): transmits one pulse per timestamp. These pulses are used to inform the neurons that a new timestamp has started;
- Transmit data (BTx): broadcasts data from the IM across all the neurons;
- Receive data (BRx): receives neuron computation ended confirmation from all the neurons.
- Master Clock: 1.8432 MHz;
- UART Clock: 115.200 kHz.

The Server sends the simulation parameters to the IM, and the IM stores the simulation parameters while broadcasting the parameters through the BTx channel using the same UART protocol that is used between the Server and the IM. If at least one spike was generated during that Biological Clock Cycle (BCC) then the IM sends those spikes back to the Server and broadcasts that information through the ZMN or the wired connections.

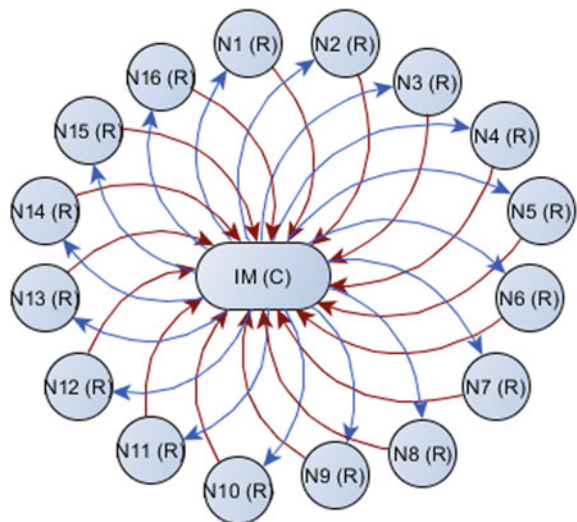
The IM Biological Clock controller generates pulses that are used to ensure that all the neurons are at the same biological clock cycle even if different types of neuron models, with different computation times, are running in different FPGAs.

Server. The Server is used to generate and send simulation parameters as well as receive and visualize the simulation results. It is connected to the IM through the COM port (RS-232). The COM port is configured with a baudrate of 115.2 kHz, 1 stop bit, 8 bits and no parity.

HNN. The HNN is composed of 16 neuron FPGAs. Each neuron FPGA has two neuron models that were described in VHDL. The IM broadcasts the configuration parameters sent by the Server to all neuron FPGAs.

During the simulation period the neuron FPGAs receive BCPs. When a new BCP is received the neuron controller provides the buffered synaptic inputs states to the neuron model and the new membrane potential is calculated. If the membrane potential reaches the threshold then a spike is generated and sent to the neuron

Fig. 3 Zigbee mesh topology



controller. The neuron controller sends the neuron ID and the spike through the ZMN to the IM and if the computation is finished the neuron sends a neuron computation ended confirmation through the BRx using a SPI protocol.

When the simulation finishes the IM sends the simulation data for that BCP and stops the simulation.

Zigbee Mesh Network (ZMN). Each XBee module was configured using the Digi X-CTU software. The XBee modules used on the neuron FPGAs were programmed as Routers and the XBee module used on the IM was configured as coordinator. Each router was programmed to send/receive data to/from the coordinator XBee (see Fig. 3).

4.2 Software Layer

A simple software test bed was developed (*Si elegans System Builder*) which allows the user to describe and configure the desired network configuration to be carried out on the FPGAs. The software is presented in a simple “wizard” format which asks the user a series of questions about their configuration requirements. These requirements comprise of information about network topology and the neural models/parameters used throughout the network. This test bed enabled testing of the described 16 HNN.

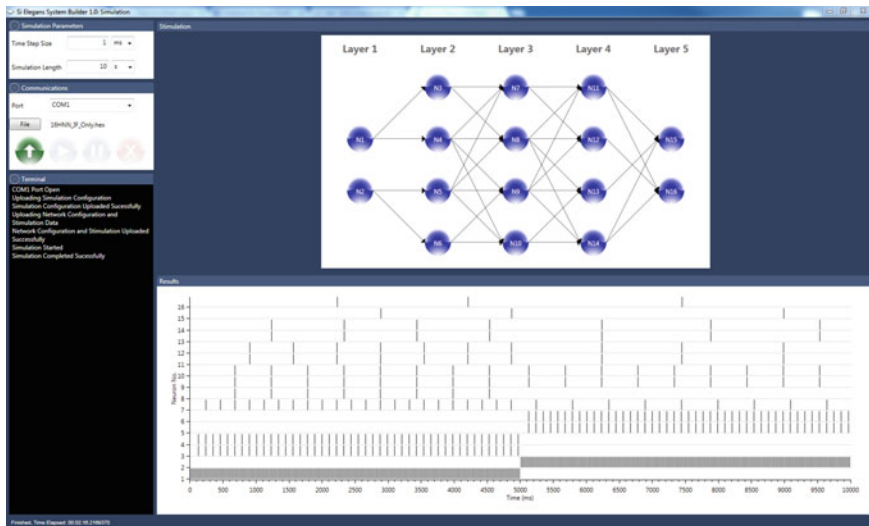


Fig. 4 Screen shot of the *Si elegans* system builder wizard

Currently the user can implement a network with a maximum of 16 neurons chosen from a pre-defined library of neural models (at present, Integrate and Fire or Leaky Integrate and Fire). Furthermore, the user can change any of the available model parameters and can implement the desired network interconnection.

Once the *Si elegans System Builder* creates the necessary files the user can upload the configuration to the FPGAs and start a simulation via a simulation tool provided by the *Si elegans System Builder* software (see Fig. 4).

This tool allows the user to interact with the hardware in several ways. Firstly, in the Simulation Parameters Pane (simulation parameters and communications windows) the user can specify the time step of the simulation, the required simulation length, the COM port used to connect to the hardware and the file to be uploaded. Below this the Terminal Window, which informs the user about the upload success and simulation progress. The Network Stimulation Pane (stimulation window) displays a graphical representation of the configuration network. Finally, the Results Pane (results window) displays simulation results to the user in real time. The main aim of this software is to provide the ISRC with a simple to use, full software test bed for testing the developed FPGA neural emulation platform. It is not intended to replace the full virtual arena being developed by partner Vicomtech.

5 Results

The 16 neuron small scale system consists of two well-known neural models were developed:

- Integrate and Fire [12]
- Leaky Integrate and Fire [12]

Simulation results of these neural models can be seen in Figs. 5 and 6 where each model has been tested individually using the Mentor Graphics Questa Sim 10.1d.

In each test case 2 synaptic input spike trains with a frequency of 250 and 100 Hz respectively were generated to stimulate the neuron. Furthermore, the following parameters were used: $C_m = 1 \text{ nF}$; $R_m = 40 \text{ M}\Omega$; $v_{th} = 10 \text{ mV}$; $v_{reset} = 2 \text{ mV}$; $v_{ref} = 5 \text{ ms}$; weight = 1.

A series of experiments was then performed on the 16 neuron small scale FPGA hardware using the feed-forward, partially connected neural network configuration described in Fig. 7, which was developed in the *Si elegans* System Builder. These experiments were first carried out with XBee wireless synaptic transmission and then with hardwired synaptic connections, thus allowing a comparison of both methods. A number of different network configurations with neurons

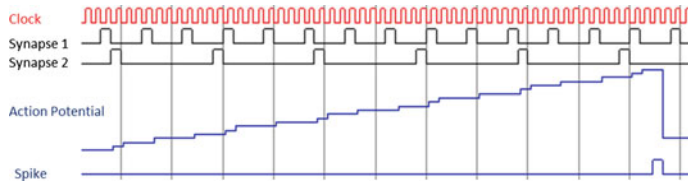


Fig. 5 Simulation results of the Integrate and Fire neuron model on Mentor Graphics Questa Sim 10.1d. Note the first row is the biological clock, rows 2 and 3 represent synaptic inputs, row 4 represents the neuron membrane voltage and row 5 represents the output spikes of the neuron

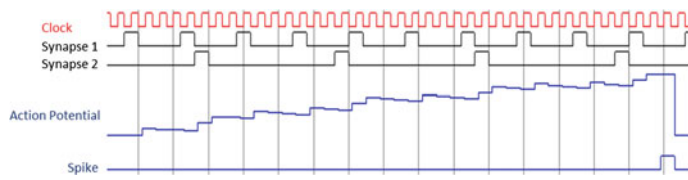


Fig. 6 Simulation results of the Leaky Integrate and Fire model on Mentor Graphics Questa Sim 10.1d. Note the first row is the biological clock, rows 2 and 3 represent synaptic inputs, row 4 is the neuron membrane voltage and row 5 represents the output spikes of the neuron

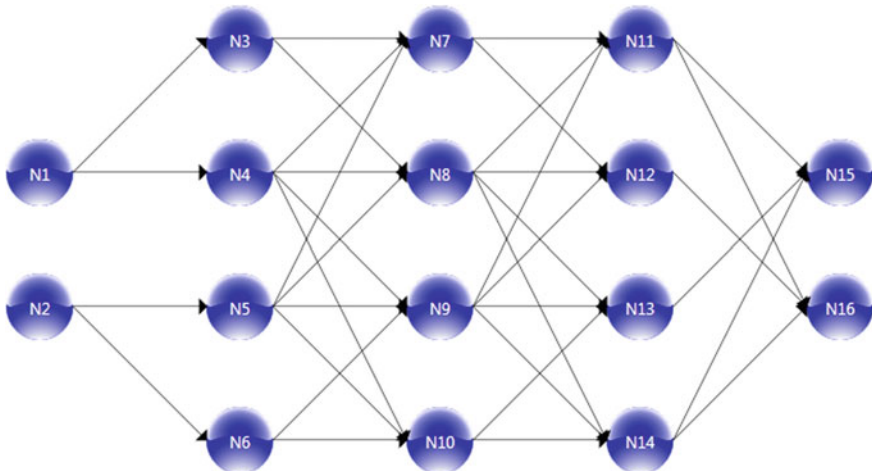


Fig. 7 Neural network topology

models/parameters were examined, to ensure that the system could handle different models at the same time.

When a simulation is started, the configuration hex stream is uploaded through the COM port to the interface manager which relays the configuration setup to the neuron boards. After uploading the configuration hex streams the Interface Manager starts the simulation. The simulations ran for 10000 Biological Clock Cycles (BCC) with a time step of 1 ms; total simulation time =10 s.

During the simulations a constant current was applied to neuron 1 for the first 5 s and then a constant current was applied to neuron 2 for the remainder of the simulation. If a neuron spikes as a result of stimulation or synaptic activity during a BCC the information is sent back to the Interface manager. All spikes during a BCC are collated and then broadcast by the Interface Manager to all neurons. Each neuron then listens for spikes that were emitted by pre synaptic neurons and a new BCC starts. Furthermore the Interface Manger relays this spike information back to the Server. Typical results generated by a simulation can be seen in Figs. 8 and 9.

Figure 8 presents a network comprised only of IF neurons with each synapse given a weight of 2. Note that when neuron 1 and 2 are stimulated with a constant current injection they fire the fastest and cause all other spiking activity throughout the network. As expected, as the information propagates through the network each successive layer's firing rate decreases. Furthermore as the stimulus changes from neuron 1 to neuron 2 the firing patterns throughout the network also change.

Figure 9 describes results from a network comprising of LIF neurons. In this case the weights were randomly initialised between 4 and 9. It is again clear that as network stimulation changes the firing patterns also change. Although these results have no biophysical meaning, they do enable testing of the small scale hardware architecture and neural model functionality.

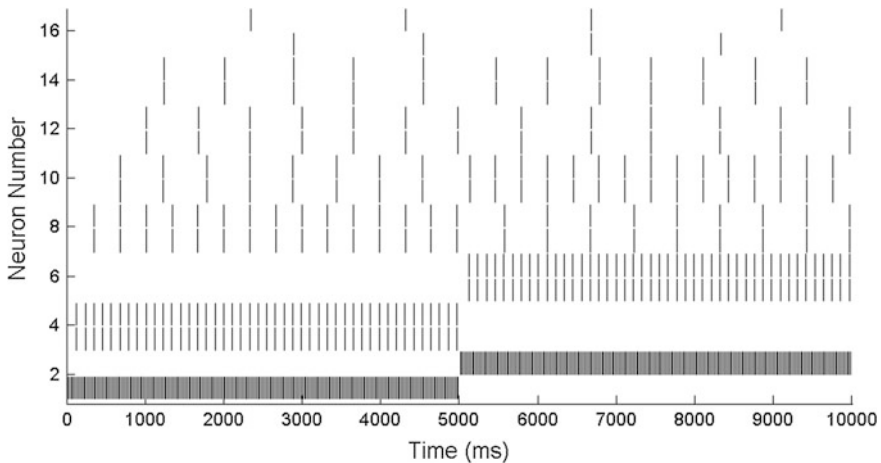


Fig. 8 Typical simulation results 1–10 s (all IF neurons)

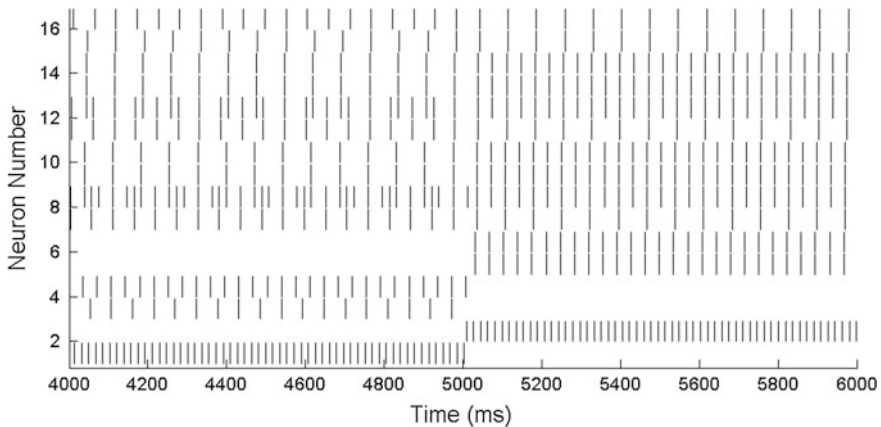


Fig. 9 Typical simulation results 4–10 s (all LIF neurons)

Results from both wired and wireless connection schemes were analysed for differences; both methods provided exactly the same results therefore no packet loss occurred during wireless simulation. However, there was a dramatic increase in simulation run time during wireless experiments. Wireless simulations required ~ 15 times more time to complete. This was a result of the 100 ms delay necessary between XBee communication transmissions.

Finally, the 16 neurons HNN was also used to develop the communications protocol that will be used in the final system. Furthermore, the use of the COM port helped the authors to validate the data payload protocol that is exchanged between

devices, however this type of communication is slower when compared with an Ethernet connection. In the near future the COM port will be substituted by an Ethernet connection which will result in a communications speed increase.

6 Conclusions and Future Work

Currently simulation of neural networks comprised of biophysical realistic models of neurons requires prohibitively long simulation times. Therefore large scale simulations generally utilise phenomenological models which do not capture the rich dynamics of biophysical models. The *Si elegans* project is a multi- platform environment which aims to emulate faithfully the small yet extremely complex nervous system of the *C. elegans* nematode. Furthermore the platform will be freely accessible to neuroscientists, enabling them to easily explore the different neural behaviours and functions of the *C. elegans* worm. The hardware framework will also be scalable, allowing neuroscientists to define new neural models and connectomes. This will ultimately lead to a better understanding of how neural systems function.

In this paper early evaluation work on the hardware architecture of the *Si elegans* framework was described, where both wired and wireless synaptic connectivity were configured and compared. The XBee solution resulted in longer run times when compared to wired connected synapses. This was due to the extra information broadcast by the XBee protocol for each spike and the required delays between transmissions, whereas the wired connection protocol only has to send a single bit for each spike. Therefore, a wireless synaptic transmission of spikes must be reduced to a single bit to achieve the fastest possible simulation times. This will be achieved via optical based synaptic interconnect boards currently under development by our partners in Istituto Italiano di Tecnologia (IIT).

The next stage of this work will be to integrate the optical based synaptic interconnect boards. During this stage all wired connectivity will be removed and the system will be retested by re-running all simulations previously carried out. This will ensure that developed system is capable of driving and communicating correctly with the new synaptic interconnect boards. The RS-232 transmission protocol which allows communication with the Server wil also be changed to Ethernet which will increase information throughput and decrease simulation run times.

Work is also currently underway to increase the neuronal model library to include more detailed neural models such as Hodgkin and Huxely, as well as including synaptic models and STDP learing.

Finally, the small scale system will be developed to full scale with custom made FPGA boards and integrated into the complete *Si elegans* system with other system components developed by our project partners National University Ireland Galway (NUIG), IIT and Vicomtech. NUIG are currently focussed on implementing a module which allows users to define new neural models using various neural modelling languages which are then automatically translated to HDL for use with

the *Si elegans* hardware. The software layer UI and virtual arena which grants the user access to the framework and provides simulation analysis tools to the user is currently under development by Vicomtech.

Acknowledgments The research leading to these results has been partially supported by the *Si elegans* project, which has received funding from the European Community's 7th Framework Programme under the Neuro BioInspired Systems Project Grant agreement 601215. We also wish to thank Altera University Program (AUP) for FPGA board donations.

References

1. Seth, S., Gankotiya, A., Jindal, A.: A Comparative study between wireless local area networks and wireless mesh networks. In: Second International Conference on Computer Engineering and Applications (ICCEA), 2010, Bali Island (2010)
2. Kaur, H., Sharma, S.: A comparative study of wireless technologies: zigbee, bluetooth LE, enocean, wavenis, insteon and UWB. In: International Conference on Recent Trends In Computing and Communication Engineering—RTCCE 2013, Hamirpur, Himachal Pradesh, India (2013)
3. Abdul Ghayum M.S.: Thesis on Comparative study of wireless protocols: Wi-Fi, bluetooth, zigbee, wirelessHART and ISA SP100, and their effectiveness in industrial automation, The University of Texas at Austin, Texas (2010)
4. Lee, J.-S., Su, Y.-W., Shen, C.-C.: A Comparative study of wireless protocols: bluetooth, UWB, zigbee, and Wi-Fi. In: 33rd Annual Conference of the IEEE Industrial Electronics Society, 2007, IECON 2007, Taiwan (2007)
5. Misra, J., Saha, I.: Artificial neural networks in hardware: a survey of two decades of progress. *Neurocomputing* **74**, 239–255 (2010)
6. Glackin, B., McGinnity, T.M., Maguire, L.P., Wu, Q.X., Belatreche, A.: A novel approach for the implementation of large scale spiking neural networks on FPGA hardware. *Comput. Intell. Bioinspired Syst.* **3512**, 552–563 (2005)
7. Ang, C., McEwan, A., van Schaik, A., Jin, C., Leong, P.: FPGA implementation of biologically-inspired auto-associative memory. *Electron. Lett.* **48**(3), 148–149 (2012)
8. Iakymchuk, T., Rosado, A., Frances, J., Batallre, J.: Fast spiking neural network architecture for low-cost FPGA devices. In: 7th International Workshop on Reconfigurable Communication-centric Systems-on-Chip (ReCoSoC), pp. 1–6 (2012)
9. Pande, S., Morgan, F., Seamus Cawley, T.B., Smit, G., McGinley, B., Carrillo, S., Harkin, J., McDaid, L.: Modular neural tile architecture for compact embedded hardware spiking neural network. *Neural Process. Lett.* **38**(2):131–153 (2013)
10. Mohamad, K., Mahmud, M., Adnan, F., Abdullah, W.: Design of single neuron on FPGA. 2012 IEEE Symposium on Humanities, Science and Engineering Research (SHUSER), pp. 133–136 (2012)
11. Salapura, V., Gschwind, M., Maischberger, O.: A fast FPGA implementation of a general purpose neuron. In: Field-Programmable Logic Architectures, Synthesis and Applications, Prague, Czech Republic, Springer Berlin Heidelberg, pp. 175–182 (1994)
12. Gerstner, W., Kistler, W.M.: Spiking Neuron Models. Cambridge University Press, Cambridge (2002)
13. Hodgkin, L., Huxley, A.F.: A quantitative description of membrane current and its application to conduction and excitation in nerve. *J. Physiol.* **117**(4):500–544 (1952)
14. FitzHugh, R.: Impulses and physiological states in theoretical models of nerve membrane. *Biophys. J.* **1**(6), 445–466 (1961)

15. Nagumo, J., Arimoto, S., Yoshizawa, S.: An active pulse transmission line simulating Nerve Axon. In: Proceedings of the IRE, vol. 50, issue 10, pp. 2061–2070 (1962)
16. Morris, B., Lecar, H.: Voltage oscillations in the barnacle giant muscle fiber. Biophys. J. **35**(1), 193–213 (1981)
17. Izhikevich, E.: Simple model of spiking neurons. IEEE Trans. Neural Netw. **14**(6):1569–1572 (2003)

Probabilistic Tractography Using Particle Filtering and Clustered Directional Data

Adelino R. Ferreira da Silva

Abstract The approach of using deterministic methods to trace white-matter fiber tracts through the brain and map brain connectivity is pervasive in currently followed tractographic methodologies. However, using deterministic procedures to support fiber mapping jeopardizes rigorous fiber tractography and may originate deficient maps of white matter fiber networks. We propose a new probabilistic framework for modeling fiber-orientation uncertainty and improve probabilistic tractography. A probabilistic methodology is proposed for estimating intravoxel principal fiber directions, based on clustering directional data arising from orientation distribution function profiles. Mixtures of von Mises-Fisher (vMF) distributions are used to support the probabilistic estimation of intravoxel fiber directions. The fitted parameters of the clustered vMF mixture at each voxel are then used to estimate white-matter pathways using particle filtering techniques. The proposed method is validated on synthetic simulations, as well as on real data experiments. The method holds promise to support robust tractographic methodologies, and build realistic models of white matter tracts in the human brain.

1 Introduction

Through the technique of diffusion magnetic resonance imaging (dMRI), the natural diffusion of water molecules in biological structures can reveal *in vivo* microscopic details about the architecture of both normal and diseased tissues. Fibrous biological tissues are typically anisotropic, hence water mobility in these tissues is not always the same in all directions. For instance, in the human brain's white matter molecular motion is favored in directions aligned with bundles of parallel fibers. White matter fiber tracking or “tractography” uses fiber-orientation estimates to

A.R.F. da Silva (✉)

NOVA CTS, Dep. de Eng. Electrotécnica, Faculdade de Ciências e Tecnologia, FCT, Universidade NOVA de Lisboa, 2829-516 Caparica, Portugal
e-mail: afs@fct.unl.pt

trace the likely paths of white-matter tracts through the brain. Tractography techniques are powerful tools to capture white matter (WM) connectivity non-invasively. Before applying tractography techniques, dMRI measurements are applied to probe the dispersion of water molecules within tissues over a time. A probability distribution on the displacement of water molecules describes the scatter pattern of molecules during the diffusion time. Since white matter axons are tiny compared to typical magnetic resonance imaging (MRI) voxels, voxels contain hundreds of thousands of axon fibers, which can adopt a wide range of complex configurations. The simpler and most commonly used method, Diffusion Tensor Imaging (DTI) uses a Gaussian distribution to model the dispersion. DTI assumes that the diffusion scatter pattern exhibits a single directional pattern, and is therefore unable to model multiple-directional fiber pathways within a voxel. Other model-based approaches, such as the multi-tensor model [1], or multi-compartment models [2, 3] have been devised to account for distinct groups of “populations” of fibers. However, model-based techniques recover but a few number of dominant fiber-orientations, and have difficulty in discriminating common anatomical fiber configurations [4]. To resolve complex orientations, model-free methods and High Angular Resolution Diffusion Imaging (HARDI) protocols have been developed. For instance, Q-ball imaging (QBI) (Tuch 2004) is one popular HARDI-based method used to resolve fiber crossings. It reconstructs the angular profile of the diffusion propagator, commonly known as the (diffusion) orientation distribution function (ODF). The ODF exhibits multiple local maxima in crossing regions, which are used as fiber orientation estimates. Two more recent model-free models are the Diffusion Spectrum Imaging (DSI) [5], and the Generalized q-Sampling Imaging (GQI) [6] methods. These methods perform non-parametric reconstructions that resolve multiple peaks in each voxel, without requiring prior knowledge of the number of fiber populations. Similarly to other methods for ODF reconstruction, DSI and GQI use shell or grid sampling schemes to extract information about the extent of diffusion anisotropy, and map vector fields that represent the fiber orientations at each voxel. In contrast to QBI, DSI and GQI are not limited to a single spherical shell and a single diffusion gradient coefficient (b -value) to characterize diffusion anisotropy.

As pointed out by [4, 7], most tractography algorithms still use the basic DTI single-fiber reconstruction and it is not clear how to generalize them to exploit the extra information that multiple fiber reconstructions provide. Even when probabilistic tractography is used to estimate the uncertainty of fiber-orientations, the information used to track through fiber configurations is limited to the principal diffusion directions. For instance, in [8] fiber-orientations are detected by a Monte Carlo streamline approach, and the sharpness of the peaks are used as indicators of uncertainty. In [7], the authors have shown that the peaks of multiple-fiber reconstructions provide useful information that can be used to improve tractography results. They used the Bingham distribution to model the peak uncertainty in fiber-orientation estimates obtained from the ODF. Hence, better peak shape uncertainty estimates provided improved tractography results. The main drawback of the above technique is that it requires a costly and complicated calibration.

The calibration procedure constructs a mapping from two Hessian (or second derivative) eigenvalues to Bingham parameters, using simulations on two-tensor mixture models with known peak directions [7].

The above considerations motivated us to devise a probabilistic framework for modeling fiber-orientation uncertainty and improve probabilistic tractography. Two key ideas govern the present development and implementation. First, we model fiber-orientation uncertainty by using directional data clustering to estimate white matter fiber orientations. A clustered-mixture-model approach to model directional ODF data based on von Mises-Fisher (vMF) distributions is used, in order to support the probabilistic estimation of intravoxel fiber directions. The generalized fractional anisotropy (GFA) [9] is applied to the reconstructed ODF in order to threshold the population of acquisition directions before clustering.

In this “clustered-vMFs” approach, each estimated voxel fiber direction is associated with a component of the fitted mixture of vMF distributions. Hence, each voxel fiber principal direction may be specified by the summary statistics of the estimated vMF component in the mixture. It is worth noting that, in opposition to [7], no calibration is required. Fitting the mixture of von Mises-Fisher (vMF) distributions to the clustered data, automatically defines the parameters defining the statistical properties of the main peak directions. Moreover, the number of fitted clusters automatically define the pattern of fibers in a voxel.

The second key idea consists in using the fitted parameters of the clustered-vMFs approach at each voxel to guide probabilistic fiber tracking using particle filtering. Several probabilistic techniques have been proposed in the literature to cope with directional uncertainty, partial volume effects, and errors in fiber orientation estimates [8, 10]. Probabilistic methods generate multiple trajectories based on a distribution of fiber bundles at a given seed point, in order to map the connection between the seed voxel and other voxels of the brain. In these techniques, Markov Chain Monte Carlo (MCMC) methods are used to sample from fiber orientation distributions. In order to make the sampling stage more effective, several authors [10–12] have proposed to apply particle filtering to recursively estimate the posterior distribution of fibers at each propagation step. In a similar vein, in this work we have used the Sequential Monte Carlo (SMC) framework [13] to model fiber trajectories. The SMC algorithm propagates for each seed a cloud of particles representing the density probability of the fiber path passing through the seed voxel. The main innovation in the present formulation consists in coupling the particle filtering process with the clustered-vMFs estimate outlined above.

The paper is organized as follows. Section 2 presents the underlying methodology supporting the proposed approach, namely the particle filtering strategy and the clustered-vMFs model. In Sect. 3 we report on experiments applied to simulated as well as to real brain data. The results of the proposed methodology are compared to those from standard streamline approaches. Section 4 provides details on the implementation environment used to support reproducible research. Section 5 draws some conclusions and points to future working directions.

2 Methods

In this section we present the underlying methodology for the proposed tractographic approach, namely the probabilistic fiber tracking model, and the clustered-vMFs model supporting the particle filtering strategy.

2.1 Fiber Tracking Model

In a particle filtering context, fiber tracking is formulated as a non-Gaussian state space model [14]. In this model, given the prior probability distribution that characterize the uncertainty of local fiber orientations, a posterior distribution of the target fiber is estimated. Given that both the prior and the posterior distribution are non-Gaussian, particle filtering techniques are well suited to estimate the complex geometry of the fiber paths, and account for directional uncertainties. In contrast, linear filtering methods such as Kalman filtering are often inappropriate to track complex configurations.

In a volume $\Omega \subset \mathbb{R}^3$, a fiber trajectory can be modeled as a sequence of n displacement vectors u_k with $k = 1, \dots, n$. From a given starting point u_0 , at each time step k , each streamline is propagated one step from its previous location $u_{k-1}^{(i)}$ with a direction vector $v_k^{(i)}$ sampled from the importance density by a step size λ , such that $u_k^{(i)} = u_{k-1}^{(i)} + \lambda v_k^{(i)}$. The state of a particle at time step k , $x_k^{(i)}$, is defined by its location $u_k^{(i)}$ and direction vector $v_k^{(i)}$.

As detailed in [14], particle filtering algorithms can be interpreted as instances of a single generic SMC algorithm. Earlier particle filtering algorithms, such as the popular Sequential Importance Sampling (SIS), suffered from a degeneracy problem as simulation time increased: variance of the estimates increased with time k . Degeneracy is a key factor conditioning the application of SIS algorithms. However, by introducing a re-sampling step degeneracy can be greatly mitigated. Modern SMC methods are a combination of SIS and resampling. SMC methods sample sequentially from a sequence of target probability densities $\pi_k(x_k)$.

As outlined in Algorithm 1, by a sequence of prediction, weighting and selection steps, the particle filter provides a discrete approximation of a posterior distribution $p(x_k | y_{0:k})$ on a time-varying parameter x_k at time step k , given the observations $y_{0:k}$ for time steps $0, 1, 2, \dots, k$, and the initial state distribution $p(x_0)$. At each time step k , N particles are propagated by sampling from an importance distribution $\pi(x_k^{(i)} | x_{0:k-1}^{(i)}, y_{0:k})$. In the weighting stage, importance weights $w_k^{*(i)}$ are assigned in accordance to the likelihood $p(y_k | x_k^{(i)})$. The discrete approximation to the posterior distribution $p(x_k | y_{0:k})$, denoted by $\tilde{w}_k^{(i)}$, is computed by normalizing the importance weights $w_k^{*(i)}$. Finally, a resampling step is used to remove particles with low weights and proliferate those with high weights. Resampling may be applied at each

time step, or alternatively, it may be applied only when the variance of the normalized weights is superior to a pre-specified threshold. The threshold, designated ε_{ESS} in Algorithm 1, is often specified in terms of the Effective Sample Size (ESS) criterion [15], which assesses the variability of the weights by,

$$ESS = \left(\sum_{i=1}^N (\tilde{w}_k^{(i)})^2 \right)^{(-1)} . \quad (1)$$

In Algorithm 1, the importance distribution $\pi(x_k | x_{0:k-1}^{(i)}, y_{0:k})$ is a vMF distribution. The initial state distribution $p(x_0)$, is the vMF distribution parameterized by one of the components of the clustered-vMFs estimate for the current voxel, as detailed in Sect. 2.2. The likelihood $p(y_k | x_k^{(i)}) = (v_k \cdot \mathcal{V}(u_k))$, is defined by a vMF distribution parameterized by the parameters of the most likely vMF cluster component, for direction v_k , at each point location u_k .

In the resampling stage, the usual practice is to attribute equal importance weights to the newly introduced particles [14]. The use of equal weights helps maintaining the diversity of the population of particles at intermediate tracking stages, which favors the exploration of new trajectories emerging from the current state.

Algorithm 1: Sequential Monte Carlo.

Input :

- \mathcal{V} Voxels' cluster statistics
- N Number of particles
- ε_{ESS} Resampling threshold

```

1 for particle  $i = 1$  to  $N$  do
2    $x_0 \sim p(x_0)$ 
3    $w_0^{*(i)} = \frac{1}{N}$ 
4 end
5 for times  $k = 1$  to  $K$  do
6   for particle  $i = 1$  to  $N$  do
7      $x_k^{(i)} \sim \pi(x_k | x_{0:k-1}^{(i)}, y_{0:k})$   $w_k^{*(i)} = w_{k-1}^{*(i)} p(y_k | x_k^{(i)})$   $\tilde{w}_k^{(i)} = \frac{w_k^{*(i)}}{\sum_{j=1}^N w_j^{*(i)}}$ 
8   end
9    $ESS = \left( \sum_{i=1}^N (\tilde{w}_k^{(i)})^2 \right)^{(-1)}$ 
10  if  $ESS < \varepsilon_{ESS}$  then
11    | Resample  $\{\tilde{w}_k^{(i)}, x_k^{(i)}\}$  according to importance weights
12  end
13 end
14

```

However, this particle filtering setting may be too rich for the resolution of the diffusion directions estimated at each voxel. White matter axon radii are in the

range [0.1, 10] μm , whereas MRI voxels typically have sides in the range [1, 5] mm. Voxels therefore contain hundreds of thousands of axon fibers [4], but the estimated principal diffusion directions are typically reduced to 2 or 3 per voxel, originating the so-called “partial volume effects” [16]. These effects introduce uncertainties in anisotropy measurements at each voxel, which influence ODF reconstruction accuracy and the anatomic validity of fiber track estimates. An alternative procedure, is to attribute new importance weights according to the weights already evolved for the population of particles. This procedure helps maintaining the selection pressure over low weighted particles and reduces trajectory irregularities, driving the sequence of distributions to a maximum a-posterior path, at the cost of particle diversity. The result is a more conservative set of estimated directions, and a reduced capability of the algorithm for exploring very long pathways. Nonetheless, it may still confer realistic fiber track estimates for brain tractography.

2.2 Clustered-vMFs Model

The fiber tracking model outlined in Sect. 2.1 uses vMF distributions as sampling distributions of interest. A d -dimensional unit random vector $\mathbf{x} \in \mathbb{S}^{d-1}$ is said to have d-variate vMF distribution if its probability density function is given by

$$f(\mathbf{x}|\boldsymbol{\mu}, \kappa) = c_d(\kappa) e^{\kappa \boldsymbol{\mu}^T \mathbf{x}}, \quad (2)$$

where $\|\boldsymbol{\mu}\| = 1$, $\kappa \geq 0$ and $d \geq 2$. The normalizing constant $c_d(\kappa)$ is given by

$$c_d(\kappa) = \frac{\kappa^{d/2-1}}{(2\pi)^{d/2} I_{d/2-1}(\kappa)}, \quad (3)$$

where $I_r(\cdot)$ represents the modified Bessel function of the first kind and order r . The density $f(\mathbf{x}|\boldsymbol{\mu}, \kappa)$ is parameterized by the mean direction $\boldsymbol{\mu}$, and the concentration parameter κ . The κ parameter characterizes how strongly the unit vectors drawn according to $f(\mathbf{x}|\boldsymbol{\mu}, \kappa)$ are concentrated about the mean direction $\boldsymbol{\mu}$. Larger values of κ imply stronger concentration about the mean direction [17]. The vMF distribution is unimodal for $\kappa > 0$, and is uniform on the sphere for $\kappa = 0$.

For directional clustering estimation, we consider a mixture of k vMF distributions [18] that serves as a model for directional ODF profile data, corresponding to multiple fiber orientations. A mixture of k vMF distributions has a density given by

$$f(\mathbf{x}|\boldsymbol{\Theta}) = \sum_{h=1}^k \alpha_h f_h(\mathbf{x}|\boldsymbol{\theta}_h), \quad (4)$$

where $f_h(\mathbf{x}|\boldsymbol{\theta}_h)$ denotes a vMF distribution with parameter $\boldsymbol{\theta}_h = (\boldsymbol{\mu}_h, \boldsymbol{\kappa}_h)$ for $1 \leq h \leq k$, $\boldsymbol{\Theta} = \{\alpha_1, \dots, \alpha_k, \boldsymbol{\theta}_1, \dots, \boldsymbol{\theta}_k\}$, and the α_h are non-negative and sum to 1. The Expectation Maximization (EM) framework is used for estimating the mean and concentration parameters of the mixture. The clustering algorithms proposed by [18] and implemented in [19] were used to fit the vMF mixture. The principal ODF profile statistics are extracted directly from the estimated clusters. The number of fibers in each voxel is automatically estimated from the reconstructed ODF profile by the vMF approach using the Bayesian Information Criterion (BIC) criterion [20]. In other words, “BIC” is used to decide on the number of components to select. All relevant statistical information about the ODF orientation and multiple fiber components may then be extracted from this fitting process.

The preceding description specifies a clustered mixture-model approach to model directional ODF data based on von Mises-Fisher (vMF) distributions. In this “clustered-vMFs” approach, each estimated voxel fiber direction is associated with a component of the fitted mixture of vMF distributions. Hence, each voxel fiber principal direction may be specified by the summary statistics of the estimated vMF component in the mixture. Based on voxel ODF reconstructions, our method estimates intravoxel fiber directions by clustering mixtures of von Mises-Fisher distributions fitted to probabilistic distributions.

As opposed to other approaches where mixture of vMF distributions are used to represent diffusion, e.g., [21], our method works directly with the sampled ODF distributions. Moreover, the proposed clustered-vMFs statistical procedure does not care for ODF reconstruction. The process of ODF reconstruction is kept independent from the process of statistical cluster estimation. The objective of the clustered-vMFs model is to gather statistical information in order to support robust probabilistic tractographic algorithms [22]. Therefore, multiple ODF reconstruction approaches can be easily integrated in the proposed framework by a simple “plug-in” technique.

Before applying the clustered-vMFs approach we need to obtain the ODF profiles at each voxel. As pointed out in the Introduction, model-free methods and HARDI protocols are more adequate than current model-based methods for resolving complex orientations. Any of the model-free methods mentioned in the Introduction, (e.g., QBI, GQI, DSI), could be used for reconstructing ODF profiles. Starting with the raw signal acquired on a shell or grid of q -space, the ODF profile is estimated at each voxel, considering a sampling density of unit vectors on a unit \mathbb{S}^2 grid or shell. To summarize anisotropic properties of the ODF and infer the underlying crossing patterns of the fibers we use the GFA metric [9],

$$GFA = \sqrt{\frac{n \sum_{i=1}^n (\psi(\mathbf{u}_i) - \langle \psi \rangle)^2}{(n-1) \sum_{i=1}^n \psi(\mathbf{u}_i)^2}}, \quad (5)$$

where $\langle \psi \rangle = (1/n) \sum_{i=1}^n \psi(\mathbf{u}_i) = (1/n)$ is the mean of the ODF, $\langle \mathbf{u} \rangle$ is the mean diffusion direction, and $\langle . \rangle$ denotes the average over ψ . The GFA metric proposed in [9], is an extension for HARDI protocols of the fractional anisotropy (FA) metric

commonly used in diffusion tensor imaging (DTI). When a threshold is applied to the estimated GFAs at each voxel, the non-thresholded unit vectors provide directional statistics information about the estimated ODF profile.

This directional clustering procedure has several advantages compared to traditional approaches for orientation mapping. In fact, current best practices perform multiple maxima extraction based on procedures which are very sensitive to the local modes that appear in the reconstructed ODFs. Signal noise and low sampling resolution yield deformed ODF reconstruction profiles, thus affecting accuracy and precision in multiple orientation evaluations. In contrast, estimating orientations from clustered directional data is much less sensitive to local modes in the reconstructed ODF profile. Moreover, the procedure is more robust to noise since it estimates orientations statistically from sampled data.

3 Experimental Results

To validate the fiber tracking model described in Sect. 2 we performed simulations with synthetic fields of diffusion profiles. Section 3.1 details the simulation methodology used for this purpose, and derives maps of fiber pathways for simulated fields of diffusion profiles. In Sect. 3, we report on fiber tracking experiments applied to real human brain data. Tractographic experiments have been applied to two Regions of Interest (ROIs) For the first ROI, seeds were placed along the Corpus Callosum (CC) region in a sagittal slice. The second ROI tests the tractography of the corticospinal tract (CST) connecting the spinal cord to the cerebral motor cortex. The results of the application of the proposed probabilistic methodology are compared to those from standard streamline approaches.

3.1 Fiber Bundle Simulation

Fiber bundle simulations were performed as follows. Firstly, we simulated diffusion profiles at each voxel by generating diffusion-weighted signals for single and multiple fibers simulations, using the method detailed in [23]. Secondly, we estimated ODF profiles by applying the model-free GQI method to extract information about the extent of diffusion anisotropy, and map vector fields that represent the fiber orientations at each voxel. Thirdly, the clustered-vMFs approach was used to obtain summary statistics of the vMF components in the mixture of von Mises-Fisher distributions. Finally, the SMC algorithm was applied to guide probabilistic fiber tracking. The parameters of the clustered-vMFs approach at each voxel were used to propagate a cloud of particles, according to the fitted density probability for the fiber bundle trajectory being tracked. Based on the resampling strategy outlined in Sect. 2.1 for path tracking, we derive a map of fiber pathways for the simulated field of diffusion profiles. Figure 1 shows an example of a

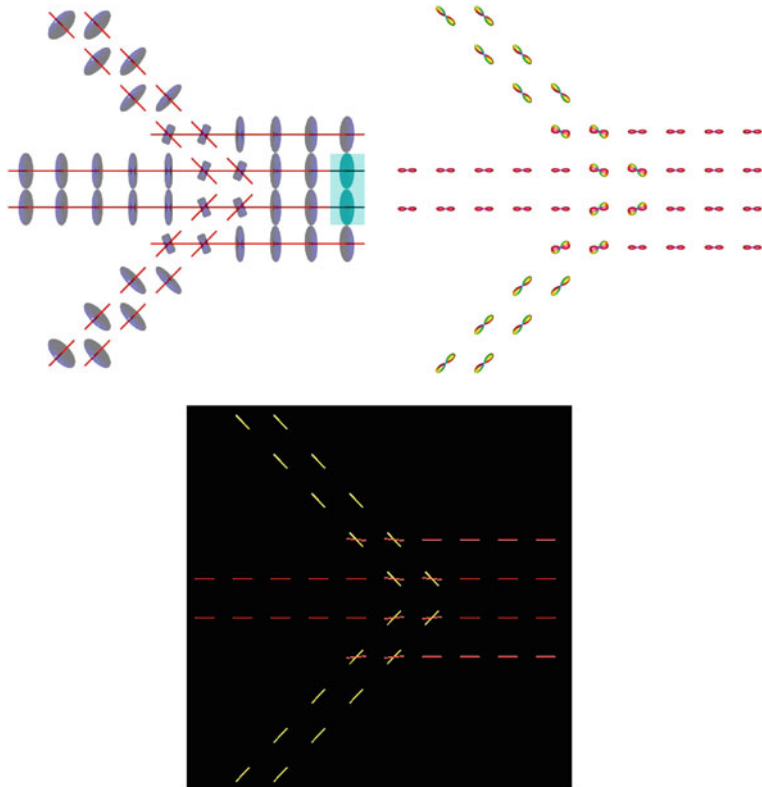
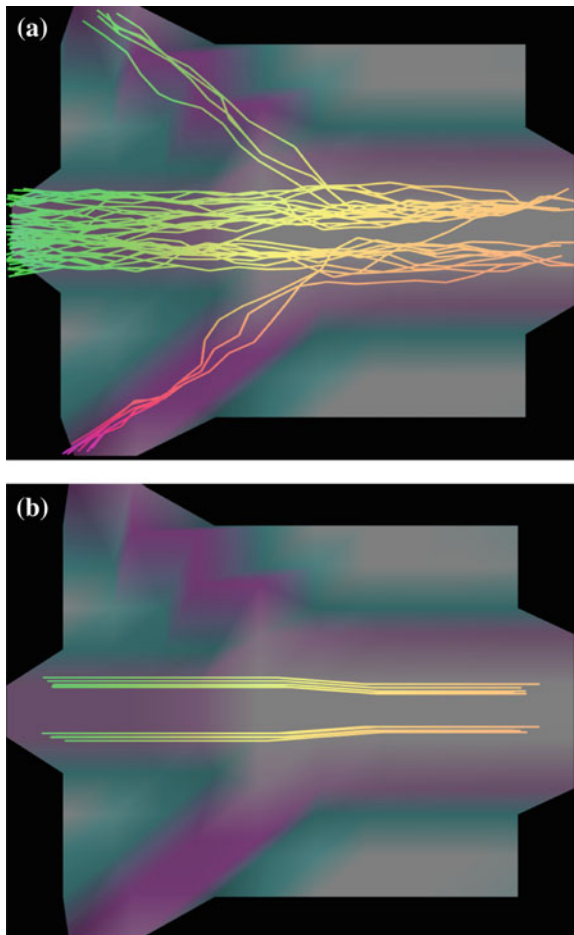


Fig. 1 Simulated diffusion field with seeds marked in *light-blue rectangle* (top left panel), field of reconstructed ODF profiles (top right panel), and field of estimated principal directions (bottom panel)

simulated diffusion field of crossing bundles (top left panel), the field of reconstructed ODF profiles (top right panel), and the field of estimated principal directions (bottom panel).

We specified two voxels as seed voxels (see the top left panel in Fig. 1), and applied the probabilistic SMC algorithm to obtain the tracks represented in Fig. 2a. The SMC algorithm was applied with 100 particles and 5 fibers per seed voxel. For comparison purposes we have also applied a standard deterministic streamline tracking procedure to the same simulation. The streamline procedure follows the tractographic approach outlined in Mori and van Zijl [24] to map fiber tracts. As seen in Fig. 2b, the streamline algorithm is unable to resolve regions of crossing fiber configurations. Typically a single directional path is selected in these regions. In contrast, the probabilistic method is able to map multiple fiber pathways in crossing fiber regions.

Fig. 2 Fiber pathways for the simulated diffusion field illustrated in Fig. 1: **a** Fibers mapped using the proposed probabilistic approach; **b** Fiber mapped using a standard streamline approach



3.2 Human Brain Data Experiments

We report on experiments using a DICOM data set provided by the “Advanced Biomedical MRI Lab, National Taiwan University Hospital”. Specifically, from <http://dsi-studio.labsolver.org/download-images> we obtained the publicly available data set “DSI 203-point 2 mm”. This data set is from a normal 24-year-old male volunteer, and has been provided as a demonstration data set in connection with the “DSI Studio” software for diffusion MR images analysis [6].

The data set was obtained with an echo planar imaging diffusion sequence with twice-refocused echo, dimension $96 \times 96 \times 60$, and slice thickness 1.9 mm. Further details on the data set specification are available from the internet address

mentioned above. We have tested our model with the two *b*-tables that accompanies the data set. One is a *b*-table for a S^2 -like grid denoted by “dsi203_bmax4000.txt”. The other is the *b*-table for the 3D-DSI sampling scheme used in the DICOM data acquisition. This *b*-table has 203 points uniformly distributed on a 3D grid limited to the volume of the unit sphere. In both tables, the *b*-values range from 0 to 4000. The ODF reconstructions were performed with 321 points uniformly distributed on the unit S^2 hemisphere.

As for the simulation procedure outlined in Sect. 3.1, we obtained estimates of the voxels’ ODF profiles using GQI basis functions. To summarize anisotropic properties of the ODF and infer the underlying crossing patterns of the fibers we used the GFA metric. A GFA threshold of 0.3 was applied on the normalized ODFs, prior to vMF clustering estimation. The SMC algorithm was then applied to estimate fiber paths. The following is a summary of tractography results applied to two ROIs. For the first ROI, 43 seeds were placed along the CC region in sagittal view, as illustrated in Fig. 3a. We then applied the clustered-vMFs method followed by SMC to track the fiber paths from each seed by propagating 150 particles, for a maximum of 300 steps. Five starting fibers were randomly placed within each voxel for tracking initiation. All selected principal diffusion directions estimated for the seed voxel were tracked. Figure 3b shows tractography results of the corpus callosum for sagittal slice 48. For comparison purposes, the same ROI and seeds were used to drive a standard deterministic streamline algorithm. Similarly, 5 starting fibers were randomly placed within each voxel for tracking initiation. The results are shown in Fig. 3c.

The second ROI used for testing was the CST, which connects the spinal cord to the cerebral motor cortex. Tractography of the CST is a challenging task. On the one hand, in some regions of the brain other fascicles may cross with the CST. On the other hand, the CST itself is made of several bifurcating sub-fascicles to ensure connections with the whole motor cortex. Unsurprisingly, standard deterministic streamline algorithms fail to map the CST accurately, because they are unable to cope with the complexity of bifurcating pathways. Five seeds used placed on each side of the CST-ROI bundle for coronal slice 53 as illustrated in Fig. 4a. This figure visualizes the location of the chosen seeds, by overlaying the GFA image with the first two main fiber directions at each voxel for coronal slice 53. Figure 4b shows tractography results of the CST for coronal slice 53 using the proposed approach. Figure 4c shows similar tractography results for the deterministic streamline algorithm.

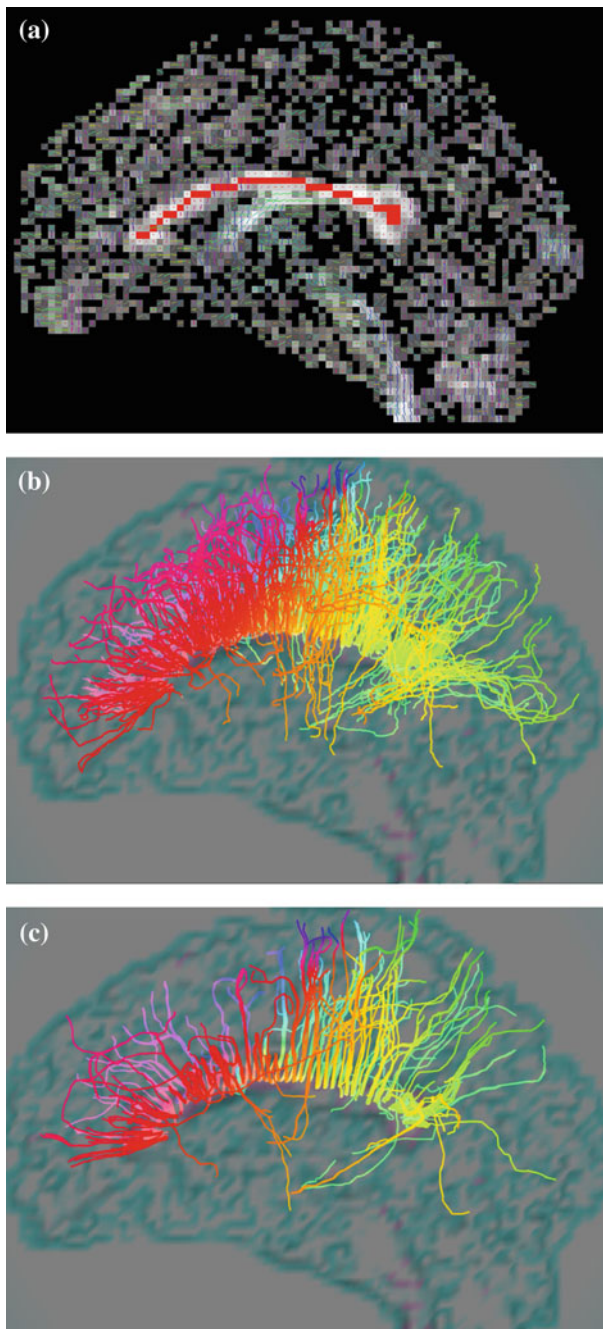
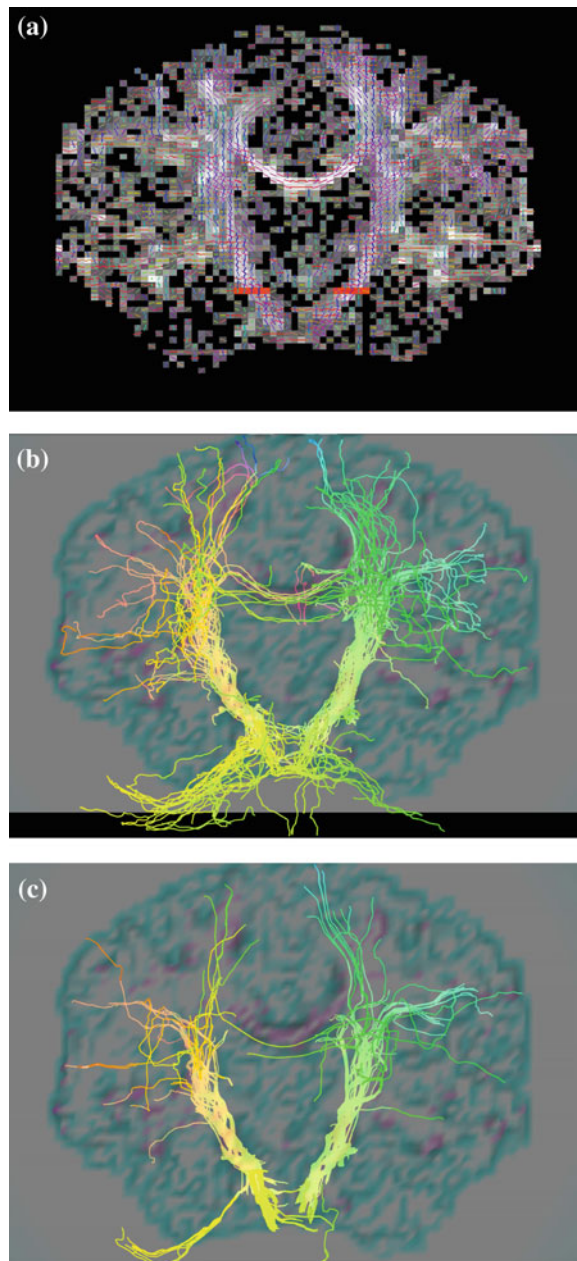


Fig. 3 Corpus callosum tractography: **a** GFA image with seeds' locations in red; **b** Probabilistic tractography using the proposed approach; **c** Tractography using a standard streamline algorithm

Fig. 4 Corticospinal tract tractography: **a** GFA image with seeds' locations in red; **b** Probabilistic tractography using the proposed approach; **c** Tractography using a standard streamline algorithm



4 Implementation and Reproducible Research

The analyses and figures described in this work were performed using software programmed entirely in **R** [25]. The **R**-package **gdimap** [26] implements the reconstruction and clustered vMF estimation methodology described in this work, and is freely available from the CRAN repository (<http://CRAN.R-project.org>). The **R** language programming system has been the platform of choice for many researchers working in the neuroscience and neuroimaging fields [27]. **R** provides a reproducible research environment to many well-developed statistical tools needed for the analysis of neuroimaging data. In particular, the packages “oro.nifti” [28], “movMF” [19], and “rgl” [29], have been used for manipulating and visualizing medical imaging data. The package “oro.nifti” is used for reading and writing NIfTI formatted data sets; “movMF” provides support for fitting and simulating mixtures of von Mises-Fisher distributions; “rgl” is an OpenGL rendering device interface, which provides an interactive viewpoint navigation facility for the **R** programming language.

5 Conclusions

We have presented a methodology to support improved probabilistic tractography in comparison with currently used approaches. The methodology builds statistical inferences at each voxel based on clusters of vMF distributions to drive sequential Monte Carlo path estimates. We have shown how the improvement of fiber directional estimates can benefit the particle filtering tracking process. Moreover, by decoupling the two stages, statistical directional estimation and probabilistic fiber tracking, the proposed methodology is well-suited to support a wide range of methods for ODF reconstruction. The methodology provides a better account of white matter pathways in regions with complex fiber configuration than streamline-oriented approaches. However, comparing results of *in vivo* fiber tracking is a difficult task in general. In the future, we intend to test the proposed methodology for performing human brain connectivity analysis. Connectivity networks may provide alternative validation tools for quantitative comparisons.

References

1. Tuch, D.S., Reese, T.G., Wiegell, M.R., Makris, N., Belliveau, J.W., Wedeen, V.J.: High angular resolution diffusion imaging reveals intravoxel white matter fiber heterogeneity. *Magn. Reson. Med.* **48**, 577–582 (2002)
2. Behrens, T.E.J., Berg, H.J., Jbabdi, S., Rushworth, M.F.S., Woolrich, M.W.: Probabilistic diffusion tractography with multiple fibre orientations: what can we gain? *NeuroImage* **34**, 144–155 (2007)

3. Assaf, Y., Basser, P.J.: Composite hindered and restricted model of diffusion (CHARMED) MR imaging of the human brain. *NeuroImage* **27**, 48–58 (2005)
4. Seunarine, K.K., Alexander, D.C.: Multiple fibres: beyond the diffusion tensor. In: Johansen-Berg, H., Behrens, T.E.J. (eds.) *Diffusion MRI: from quantitative measurement to in vivo neuroanatomy*. Academic Press, Amsterdam (2009) 56–74
5. Wedeen, V.J., Hagmann, P., Tseng, W.Y.I., Reese, T.G., Weisskoff, R.M.: Mapping complex tissue architecture with diffusion spectrum magnetic resonance imaging. *Magn. Reson. Med.* **54**, 1377–1386 (2005)
6. Yeh, F.C., Wedeen, V.J., Tseng, W.Y.I.: Generalized q-sampling imaging. *IEEE Trans. Med. Imaging* **29**, 1626–1635 (2010)
7. Seunarine, K.K., Cook, P.A., Hall, M.G., Embleton, K.V., Parker, G.J.M., Alexander, D.C.: Exploiting peak anisotropy for tracking through complex structures. In: Proceedings of 11th IEEE International Conference on Computer Vision Workshop on MMBIA, Rio de Janeiro (2007)
8. Parker, G., Alexander, D.: Probabilistic Monte Carlo based mapping of cerebral connections utilising whole-brain crossing fiber information. In: Proceedings of IPMI, pp. 684–695 (2003)
9. Tuch, D.S.: Q-ball imaging. *Magn. Reson. Med.* **52**, 1358–1372 (2004)
10. Zhang, F., Hancock, E.R., Goodlett, C., Gerig, G.: Probabilistic white matter fiber tracking using particle filtering and von Mises-Fisher sampling. *Med. Image Anal.* **13**, 5–18 (2009)
11. Pontabry, J., Rousseau, F., Oubel, E., Studholme, C., Koob, M., Dietemann, J.L.: Probabilistic tractography using Q-ball imaging and particle filtering: application to adult and in-utero fetal brain studies. *Med. Image Anal.* **17**, 297–310 (2013)
12. Rowe, M.C., Zhang, H.G., Oxtoby, N., Alexander, D.C.: Beyond crossing fibers: tractography exploiting sub-voxel fibre dispersion and neighbourhood structure. In: IPMI, pp. 402–413 (2013)
13. Doucet, A., Godsill, S., Andrieu, C.: On sequential monte carlo sampling methods for bayesian filtering. *Stat. Comput.* **10**, 197–208 (2000)
14. Doucet, A., Johansen, A.M.: A tutorial on particle filtering and smoothing: fifteen years later. In: Crisan, D., Rozovsky, B. (eds.) *The Oxford Handbook of Nonlinear Filtering*. Oxford University Press, Oxford (2011)
15. Liu, J.S.: *Monte Carlo Strategies in Scientific Computing*. Springer Series in Statistics. Springer, New York (2001)
16. Alexander, A.L., Hasan, K.M., Lazar, M., Tsuruda, J.S., Parker, D.L.: Analysis of partial volume effects in diffusion-tensor MRI. *Magn. Reson. Med.* **45**, 770–780 (2001)
17. Mardia, K.V., Jupp, P.: *Directional Statistics*, 2nd edn. Wiley, New York (2000)
18. Banerjee, A., Dhillon, I.S., Ghosh, J., Sra, S.: Clustering on the unit hypersphere using von Mises-Fisher distributions. *J. Mach. Learn. Res.* **6**, 1345–1382 (2005)
19. Hornik, K., Grün, B.: Mixtures of von Mises Fisher Distributions. R package version 0.1-0 (2012)
20. Schwartz, G.: Estimating the dimension of a model. *Ann. Stat.* **6**, 461–464 (1979)
21. Rathi, Y., Michailovich, O., Shenton, M.E., Bouix, S.: Directional functions for orientation distribution estimation. *Med. Image Anal.* **13**, 433–444 (2009)
22. Ferreira da Silva, A.: Facing the challenge of estimating human brain white matter pathways. In: Madani, K., Kacprzyk, J., Filipe, J. (eds.) *Proceedings of the 4th International Joint Conference on Computational Intelligence*, SciTePress, pp. 709–714 (2012)
23. Ferreira da Silva, A.: Computational representation of white matter fiber orientations. *Int. J. Biomed. Imaging Article ID* 232143
24. Mori, S., van Zijl, P.C.M.: Fiber tracking: principles and strategies—a technical review. *NMR Biomed.* **15**, 468–480 (2002)
25. R Development Core Team: R: A Language and Environment for Statistical Computing. R Foundation for Statistical Computing, Vienna, Austria. (2010)
26. Ferreira da Silva, A.: gdimap: Generalized Diffusion Magnetic Resonance Imaging. R package version 0.1-1 (2012)

27. Whitcher, B.: CRAN Task View: Medical Image Analysis. Version 2012-03-30 (2012)
28. Whitcher, B., Schmid, V.J., Thornton, A.: Working with the DICOM and NIFTI Data Standards in R. *J. Stat. Softw.* **44** (2011)
29. Adler, D., Murdoch, D.: rgl: 3D Visualization Device System (OpenGL). R package version 0.92.879 (2010)

Post-stroke Robotic Upper-Limb Telerehabilitation Using Serious Games to Increase Patient Motivation: First Results from ArmAssist System Clinical Trial

**Cristina Rodríguez-de-Pablo, Maša Popović, Andrej Savić,
Joel C. Perry, Aitor Beloso, Tijana Dimkić Tomić and Thierry Keller**

Abstract Research findings indicate that intensive therapy is essential for achieving better outcome in post-stroke rehabilitation. However, with the increasing number of stroke patients and limited healthcare resources, it is difficult to provide the needed amount of therapy. Robot-assisted rehabilitation based on serious games

C. Rodríguez-de-Pablo (✉) · A. Beloso · T. Keller
Rehabilitation Technologies Health Division, TECNALIA, San Sebastian, Spain
e-mail: cristina.rodriguez@tecnalia.com

A. Beloso
e-mail: aitor.beloso@tecnalia.com

T. Keller
e-mail: thierry.keller@tecnalia.com

M. Popović
Laboratory for Experimental Psychology, Faculty of Philosophy,
University of Belgrade, Belgrade, Serbia
e-mail: beumas@yahoo.com

A. Savić
Tecnalia Serbia Ltd, Belgrade, Serbia
e-mail: andrej.savic@tecnalia.com

A. Savić
Signals and Systems Department, School of Electrical Engineering,
University of Belgrade, Belgrade, Serbia

J.C. Perry
Mechanical Engineering Department, University of Idaho, Moscow, ID, USA
e-mail: jperry@uidaho.edu

T.D. Tomić
Clinic for Rehabilitation Dr Miroslav Zotović, Belgrade, Serbia
e-mail: tijanatomic1985@gmail.com

T.D. Tomić
School of Medicine, University of Belgrade, Belgrade, Serbia

may offer the solution for providing a more autonomous and scalable training that can be transferred out of the clinic and into home environments. Robots offer precision and repeatability of movements that can be used to provide safe and intensive rehabilitation exercises, both at home and in the clinic. Serious games can provide an enjoyable and effective way to motivate patients to increase both the quality and quantity of therapy. In addition, these technologies can also be used to remotely assess the motor performance of patients and the therapy progress. The ArmAssist is a recent example of a low-cost robotic system designed specifically for post-stroke upper-limb telerehabilitation. The system incorporates a set of serious games for assessment and training, further described in this paper. Preliminary results from the ongoing clinical study reveal very positive responses from 10 patients and 2 therapists about the usability and integration of the system in the clinical setting. Training with this system is shown to be beneficial and enjoyable, and highly motivates patients to continue and endure longer durations of training. More data and analysis is required to extract further conclusions.

Keywords Serious games • Upper-limb rehabilitation • Robotic rehabilitation • Quantitative assessment • Reach training • Motivation • Stroke • Home-based telerehabilitation

1 Introduction

Research confirms that better results in terms of rehabilitation outcome are obtained in specialized care centers where patients receive more therapy per day and with more quality for extended periods of time [1, 2].

However, the amount of professionally-supported rehabilitation training provided to the average patient is still far from the ideal. A Dutch report published in 2008, reported that the average treatment time for stroke patients in skilled nursing facilities was about 4.5 h per week, and only about 2 of them was spent in physical therapy [3].

Healthcare resources are suffering from constant cutbacks due to economic constraints and the prevalence of stroke continues to increase dramatically together with the aging of the population. As a matter of fact, European statistics as a whole report that nearly 1 million people experience a first or recurrent stroke each year [4]. In that context, the amount of intensive therapy required cannot be provided in the regular way that rehabilitation training has been provided up to now. There is a need for more autonomous and scalable training that can be transferred out of the clinic. Robot-assisted rehabilitation based on serious games may offer that training.

Robots offer precision and repeatability of movements that can be used to provide safe and intensive rehabilitation exercises. Serious games can provide an enjoyable and effective way to motivate patients to increase both the quality and quantity of therapy by decreasing the monotony of performing hundreds of repeated motions and by providing challenging performance feedback. In addition, these

technologies can also be used to remotely assess the motor impairment of patients without the need for the therapist to be present.

The introduction of gaming to rehabilitation is based on research findings that indicate patient motivation as highly important for therapeutic outcome [5]. Patient cooperation and satisfaction with a given treatment is essential in achieving successful rehabilitation results [6]. Gaming is renowned for its ability to provoke high levels of engagement and hold attention for long periods of time; thus, the incorporation of gaming into stroke rehabilitation treatments has been widely accepted in the past years. There is evidence that the use of gaming may be beneficial in motor function improvement when compared with conventional therapy [7–9]. A recent study investigating effects of gaming in rehabilitation shows higher improvement in some areas of upper extremity motor function, increased patient motivation and prolonged endurance in exercising, compared to a non-gaming treatment of the same intensity [10, 11].

Several commercial games, which combine entertainment with exercise, have been developed and the use of such games has shown superior results in some cases in comparison to other types of recreational therapy [7]. However, research has indicated that most people with motor function problems may have difficulty playing commercial games out-of-the-box [12]. This raises the prospect of games being designed specifically for rehabilitation.

Therefore, a large increase in robotic rehabilitation based on serious games has been seen over the last years [13, 14]. Recent commercial players in the field include Hocoma, Tyromotion, HomeTelemed, MediTouch, YouRehab, NeuroAtHome and Virtualware.

However, even with the number of strong commercial players getting involved, current success is still rather limited. The solution may lie in the development of a system that can be easily integrated with current practice and which can verify its effectiveness correlating the results of both assessment and training tools with the assessment scales and physical therapy performed at the clinic.

Towards this end, this paper presents a new version of 5 games for assessment and 5 games for training of post-stroke arms used in conjunction with the ArmAssist rehabilitation device and the TeleReha web platform for at-home telerehabilitation. The ArmAssist allows planar movement of the arm by supporting the arm against gravity while measuring the movement parameters (2D position, orientation and arm support/lifting force) that are used to control the games. The TeleReha platform allows the patient to perform game-based rehabilitation both at the clinic and at home, while the doctor is able to monitor the progress, update the therapy correspondingly, and communicate with the patient when necessary. The other system components and functionalities have been previously described in publications [15–17]. The assessment games are specifically designed to not only measure the effectiveness of the training, but also to compare the assessment results with the standard clinical assessment scales. The training games include cognitive components and are designed to motivate the patient to train for long periods of

time. Previous versions of the system have been improved based on feedback from usability testing. The final design is currently being used in a clinical study and preliminary results about usability and patient motivation are presented.

2 Games

2.1 Design Process

A first set of requirements for the games was defined after a comprehensive review of the key elements that promote the rehabilitation process and the role of gaming in robot-aided rehabilitation therapy was performed [18]. A more detailed list of requirements and games to be developed was drawn out, integrating this preliminary information with a series of interviews and focus groups with clinicians.

Then, an iterative approach was used for the game design and implementation, meaning that the games were tested by patients and therapists all along the implementation process.

Throughout the game design and implementation process, game design principles and ergonomic and user interface design standards were closely observed. Design criteria considered included aspects such as clarity of instructions and feedback, optimization of the level of challenge in order to keep patient motivation, consistency between games, suitability toward visual or cognitive impairments, and robustness, i.e., tolerance to user error. A detailed description of the methods used for the design was already presented in [19].

A first version of the games was implemented and tested in a 12-week clinical pilot test with 9 patients. This usability testing and its results were further described in [20]. Then, a second version of the games was developed in order to first, include the usability feedback obtained in previous testing and second, improve the assessment methodology in order to be able to properly evaluate the effectiveness of the system and compare the results of that assessment with the standard scales used at the clinic. Finally, a shorter usability testing of the new version of the software was carried out in the Rehabilitation Service at ‘Hospital Universitario de Álava- Sede Txagorritxu’ (Spain). The feedback extracted from that testing was used for the design of the final version of the software, which is currently being used in an ongoing clinical study.

2.2 Requirements

In this section, the requirements for the redesign of the games are presented. A detailed list of the initial requirements of the games was already presented in [19].

After an initial *Force Calibration*, assessment games are composed of short evaluation of *Range of Movement*, *Range of Force*, *Control of Movement*, and *Control of Force*. Training games include *Words*, *Point to Point*, *Memory*, *Jigsaw Puzzle* and *Solitaire* games. A detailed description of the games can be found in Sect. 2.3.

The main goal of the redesign was to improve the games in order to be able to properly evaluate the effectiveness of the system and compare the assessment results with the standard scales used at the clinic. For that, first of all, levels in the assessment games needed to be removed in order to facilitate intra- and inter-patient comparison. Game levels had to be kept, however, for the training games in order to adapt the challenge, motivate the patient and avoid frustration. Also, it was necessary to make some of the games simpler and faster; for example different versions of the *Control of Force* assessment game were developed and later determined to be too time consuming and cognitively taxing for a rapid assessment. Others needed a redesign in order to avoid undesired movements; therefore, a new version of the *Control of Movement* game asks only for reach movements, and the new *Range of Movement* game measures only when the user stops in order to avoid counting ballistic movements. It was observed to be of major importance the fact that the score was perfectly aligned with the metric being evaluated, as that is what the patients focused on when trying to improve. In that way, the reaching movement requirements have been removed from the new *Control of Force* in order to focus on the control of the lifting force and its smoothness evaluation. And lastly, some improvements were needed in the data collection to address some issues detected in the post-processing work of data from the previous games.

In addition, most of the feedback obtained in the usability testing was taken into account for the redesign. Some examples of the changes included are:

- The improvement of the selection/deselection strategies, with an optimization of the timing in the waiting strategy and a refinement of the feedback in the lifting force strategy (see Sect. 2.3, for more details on the selection strategies);
- The improvement of feedback, e.g., in the *Point to Point* game when a piece is inserted; this was not always properly understood by patients and they kept trying to insert it;
- The clarification of some instructions, e.g., providing a hint in the *Words* game or allocating a concrete space where the *Jigsaw Puzzle* has to be assembled;
- The improvement of the visualization, e.g., making the back image of the cards in the *Memory* game unmistakable with the content itself;
- The empirical adjustment of the time-outs and level parameters.

2.3 *Description of Games*

2.3.1 General Features

There exist two kinds of games. The assessment games are short tasks (1–2 min) designed to provide the therapist with an objective evaluation of the different parameters that define the arm movement and to adjust the training games correspondingly. The training games are longer, more complex and entertaining tasks, which can also integrate cognitive components and whose objective is to motivate

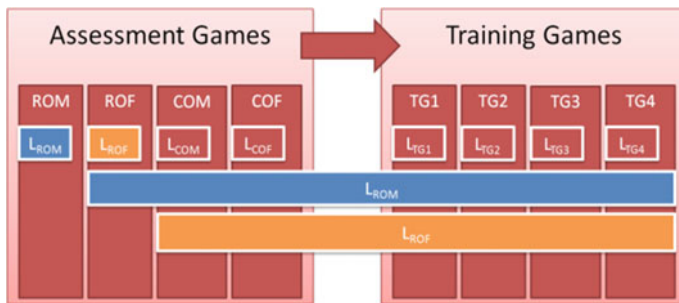


Fig. 1 Influence of the result obtained at ROM and ROF in the other games

the patient to train harder and longer. In both of them, reach extension movements are encouraged, which require simultaneous abduction/adduction of the shoulder and extension of the elbow.

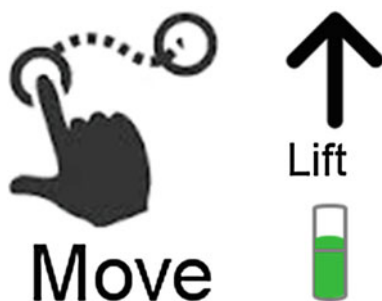
In all the games (Fig. 1) the level is composed of two aspects: the Movement level (ROM) and the Force Level (ROF). The ROM, the range of movement that each game requires, is determined by the performance of the patient in the first assessment game, *Range of Movement*. For accessibility reasons, the visualization of the games is always the same, that is, the objects keep their sizes and their positions; however, the area of the mat where the ArmAssist has to be moved varies according to the range of motion of the patient. This avoids some visualization problems when the range is too small and has proven to be well understood by patients. The ROF is the range of vertical force required by each game, i.e. the percentage of the arm weight that the patient must lift. This is determined by the performance of the patient at the second assessment game, *Range of Force*.

Furthermore, in the training games a task level component is included. This is avoided in the assessment games in order to facilitate the intra- and inter-patient comparison of the evaluation results. Each game presents five levels and is scored based on a combination of evaluated features. The game levels are automatically adapted by the platform based on performance. The adaptation method adopted is the following: a game score of 100 % or two consecutive scores of at least 80 % prompt a level increase. Still, if considered inadequate, the level can be modified by the therapist from within the platform at any time.

Each time that a game starts, the user will be asked to move the device slowly over the mat in order to calibrate the device position. This will not take more than 2 s. Also, before playing any game, the user is asked to calibrate the weight of his arm in a relaxed state in order to calibrate the vertical force component of the device. This second calibration needs to be done only once; however, it can be repeated when desired for changes in the position of the table or chair that may affect the weight of the arm.

There are two strategies for selection/deselection of objects in the training games. ArmAssist's natural strategy is the use of the vertical force, that is, to lift the arm to pick up a piece, and move and relax the arm to leave it. However, for some

Fig. 2 Indications for the two selection strategies



patients this strategy has proven to be more difficult to understand or to control in the early stages of rehabilitation. Therefore, another strategy is provided which does not require the use of the vertical force, requiring instead a brief pause over the piece to select it. The piece will be deselected when the patient pauses after having moved it. Moreover, in order to avoid unwanted selections, to reactivate the selection of a part, the user must bring the cursor outside of the part in question and then place it back over the part again. Proper timing is the key for this strategy to work properly. When the therapist deems appropriate, he will enable the use of force in the patient's profile. In both cases, the strategy that should be used to pick or drop an object is indicated by a message and icon at the top of the screen (Fig. 2). In order to facilitate the comprehension of the vertical force selection strategy, the feedback force is also displayed, indicated in green when the required threshold lifting force is being performed, and in red when not.

Strict overall times and intermediate countdowns in the case of inactivity are employed in all the assessment games to ensure that assessments are carried out efficiently. The intermediate countdowns ensure, for example, that the cursor is placed at the required area or that the achieved value is improved in a determined amount of time. In the training games, the total time can be assigned by the therapist. In the games in which the time is associated with the task level, the game will be launched successively as many times as necessary to complete the total time assigned. A 'direct exit' has been enabled in case the user or therapist wants to finish a game before the assigned training time; this can be done by pressing the center bar of the device with both hands. However, when exited in this way, no data is stored, nor the level updated, etc. thus, it should not be used as a normal course of action.

General performance indicators are stored for all the games in each session, with 100 being the maximum score for all the games. During the assessment games, full force and trajectory information is also stored in order to allow a detailed post-processing analysis. The data collection has been improved in order to solve some problems found in previous data analyses. The sampling frequency has been increased from 10 to 100 Hz and descriptive data of every sequence of the game is collected. In addition, data is split in blocks, each block corresponding to analog groups of movements, e.g., extension and flexion; for each of them the target position and force, events, times, and performance are stored.

2.3.2 Assessment Games

The *Force Calibration* game (Fig. 3a) serves to weigh the patient's arm in a relaxed position and thereby calibrate the vertical force characteristic of the device. Therefore, it should be performed before any other game. Moreover, without any limitation of time, it helps the patient to have an initial contact with the vertical force characteristic of the device, which generally causes some confusion for the patients at first. In this way, the patient can try as much as needed to use this feature and see the feedback result of his actions on the screen. When the patient understands this concept and is prepared, correct posture of the torso and the relaxation of the arm must be checked and then the calibration can be started. This arm weight calibration needs to be done only once; however, it can be repeated at any time.

The *Range of Movement* game (Fig. 3b) evaluates the range of extension movements from a central position towards the different directions of the transverse plane. This game, being the one that defines the ROM required by all the rest of the games, should always be the first game played; or just after the *Force Calibration* game in the case that the force calibration was not previously performed. In the game, different sectors in a semicircle have to be deleted with a reach extension movement of the arm from the central ball to the furthest point reached in that direction as indicated by a white arrow. The patient needs to stop at the furthest point reached in order for the result for that sector to be saved, thereby avoiding the acceptance of ballistic movements. Then he must return to the centre ball and start again with another sector. In order to improve the user feedback, there are two ways in which sectors are visually erased (Fig. 3b): instantaneously as the cursor passes (in light green), which gives real-time feedback to the user; and once they stop

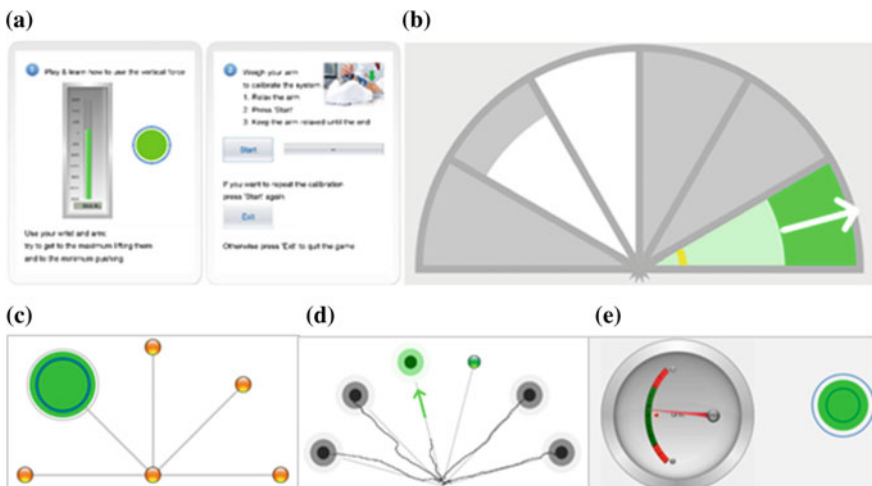


Fig. 3 Assessment games: **a** Force Calibration. **b** Range of Movement. **c** Range of Force. **d** Control of Movement. **e** Control of Force

(in white), when the score is really saved, and that part of the sector is deleted permanently. The patient must ensure that he remains upright during the game. The game detects if the patient leans over the table in order to achieve a greater range of movement; in that case, the game is interrupted until he corrects the posture. The score for each sector is the percentage of the maximum range that the patient is able to reach, being the maximum defined for a healthy patient. The final score is the average of the values for all the sectors.

The *Range of Force* game (Fig. 3c) assesses the arm support/lifting capacity in different positions of the plane by placing the cursor over a circular target and lifting the arm. As the arm is unloaded from the device, the size of the target is increased in proportion to the lifting force in order to reach the diameter of a peripheral ring, which indicates the target unloading level. This game, being the one that defines the ROF required by the rest of the games, should always be the second game played, after the *Range of Movement* game. The points are located at half of the ROM achieved for each of the sectors described in the *Range of Movement* game. For each of them, the score is the percentage of the maximum lift force, the maximum being the complete lift of the patient's arm. The final score is the average of the values for all the points.

The *Control of Movement* game (Fig. 3d) evaluates the patient's motion control when he has to follow a path from one point to another and stop in a very restricted time. For that, the user must first, move the cursor to the centre ball; second, to the target that is blinking and stop in the centre as quickly as possible. Then, he/she must go back to the centre and start the task over moving to the new ball that blinks. As in the *Range of Movement* game, the patient must ensure that he remains upright during the game; otherwise, the game will be interrupted until he corrects the posture. The location of the target points is the same as for the *Range of Force* game. For each of them, the score is based on how close to the centre of the target the user is able to stop in that short amount of time, and the final score is the average of all the values.

The *Control of Force* game (Fig. 3e) evaluates the patient's ability to control the level of vertical force, that is, the ability to lift and hold the arm position against gravity. Keeping the arm in a centered position on the mat, the patient must lift the arm slightly trying to keep the needle in the middle of the dial, always in the green area. This area will become narrower, and therefore will require a greater control of the arm position as the time passes. The patient should keep this position until the progress bar completes. The goal value is based on the ROF evaluated in the *Range of Force* game. The final score reflects the percentage of time that the user is able to keep the arm in between the ranges defined. In all these games, inactivity countdowns that ensure the brevity of the assessment may affect the scores; e.g., in the *Range of Movement* game, if the maximum range achieved in a sector is not increased in a certain amount of time, that sector is considered evaluated and the next one will start.

2.3.3 Training Games

These games aim to train the reach extension movements of the arm in an enjoyable way, generally having to pick objects and move them to different positions of the plane. To accomplish this, the user has to first, place the cursor over the corresponding object and stop briefly, or lift the arm in the case that the vertical force component is being used, which will be indicated; second, move it to the corresponding position; and third, stop briefly again or rest the arm in the previously mentioned case. Each game presents five levels and is scored based on a combination of evaluated features, generally reflecting the percentage of the game completed (e.g., percentage of elements inserted, percentage of puzzle completed, etc.). Time available is also adjusted according to the level in each case.

In the *Words* game (Fig. 4a), the missing letters in the words have to be completed with the spare letters at the bottom of the screen. The letter will go back to its initial position if it is introduced into the wrong space or is released, that is, if the user stops for 1 s after moving the piece or rests the arm. As the level increases, the number of missing letters to be filled in each word, the difficulty of the word, and the difficulty of the task also increase. Task difficulty, for example, increases by having to fill in vowels or consonants and the accuracy needed for a letter to be considered selected or introduced. In the *Point to Point* game (Fig. 4d), each object has to be placed in its box. The levels are defined by the number of elements to be introduced and the accuracy needed for an object to be considered selected or introduced. For the *Memory* game (Fig. 4c) the user has to discover pairs of matching cards, remembering the ones previously discovered by the user or the

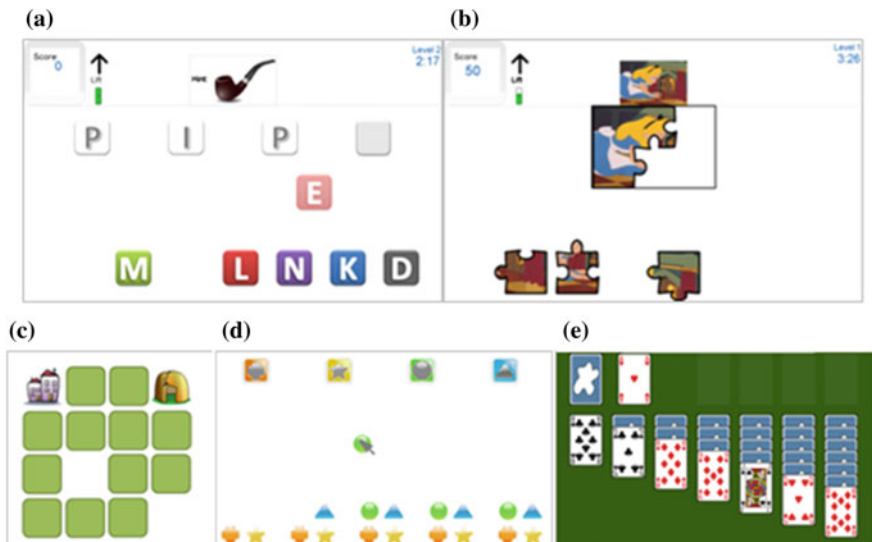


Fig. 4 Training games: **a** Words. **b** Jigsaw Puzzle. **c** Memory. **d** Point to Point. **e** Solitaire

opponent (the PC). The number of pairs and the intelligence of the PC define the levels. The users can also train by putting together a *Jigsaw Puzzle* (Fig. 4b) whose number and size of pieces increase with the levels. As a fifth training game, the user can play the typical *Solitaire* game (Fig. 4e) with different numbers of cards dealt and times to complete the task.

3 Testing

Currently, a clinical study is being conducted in the Clinic for Rehabilitation ‘Dr Miroslav Zotović’ in Belgrade, Serbia. The main purpose of this study is to determine the effectiveness of the training and the correlation between ArmAssist assessment results and standard clinical assessment scales. This study is also aimed at further investigation of usability and integration of the system in the clinical setting, as well as exploration of full patient experience and motivation in training with the ArmAssist.

Patients included in this study are 40–70-year-old stroke survivors in the sub-acute phase with unilateral paresis, able to understand simple instructions, and who have some voluntary movements in elbow and shoulder joints. The program lasts 4 weeks, where the first week is intended for patient’s familiarization with the system and the next 3 weeks for ArmAssist-based therapy, during which patients have at least 1 h of conventional therapy and at least 30 min of additional therapy per day, 5 days per week. The study consists of three groups—(1) Experimental group; (2) First control group; and (3) Second control group. The difference between the three groups is in terms of the additional therapy they receive, which consists of training with ArmAssist for the experimental group, conventional therapy for the first control group and properly matched work therapy, i.e. planar reaching movements, for the second control group. Each group comprises 15 patients; however, for the time being, only 10 patients of the experimental group and 6 of the first control could be included for this study.

All patients will be assessed at the beginning and the end of the program. The Fugl-Meyer Assessment, the Action Research Arm Test, the Barthel index, the Modified Rankin scale, the Beck depression scale, the Wolf Motor Function test and the Modified Drawing Test are among the measurements used [21–27].

In addition, an experimental psychologist interviews patients at the end of the program. Two questionnaires are administered to the ArmAssist group patients, and additional questions are discussed in order to fully evaluate patient experience with the system. The ArmAssist usability evaluation questionnaire, consisting of 15 items for patients and 18 for therapists, is administered to evaluate ease of use, comfort, pain, fatigue, enjoyment, benefits, desire to continue using the system, possible difficulties and recommendations for improvement [28]. The Intrinsic motivation inventory (IMI) is used to evaluate patient motivation for the received treatment [29]. The IMI assesses participants’ interest/enjoyment, perceived competence, effort, value/usefulness, felt pressure and tension, and perceived choice

while performing a given activity, thus yielding six subscale scores. Following the instructions,¹ and based on our previous work, we have constructed our own IMI questionnaire consisting of 20 items relevant for this study [10, 30].

4 Results

Preliminary results from the ongoing clinical study reveal very positive responses from patients and therapists about the usability and acceptance of the ArmAssist. The system clearly integrates well in the clinical setting. Analysis of answers obtained from ten patients and two therapists on the ArmAssist usability evaluation questionnaire indicates that it is easy to learn how to use the system (hardware and software) and easy to remember how to use the system effectively each time they work with it. While therapists are familiar with this kind of technology, patients usually are not, but still had no problems in using the system. Both patients and therapists feel that the system motivates patients to train longer, which is beneficial in patient recovery, and they would highly recommend it to other people for training.

Therapists feel that the system is enjoyable for patients and that the selected games are adequate for training. They find the outcome results of the training to be sufficient and clearly presented.

Most patients were very excited to train with the ArmAssist. They especially enjoyed the combination of using cognition and arm movements while training. Different patients showed preference for different games. However, as earlier revealed in the usability testing, patients expressed preference for a larger variety of games as they got bored after a certain period. Some patients also expressed a need for higher levels of challenge as they found the games to be too easy. For that reason, new games are being developed. These games will be designed to be more challenging and to keep the patient motivated for longer periods of time.

The knowledge of performance clearly motivated the patients to continue the training and to improve in every session. For that reason, as already observed in the initial usability testing, in order to avoid frustration, the difference between assessment and training games must be clear for the patients; the significant difference being that the maximum values for the first ones are defined by healthy patients and are not adapted to their capacity as in the case of the second ones. Further observation of the training sessions revealed that it might be necessary to visibly hide the performance scores in the assessment games and keep them only in the training games. During assessment, patients often tried making compensatory body movements in order to achieve the maximum score. This way, an error in assessment can be made and carried on to the training games. In order for this to be

¹<http://www.selfdeterminationtheory.org/>.

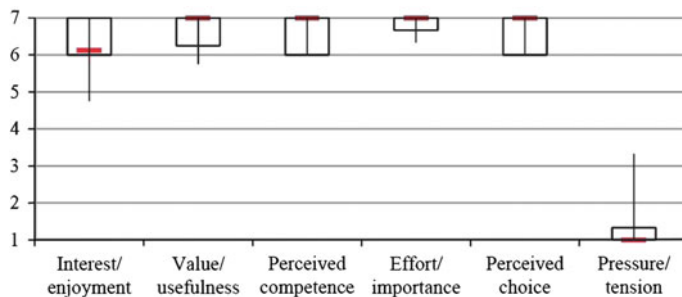


Fig. 5 Box and whiskers diagram of IMI subscale scores. The score range is from 1 (lowest score) to 7 (highest score)

avoided, the performance scores should not be shown to patients during assessment. Instead, qualitative feedback could be shown in order to improve motivation.

Other recommendations for improvement include adjustments of game display on the screen for visually impaired patients. This has already been incorporated in the design but needs further improvement in order for visually-impaired patients to be able to effectively use the system. The seating arrangement during training also needs to be adapted to various body constitutions for better comfort.

Analysis of answers obtained with the IMI questionnaire from patients reveals very high patient motivation in using the ArmAssist. The IMI subscale scores (6) for ten patients are presented in the form of a box-and-whisker diagram, depicting inter-quartile ranges (Fig. 5). Red lines denote medians, while the bottoms and tops of the boxes denote the 1st and 3rd quartile, respectively.

Eight out of ten patients have very high scores (6 and higher) on the interest/enjoyment subscale (with median score for all patients being 6.1 and IQR 1, on a scale from 1 to 7). Only one patient has a score lower than 5 on this subscale. The interest/enjoyment subscale is considered the self-report measure of intrinsic motivation and is the only subscale that assesses intrinsic motivation, per se [31]. The results obtained in this study suggest that the patients enjoyed exercising with the ArmAssist and experienced the games as very interesting.

Very high patient scores (with median 7 and IQR 0.75) on the value/usefulness subscale contribute to higher patient motivation during the rehabilitation treatment. The idea behind the value/usefulness concept is that people internalize and become self-regulating with respect to activities that they experience as useful or valuable for themselves [29]. These results suggest that patients experienced exercising with the ArmAssist as useful and valuable for the recovery of motor function of upper extremities and many of them have expressed great satisfaction in the level of recovery.

All ten patients have very high scores (6 and higher) on the perceived competence subscale (with median 7 and IQR 1). This contributes to the positive aspect of exercising with the ArmAssist. The perceived competence concept is theorized to be a positive predictor of both self-reported and behavioral measures of intrinsic

motivation [31]. Patient awareness of their own ability to perform the task and awareness of performance improvement during the rehabilitation period are very important, and overall contribute to patient interest in continuing treatment.

Very high scores (with median 7 and IQR 0.33) on the effort/importance subscale contribute to higher patient motivation as well. These results suggest that patients have put a lot of effort and energy into performing these exercises well because they experienced exercising with the ArmAssist as important for their recovery.

Very high scores (with median 7 and IQR 1) are observed on the perceived choice subscale. Perceived choice is theorized to also be a positive predictor of both self-report and behavioral measures of intrinsic motivation. The results obtained in this study may suggest that patients are enjoying the gaming aspect of exercising with the system, and not experiencing this additional exercise as an obligation that should be fulfilled as part of the entire rehabilitation program.

Low scores (with median 1 and IQR 0.33) on the felt pressure/tension subscale, which are obtained in this study, are favorable. The pressure/tension concept is theorized to be a negative predictor of intrinsic motivation, thus, low scores on this subscale show that most participants were at ease while performing the exercises [29]. Even patients who reported having pain during exercising did not feel tense or anxious, and were motivated to continue training.

5 Conclusions

A new version of assessment and training games has been developed for at-home post-stroke arm rehabilitation. The aim was to include feedback gathered in previous usability testing and to improve the assessment methodology in order to be able in the future not only to measure the effectiveness of the system, but also to compare the assessment results with the standard assessment scales currently used in clinical settings. Preliminary results from an ongoing clinical study reveal very positive responses from patients and therapists about the usability and integration of the system in the clinical setting. Training with this system is shown to be beneficial and enjoyable, and highly motivates patients to continue and endure longer durations of training. Future work comprises the further analysis of data obtained from the ongoing clinical study, the corresponding redesign of games according to the results obtained, and the development of new training games.

Acknowledgments The authors would like to thank the Rehabilitation Service at the ‘Hospital Universitario de Álava- Sede Txagorritxu’ for their contributions to the design of the games; the “Clinic for Rehabilitation Dr Miroslav Zotović” for their contribution to these results, and H. Zabaleta, D. Valencia and J. Arcas for their contributions to the whole system.

References

1. Sluijs, E.M., Kok, G.J., van der Zee, J.: Correlates of exercise compliance in physical therapy. *Phys. Ther.* **73**(11), 771–782 (1993)
2. Kwakkel, G., Wagenaar, R.C., Koelman, T.W., Lankhorst, G.J., Koetsier, J.C.: Effects of intensity of rehabilitation after stroke a research synthesis. *Stroke* **28**(8), 1550–1556 (1997)
3. Peerenboom, P., Spek, J., Zekveld, I., Cools, H., van Balen, R., Hoogenboom, M.: Revalidatie in de AWBZ, omvang, aard en intensiteit. Etc Tangram en LUMC/PHEG Verpleeghuisgeneeskunde 31 (2008)
4. Hesse, S., Werner, C., Pohl, M., Rueckriem, S., Mehrholz, J., Lingnau, M.: Computerized arm training improves the motor control of the severely affected arm after stroke a single-blinded randomized trial in two centers. *Stroke* **36**(9), 1960–1966 (2005)
5. Maclean, N., Pound, P.: A critical review of the concept of patient motivation in the literature on physical rehabilitation. *Soc. Sci. Med.* **50**(4), 495–506 (2000)
6. Chen, C.Y., Neufeld, P.S., Feely, C.A., Skinner, C.S.: Factors influencing compliance with home exercise programs among patients with upper-extremity impairment. *Am. J. Occup. Ther.* **53**(2), 171–180 (1999)
7. Saposnik, G., Teasell, R., Mamdani, M., Hall, J., McIlroy, W., Cheung, D., Thorpe, K.E., Cohen, L.G., Bayley, M.: Effectiveness of virtual reality using Wii gaming technology in stroke rehabilitation a pilot randomized clinical trial and proof of principle. *Stroke* **41**(7), 1477–1484 (2010)
8. Housman, S.J., Scott, K.M., Reinkensmeyer, D.J.: A randomized controlled trial of gravity-supported, computer-enhanced arm exercise for individuals with severe hemiparesis. *Neurorehabil. Neural Repair* **23**(5), 505–514 (2009)
9. Piron, L., Turolla, A., Agostini, M., Zucconi, C., Cortese, F., Zampolini, M., Zannini, M., Dam, M., Ventura, L., Battauz, M.: Exercises for paretic upper limb after stroke: a combined virtual-reality and telemedicine approach. *J. Rehabil. Med.* **41**(12), 1016–1020 (2009)
10. Popović, M.D., Kostić, M.D., Rodić, S.Z., Konstantinović, L.M.: Feedback-mediated upper extremities exercise: increasing patient motivation in poststroke rehabilitation. *BioMed. Res. Int.* **2014**, 11 (2014)
11. Kostić M., Popović M., Popović D. (2014) The robot that learns from the therapist how to assist stroke patients. In: New Trends in Medical and Service Robots. Springer, New York, pp. 17–29
12. Rand D., Kizony R., Weiss P.: Virtual reality rehabilitation for all: Vivid GX versus Sony PlayStation II EyeToy. In: 5th International Conference on Disability, Virtual Environments and Associated Technologies, pp. 87–94 (2004)
13. Robertson, J.V., Roby-Brami, A.: Augmented feedback, virtual reality and robotics for designing new rehabilitation methods. In: Rethinking Physical and Rehabilitation Medicine. Springer, New York, pp. 223–245 (2010)
14. Brewer, B., McDowell, S., Worthen-Chaudhari, L.: Poststroke upper extremity rehabilitation: a review of robotic systems and clinical results. *Top. Stroke Rehabil.* **14**(6), 22–44 (2007)
15. Zabaleta, H., Valencia, D., Perry, J., Veneman, J., Keller, T.: Absolute position calculation for a desktop mobile rehabilitation robot based on three optical mouse sensors. In: 2011 Annual International Conference of the IEEE Engineering in Medicine and Biology Society, EMBC, 2011. IEEE, pp. 2069–2072
16. Perry, J.C., Zabaleta, H., Beloso, A., Rodríguez-de-Pablo, C., Cavallaro, F.I., Keller, T.: ArmAssist: development of a functional prototype for at-home telerehabilitation of post-stroke arm impairment. In: 2012 4th IEEE RAS & EMBS International Conference on Biomedical Robotics and Biomechatronics (BioRob), 2012. IEEE, pp. 1561–1566
17. Ruiz-Ruano, J.A., Perry, J.C., Rodríguez-de-Pablo, C., Keller, T.: Telereha: online/offline web platform for telerehabilitation of post-stroke arm impairment. In: Converging Clinical and Engineering Research on Neurorehabilitation. Springer, New York, pp. 991–995 (2013)

18. Perry, J.C., Andureu, J., Cavallaro, F.I., Veneman, J., Carmien, S., Keller, T.: Effective game use in neurorehabilitation: user-centered perspectives. *Handbook of Research on Improving Learning and Motivation through Educational Games*, Ch. 32. IGI Global, Pennsylvania, pp. 683–725 (2010)
19. Rodríguez-de-Pablo, C., Perry, J.C., Cavallaro, F.I., Zabaleta, H., Keller, T.: Development of computer games for assessment and training in post-stroke arm telerehabilitation. In: 2012 Annual International Conference of the IEEE Engineering in Medicine and Biology Society (EMBC), 2012. IEEE, pp. 4571–4574
20. Perry, J.C., Rodriguez-de-Pablo, C., Cavallaro, F.I., Beloso, A., Keller, T.: Assessment and training in home-based telerehabilitation of arm mobility impairment. *J. Access. Des. All* **3**(2), 32 (2013)
21. Sanford, J., Moreland, J., Swanson, L.R., Stratford, P.W., Gowland, C.: Reliability of the Fugl-Meyer assessment for testing motor performance in patients following stroke. *Phys. Ther.* **73**(7), 447–454 (1993)
22. Van der Lee, J.H., de Groot, V., Beckerman, H., Wagenaar, R.C., Lankhorst, G.J., Bouter, L.M.: The intra-and interrater reliability of the action research arm test: a practical test of upper extremity function in patients with stroke. *Arch. Phys. Med. Rehabil.* **82**(1), 14–19 (2001)
23. Collin, C., Wade, D., Davies, S., Horne, V.: The Barthel ADL Index: a reliability study. *Disabil. Rehabil.* **10**(2), 61–63 (1988)
24. De Haan, R., Limburg, M., Bossuyt, P., Van der Meulen, J., Aaronson, N.: The clinical meaning of Rankin ‘handicap’ grades after stroke. *Stroke* **26**(11), 2027–2030 (1995)
25. Beck, A.T., Ward, C.H., Mendelson, M., Mock, J., Erbaugh, J.: An inventory for measuring depression. *Arch. Gen. Psychiatry* **4**, 561–571 (1961)
26. Wolf, S.L., Catlin, P.A., Ellis, M., Archer, A.L., Morgan, B., Piacentino, A.: Assessing Wolf motor function test as outcome measure for research in patients after stroke. *Stroke* **32**(7), 1635–1639 (2001)
27. Kostić, M.D., Popović, M.D.: The modified drawing test for assessment of arm movement quality. *J. Autom. Control* **21**(1), 49–53 (2013)
28. Posteraro, F., Mazzoleni, S., Aliboni, S., Cesqui, B., Battaglia, A., Carrozza, M.C., Dario, P., Micera, S.: Upper limb spasticity reduction following active training: a robot-mediated study in patients with chronic hemiparesis. *J. Rehabil. Med.* **42**(3), 279–281 (2010)
29. Deci, E.L., Ryan, R.M.: *Intrinsic Motivation and Self-determination in Human Behavior*. Springer Science & Business Media, New York, p. 371 (1985)
30. Kostić, M., Kovačević, P., Popović, M.: Playing games in Virtual Reality: motivation of patients during neurorehabilitation. *Proc. Infoteh* **11**, 692–696 (2012)
31. Ryan, R.M., Mims, V., Koestner, R.: Relation of reward contingency and interpersonal context to intrinsic motivation: A review and test using cognitive evaluation theory. *J. Pers. Soc. Psychol.* **45**(4), 736 (1983)

Comparison of Electro-Optical Strategies for Mimicking *C. elegans* Network Interconnectivity in Hardware

Lorenzo Ferrara, Alexey Petrushin, Carlo Liberale, Dara Brannick,
Brian Connolly, Pat Mitchell and Axel Blau

Abstract With exactly 302 neurons and about 8000 connections, the hermaphrodite of the soil-dwelling ringworm *Caenorhabditis elegans* features one of the simplest nervous systems in nature. The *Si elegans* project will provide a reverse-engineerable model of this nematode by emulating its nervous system and embodying it in a virtual world. The hardware will consist of 302 individual FPGAs, each carrying a neuron-specific neural response model. The FPGA neurons will be interconnected by an electro-optical connectome to distribute the signal at the axonal output or gap-junction pin of an FPGA neuron onto the respective synaptic input or gap-junction pins of postsynaptic FPGA neurons. This technology will replicate the known connectome of the nematode to allow for a biomimetic parallel information flow between neurons. This chapter focuses on the comparison of different electro-optical connectome concepts and on the required implementation steps with their advantages and disadvantages being explained.

L. Ferrara · A. Petrushin · A. Blau (✉)

Neuroscience and Brain Technologies Department, Istituto Italiano di Tecnologia,
via Morego 30, 16163 Genoa, Italy

e-mail: axel.blau@iit.it

L. Ferrara

e-mail: lorenzo.ferrara@iit.it

A. Petrushin

e-mail: alexey.petrushin@iit.it

C. Liberale

BESE Division, KAUST (King Abdullah University of Science and Technology),
Thuwal 23955-6900, K.S.A

e-mail: carlo.liberale@kaust.edu.sa

D. Brannick · B. Connolly · P. Mitchell

Accutron Ltd, National Technology Park, Limerick, Ireland

e-mail: dbrannick@accutron.ie

B. Connolly

e-mail: brian.connolly@accutron.ie

P. Mitchell

e-mail: pat.mitchell@accutron.ie

1 Introduction

Caenorhabditis elegans, a soil-dwelling nematode, is one of the best characterized organisms. The adult hermaphrodite is comprised of exactly 959 cells, including 95 body wall muscle cells, 302 neurons and about 8000 connections, of which about 2000 are electrical junctions. The spatial organization of neurons and their inter-connectivity is largely known and almost fully mapped. The most up-to-date wiring information covers 279 neurons of the somatic nervous system, excluding 20 neurons of the pharyngeal system and three neurons that appear to be unconnected from the rest [2, 7, 8]. A highly compressed view on the overall connectivity matrix is given in Fig. 1. Its data is based on work by Chklovskii's [2] and Kawamura's [5] groups, which was modified by Bhatla [1] for easier processing.

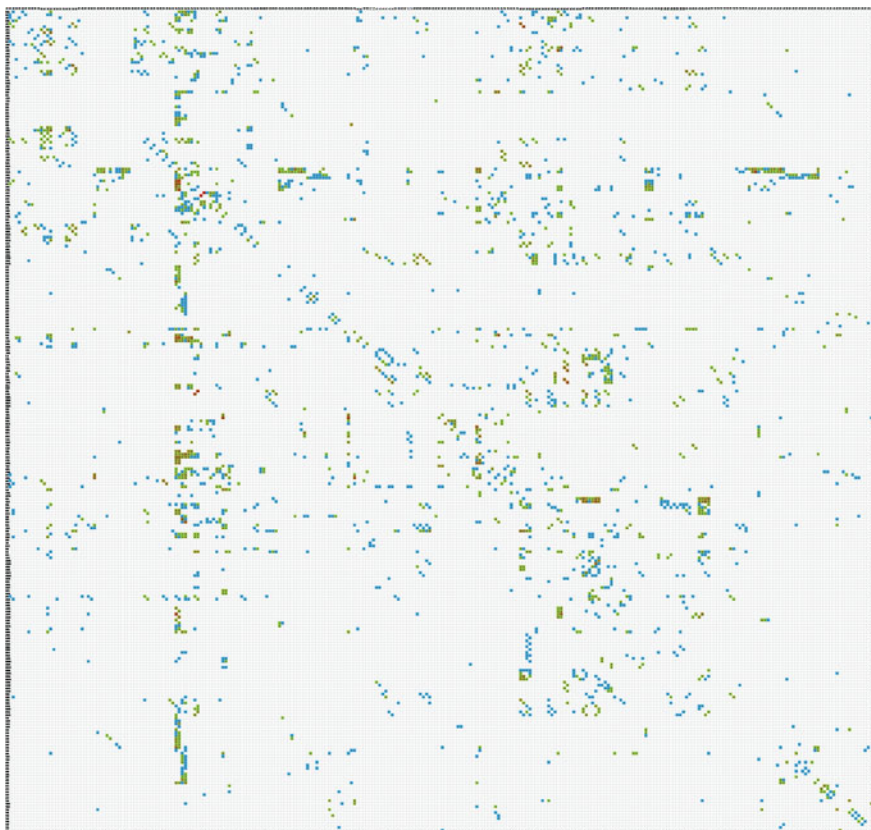


Fig. 1 Connectivity matrix of currently 279 neurons (not including the pharynx network) based on the *Neural Connectivity II* dataset by Varshney et al. [11] and the *Database of Synaptic Connectivity of C. elegans for Computation* by Oshio et al. [5]. It was compiled by Nikhil Bhatla [1]. Presynaptic neurons listed in the row headers connect to their postsynaptic target neurons listed in the column headers via one (blue) or several simultaneous chemical or electrical synaptic connections (gradient green to red). Due to page size limitations, the names of the individual neurons along the *left* and *top* edges are not legible

Despite its seemingly low complexity, some experimental key information on neural function is still missing. For instance, little is known on the excitatory or inhibitory identity of a synaptic connection, on its weight and its transmission properties. Equally sparse is our knowledge on the information coding and signal propagation modalities. This lack makes it difficult to understand how the rich behavioural repertoire of the worm is coded for. Although new experimental tools became available recently (e.g., optogenetics) that may help in answering these questions, the *Si elegans* project suggests an alternative, hypotheses-driven route to supply the missing data. *Si elegans* aims at providing a synthetic modelling platform for the testing and validation of neural coding mechanisms. It will consist of a highly parallel, modular, user-programmable and scalable hardware architecture. Neurons will be represented by reconfigurable field-programmable gate arrays (FPGAs), which exchange information via a light-based connectome. Any property of each individual neuron can be programmed at almost arbitrary detail. This hardware computing framework will be embodied by a virtual representation of the nematode, which will be allowed to interact with a realistic, physics-based virtual environment. The closed-loop platform will allow mimicking *C. elegans* in real time to let complex and realistic behavior emerge. Because all events will be traced and stored, the underlying information processing principles can be abstracted from the response characteristics of the network. This *Si elegans* platform will be made available to the scientific community through an open-access web portal for its peer-validation and use.

2 Concepts for a Biomimetic Connectome Emulation

2.1 Parallelized Signal Propagation Through Structured Light

The information flow in the emulated *C. elegans* network will be based on an electro-optical connection scheme between FPGAs according to the synaptic connectivity map (or any future update of it) depicted in Fig. 1. Conceptually, the architecture will require one light source per FPGA neuron being triggered by one of its output pins to emulate a neural membrane potential swing or gap-junction current. For each FPGA neuron, an optical system made of neuron-specific micromirrors will multiply and distribute this signal onto an array of individual photodetectors (PDs) of postsynaptic FPGAs (Fig. 2). Each photodetector is tied to the respective synaptic input or gap-junction pins of those target FPGA neurons that the presynaptic neuron interconnects with. This strategy shall ensure that a signal will arrive in parallel at all target neurons with a precise and predictable timing. Precise spike-time coding is believed to be key for the reliable processing of information in biological nervous systems [3, 4, 9, 10]. To place the photodetectors in line of sight

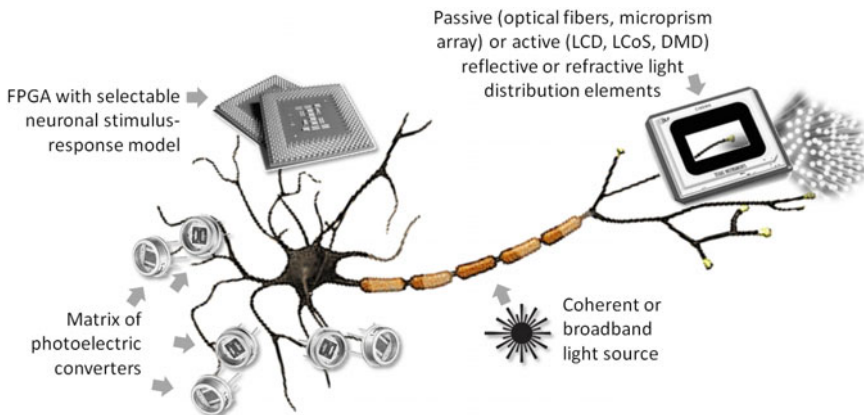


Fig. 2 Hardware components for the emulation of a neuron

with respect to the firing neural system, they will be mounted on so-called synaptic boards (SBs). Their design and layout influences the light projection requirements in mutual dependency with the distribution of the FPGA neurons.

2.2 Geometry and Layout Considerations

Each synaptic connection will be represented by one photodetector. *C. elegans* neurons can form between 1 and 350 connections to other neurons at a time. This constraint offers four options:

1. Design several different synaptic boards with a specific number of photodetectors for neurons whose number of connections fall in a certain range (e.g. 1–30, 31–60, 61–180, 180–350). This would reduce the number of required photodetectors to a minimum, but increase the design and synaptic board arrangement effort.
2. Design two types of synaptic boards, a smaller one for the majority of neurons with a low number of connections (for example, 263 neurons have less than 60 connections) and a bigger one for the rest of the neurons. This would be a compromise between the required resources and the design effort.
3. Design one type of synaptic board with the maximum number of photodetectors to both simplify the PCB board design process and the distribution of the resulting synaptic boards at the cost of increasing the space requirements and number of required photodetectors.
4. Design one type of daisy-chainable synaptic board with a relatively low number of photodetectors, which would allow by their combination the increase of the overall number of available photodetectors if needed. This would be a compromise between a low design effort and increased cost for the additional connectors.

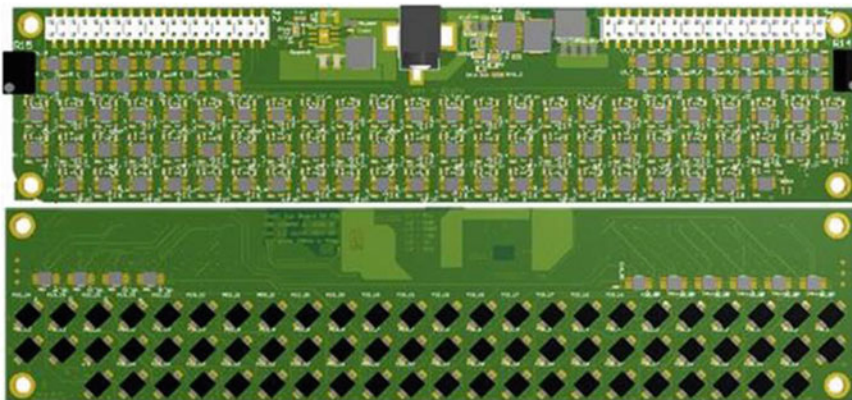


Fig. 3 Rear (*top*) and front (*bottom*) layout of a synaptic board with 68 photodetectors, amplifier electronics, connectors, power supply and board fixation holes

The number of photodetectors determines the synaptic board layout because the available area will not only accommodate the detectors, but also the signal conditioning electronics and the high-density connector to the FPGA neuron board. In addition, the synaptic board may also carry the axonal output module consisting of the light source, a micromirror chip and the optical projection system. A design example without axonal module is shown in Fig. 3.

2.3 Photodiode and Power Requirements

Among the tested photodiodes, PD70-01C (Everlight) has the best sensitivity, highest efficiency in the visible spectrum and a relatively low parasitic capacitance. It has an overall dimension of 3.9 mm by 6.4 mm and a sensitive area of 3.5 mm by 4 mm. To lower its junction capacitance, the photodiode will be connected in reverse voltage. Device characteristics are listed in Table 1. Figure 4 shows an image of the detector and its terminal capacitance versus the reverse voltage.

The electronics of the synaptic board will require ± 3 V voltage lines. The maximum estimated current consumption per photocell is 12.6 mA. The power requirement depends on the design of the synaptic board as discussed in Sect. 2.2. The expected power consumption for two synaptic boards with a different number of photodetectors is listed in Table 2.

Table 1 Photodiode characteristics

Photodiode	Manufacturer	λ with max sensitivity	Sensitivity at $\lambda = 620$ nm	I_{dark}	C_p
PD70-01C	Everlight	940 nm	70 %	30 nA	25 pF

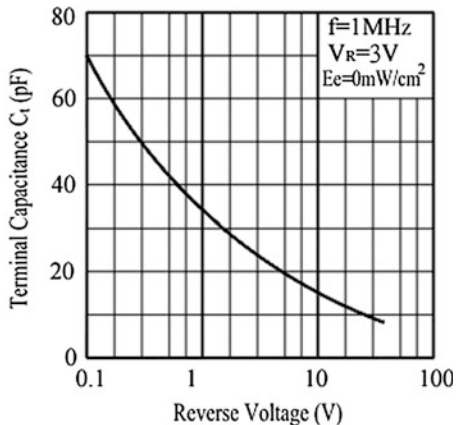


Fig. 4 PD70-01C photodiode (*left*) and its terminal capacitance versus reverse voltage (*right*)

Table 2 Synaptic board power consumption

	Single cell (mA)	Board
Small SB (68 PDs)	12.6	1 A @ ± 3 V
Large SB (370 PDs)	12.6	6.5 A @ ± 3 V
PD reverse voltage		-3 V ÷ -15 V

2.4 The Axonal Output Module

To emulate the firing of a neuron, we have to simultaneously trigger the photodetectors on the synaptic boards to which it is connected. This requires the light source dedicated to each neuron to be structured into parallel rays by means of a micromirror array and to be distributed to the photodetectors on the synaptic boards by a lens system. Active micromirror devices like the digital micromirror device (DMD) pioneered by Texas Instruments have been selected as the most efficient and flexibly reconfigurable solution. In digital light processing (DLP) projectors, each mirror generates one pixel in the projected image. The number of mirrors corresponds to the resolution of the image. Mirrors can be rapidly toggled between $\pm 12^\circ$ to reflect the light either through a projection lens or onto a light sink. When no data signal is applied, individual mirrors are held electrostatically in their previous state by three static memory elements underneath each mirror. This allows the creation of a quasi-static light distribution pattern that, upon demand, can be reconfigured by means of a commercial DMD controller (e.g. DLP® LightCrafter™, Texas Instruments) (Fig. 5). Mirrors can be binned to increase the light intensity at the projection screen at the cost of decreasing the overall image resolution.

As mentioned above, the design of the synaptic board also depends on the DMD technology; different models of DLPs hold different numbers of mirrors of different dimension and arrangement. Table 3 lists the characteristics of some DMD models.

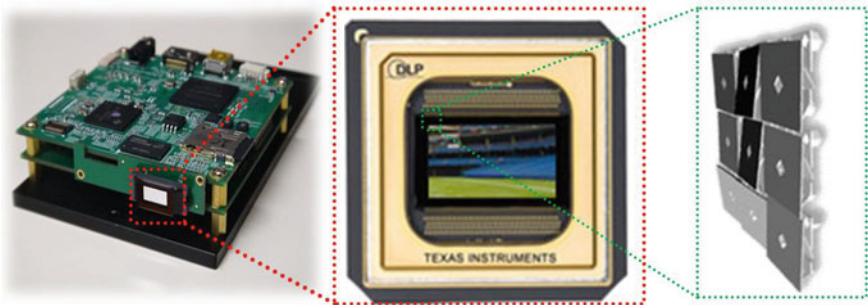


Fig. 5 Example of a commercial DMD controller (*left*), a DMD chip (*middle*) and the three-state positioning of micromirrors ($+12^\circ$ *light grey*, -12° *black*, 0° *dark grey*; *right*). Images by TI adapted from [6] with permission

Table 3 DLP characteristics

DLP model	Number of mirrors	Distribution	Pixel pitch (μm)
3000	608 x 684	Diamond	7.56
4500	912 x 1,140	Diamond	7.56
6500	1,920 x 1,080	Orthogonal	7.56

The choice of the light source affects the flexibility of the projection scheme. There are two sources to choose from: LEDs and lasers. The main advantage of an LED is its low price and switching speed. It reaches full power in tens of nanoseconds. Being a non-coherent source, different types of LEDs can be used in the same optical system without interference phenomena. On the other hand, coherent laser light can be used for both conventional or for holographic projection. Although lasers are less responsive, their intensities outperform LEDs. Preliminary tests show that any optical power higher than $4 \mu\text{W}$ per photodiode will be sufficient to trigger it.

3 Comparison of Different Synaptic Board and Projection Scheme Installation Scenarios

Synaptic and FPGA boards can be arranged in different ways depending on the optical alignment requirements, the size of the room, the cost of the entire structure, the compactness of the solution, the willingness of using cables and racks, and the vibration of the environment. Finding the most effective solution is therefore challenging. Among the possible solutions, five are analyzed with respect to their advantages and drawbacks.

3.1 19" Rack with Synaptic Boards Directly Plugged into Neural FPGA Boards

Features. The first idea relies on a common arrangement for FPGAs and synaptic boards in the same rack. Each FPGA will directly connect to the back side of a synaptic board by means of two 200-pin backplane connectors (Fig. 6).

The connectors input and output are tilted by 90° for a perpendicular arrangement of the synaptic board with respect to the FPGA board. This allows for a rack-based arrangement where the FPGA boards are inserted into the rack's rails while the synaptic boards create a synaptic plane in front of the rack (Fig. 7). Each alternative board pair is inverted to give air flow clearance between the FPGA boards.

Advantages. This scheme ensures a simple, reliable and space-saving connection between the boards because the FPGAs can be densely packed without compromising good ventilation. Moreover, apart from two connector pairs, there are no extra costs or weight loads due to cabling. The total arrangement is elegant and efficient.

Disadvantages. Debugging or checking on the FPGA/synaptic board connections may be difficult and cause optical misalignment due to their stiffness. The alignment itself could be an issue if individual synaptic boards were shifted or tilted to each other, thereby causing the pixel projection to miss the centers of the photodetectors. Another problem, especially in case of a projection with low-density micromirror DLPs (e.g. less than 1 Mpixel), is the waste of space due to the rack

Fig. 6 Direct connection between FPGA board (*left*) and synaptic board (*right*) by a pair of 90° extensions for instrumentation (PXI) connectors (box)

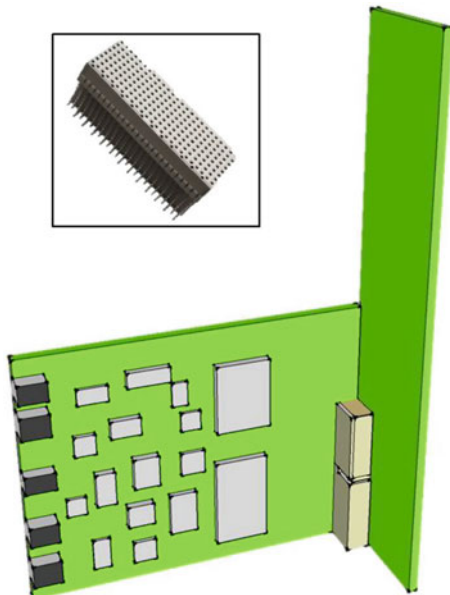
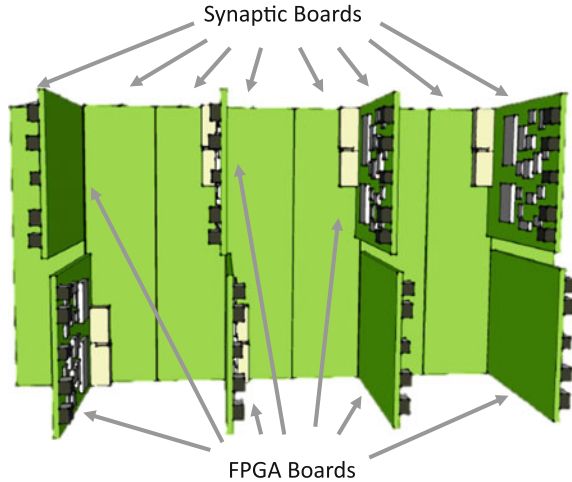


Fig. 7 Example of a combined FPGA and synaptic board distribution in a row of a conventional rack. The rack is not shown for clarity



frames and fixed dimensions, which may not necessarily match the DLP projection ratio. Moreover, the emulated neurons vary in their number of synaptic connections (from 1 to 350) resulting in an inefficient light distribution for low connectivity scenarios.

3.2 Separate Synaptic Frame in Front of 19" FPGA Racks

Features. A second approach addresses two main system requirements: Sufficient cooling of the FPGA boards and alignment stability of the synaptic boards. These can be warranted by housing the FPGA boards in standard 19" racks whereas the synaptic boards were mounted on a rigid frame being mechanically decoupled from the FPGA racks. This allows the cooling of the FPGA boards by fans being installed in the base of the racks without their vibration affecting the synaptic boards. If the synaptic boards are mounted on hinges, they can be swiveled and locked in place at any required angle to maximize their optical coupling with the micromirror array (Fig. 8). Furthermore, the FPGA boards can be removed from the back of the rack without influencing the synaptic board installment.

In this case, a FPGA board will be connected to its corresponding synaptic board by several standard high-density low-cost ribbon cables. Each synaptic board can be fitted with an inertia sensor to monitor vibrations, which might cause optical misalignment. The signals of two extra photodiodes placed diagonally at two corners of a synaptic board, when brought to the analog inputs of the FPGA, should assist with mechanical and optical alignment. Moreover, the entire synaptic framework can be fabricated in a concave shape angle (Fig. 9) to reduce any projection distortion.

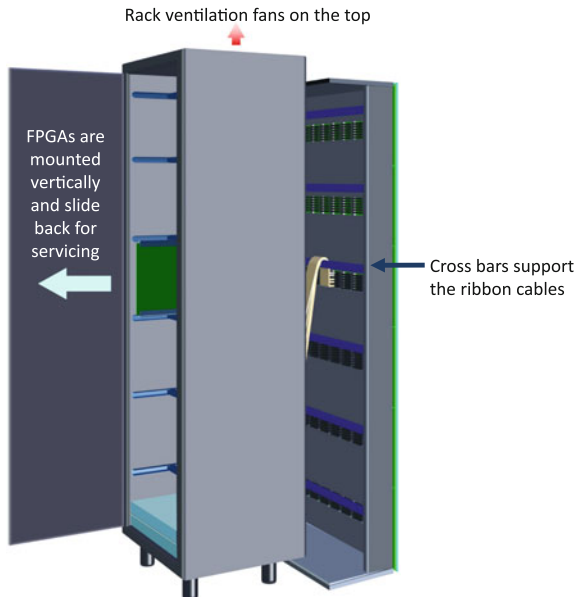


Fig. 8 FPGA rack connected to stand-alone synaptic rack by ribbon connectors

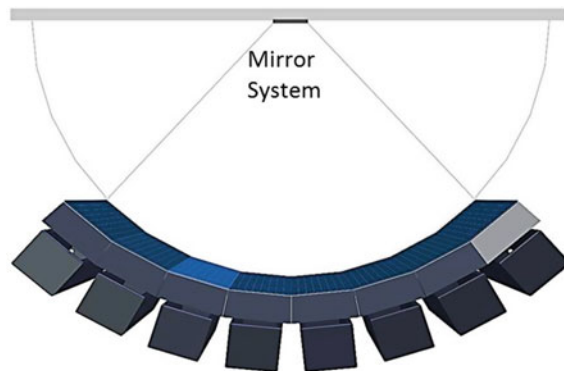


Fig. 9 Possible concave arrangement of 8 FPGA racks with the synaptic framework in front of it. In this example, the projection starts from the synaptic screen and is back-reflected by means of a mirror on the opposite wall

To allow for the maximum flexibility, the FPGA board and the synaptic board can be connected through a daughter board (Fig. 10) that will convert between different connectors. For example, an FPGA board may be equipped with 6 high-speed mezzanine card (HSMC) connectors, whereas the synaptic board carries 6 insulation-displacement contact (IDC) connectors; the daughter board will then

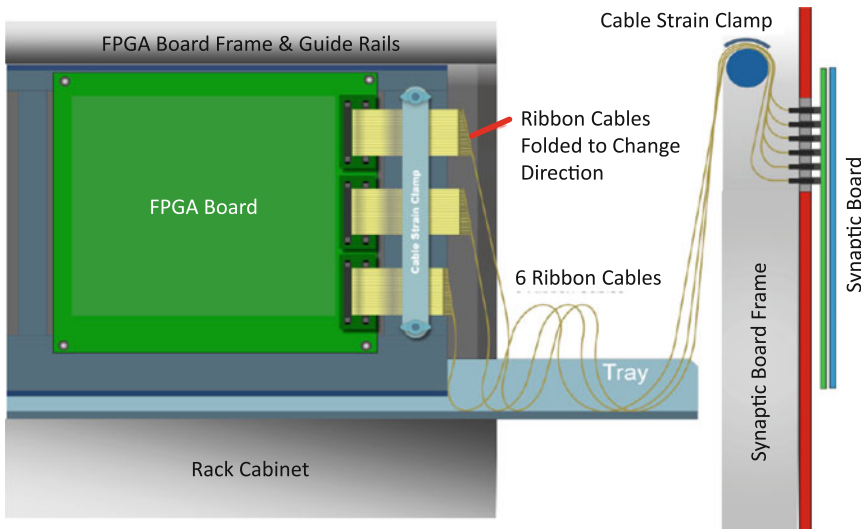


Fig. 10 Connection between FPGA board HSMC connectors to synaptic board IDC connectors by means of a connector conversion daughter board. The cable strain clamp prevents misalignment in case an FPGA board needs to be removed

covert between the two standards. Additional cable clamps would furthermore allow the two main boards to be disconnected without alignment loss.

Advantages. Decoupling the synaptic receivers from the FPGA boards gives additional design freedom and allows for a better alignment of the photodetectors with the projection system. The alignment is furthermore facilitated by the ability to tilt and turn individual synaptic boards through hinges located on the synaptic frame (not shown). Moreover, dedicated detectors for centering a synaptic board will guarantee a proper optical projection. Furthermore, the daughter board will add “hot plug” functionality without alignment loss to the system. The daughter board itself adds freedom in the choice of connectors on the two boards, thereby allowing the two being designed independently from each other. It also prevents accidental mating cycle-related damage to the FPGA board. Because the synaptic board frame is custom-made, its design can be optimized to minimize the empty spaces between boards thereby maximizing the effective projection area. Finally, the photodetectors from one synaptic board can be assigned to a different FPGA thanks to multiple cables. That way, the neurons with a higher number of connections can use photodetectors from neighbor synaptic boards that engage in fewer connections, thereby permitting the reduction of the board area and the number of photodetectors on each board.

Disadvantages. Boards in two separate racks need to be connected by several long and heavy cables. Moreover, the ribbon cables will make it difficult to check for wrong addressing or damage. In order to access the cabling, the synaptic boards need to be detached from their frame. The custom racks will furthermore increase the installation costs.

3.3 Custom-Made Frame for the Arbitrary Positioning of Synaptic Boards Directly Plugged into Neural FPGA Boards

Features. As in the first scenario, the FPGA boards will be directly connected to the back side of each synaptic board through a 90° connector. This time, however, the synaptic boards instead of the FPGA boards are fixed to a custom-made frame. This will permit an arbitrary distribution and geometry of the synaptic boards. Boards for highly connected neurons can be bigger than boards with few connections. The final geometry will be dictated only by the required projection area and the synaptic board dimensions and can therefore be optimized to match the optical path and to minimize optical losses. An example of such arrangement with a high degree of design freedom is shown in Fig. 11.

Advantages. The main advantage is the freedom in choosing synaptic board geometries that grant the most effective addressing of the photodetectors. Because the boards are individually attached to a custom-made frame, they can be individually aligned for a best match with the projected pixels. The panel-like arrangement will furthermore allow reducing the required area. The smaller the overall projection screen, the closer the micromirrors can be placed in front of it, thereby increasing the delivered energy to each photodetector. Each board will be attached to bars by screws, allowing for its independent removal and reinsertion in case of its malfunctioning without compromising the alignment. As discussed for the first solution, overall system complexity and costs will be low because of the absence of additional cabling.

Disadvantages. The absence of standard racks may make the FPGA structure less stable. The design of a sturdy custom-made installation and support frame may be demanding and costly. It has to take into account that the access to centrally

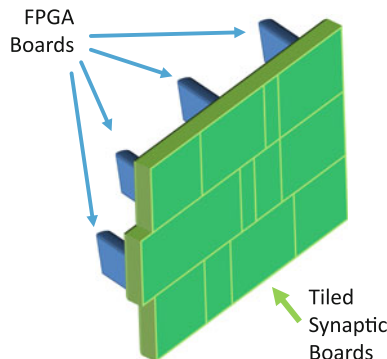


Fig. 11 Synaptic board installation with different board geometries, each optimized for the particular number of connections of each neuron. The FPGA boards are connected by 90° PXI connectors to the back of the synaptic boards. The custom-made installation frame is not shown

installed boards may be obstructed and that an uneven pitch of the FPGA boards could cause local overheating or structural imbalance.

3.4 Synaptic/FPGA Board Integration

Features. This architecture considers a high integration of the FPGA and the synaptic board. As shown in Fig. 12, the photodiode array is soldered directly to the rear side of the FPGA board. The circuitry and amplifiers for the photodetectors will be placed on the same face, being covered by means of a thin sheet of light absorbing material that will only expose the active area of the photodetectors. This solution would also require the design of a custom-made board frame to face the photodetector side towards the optical projection system.

Advantages. The design is very elegant, compact and low cost because neither cables nor connectors are required. The photodetectors can be soldered directly on the back side of the FPGA board in any desired layout.

Disadvantages. The integration of the FPGA and synaptic board, although simple, is problematic in case of failure, making it hard to test faulty connections. Furthermore, the geometry of the synaptic panel is dictated by the FPGA board dimensions and the arrangement of components thereon, making it less compatible with the projection requirements. Finally, a fault in any of the two systems would require the costly replacement of the entire board.

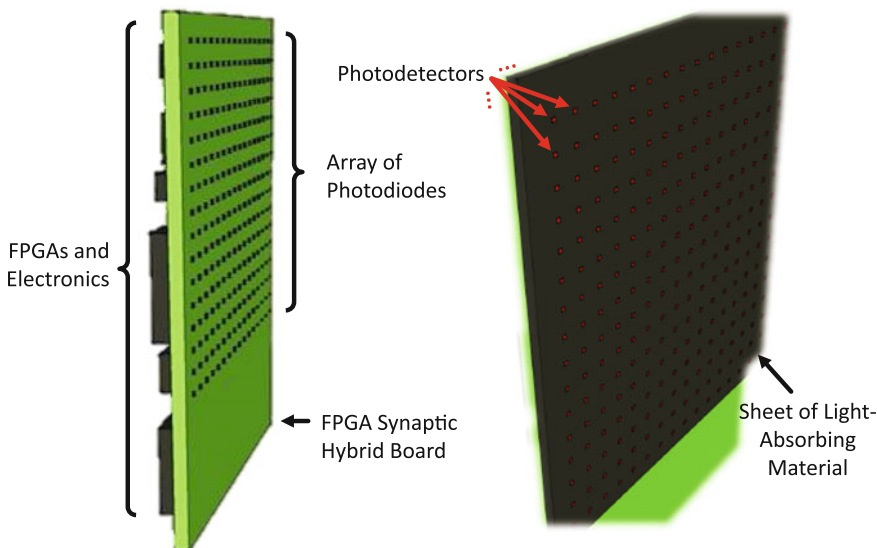


Fig. 12 Design of synaptic board directly integrated on the back side of the FPGA board before (left) and after (right) the application of a thin sheet of light-absorbing material that covers the electronics and only exposes the PDs

3.5 Selectable Electro-Optical Communication Through Bifunctional Synaptic Boards

Features. The last solution features both a wire-based connection scheme and an optical synaptic board. As shown in Fig. 13, each synaptic board is connected to adjacent boards by two 400-pin pass-through connectors. These connectors pass a bus of 302 lines around all of the 302 synaptic boards. All of these 302 lines are fed back to the FPGA through a separate 90° 400-pin connector.

The firing signal from the FPGA board is buffered and its output is connected to 302 ‘shorting links’ on each synaptic board. One shorting link per synaptic board is joined connecting the output of the FPGA to its respective line of the 302 line bus. For example, synaptic board 1 would have link 1 shorted, synaptic board 2 would have link 2 shorted etc. These shorting links would be a pair of surface-mount technology (SMT) resistor pads, which would be shorted by either soldering a zero Ohm resistor between them or by their bridging with a jumper. Each neuron would have its buffered firing signal appear separately on all of the synaptic boards. Each FPGA board would have all 302 signals fed back to the FPGA. The FPGA would then selectively enable the required neuron inputs and outputs as part of its neuronal response model. The whole instalment will look as depicted in Fig. 14. On each synaptic board will also be installed an array of 400 photodetectors, back-connected to the FPGA, to provide an optical alternative for the connectome.

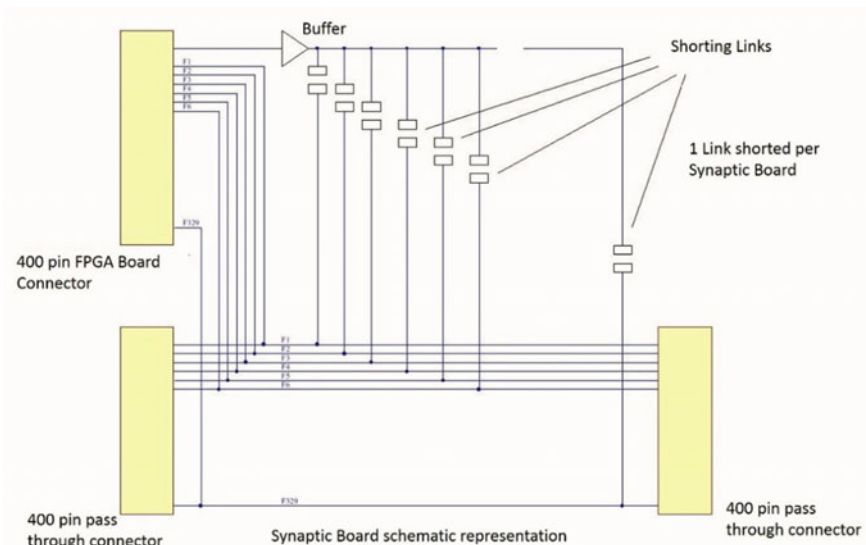


Fig. 13 Schematic of the daisy-chained, purely electrical connection scheme between an FPGA board and its synaptic boards with two pass-through connectors to neighbor boards

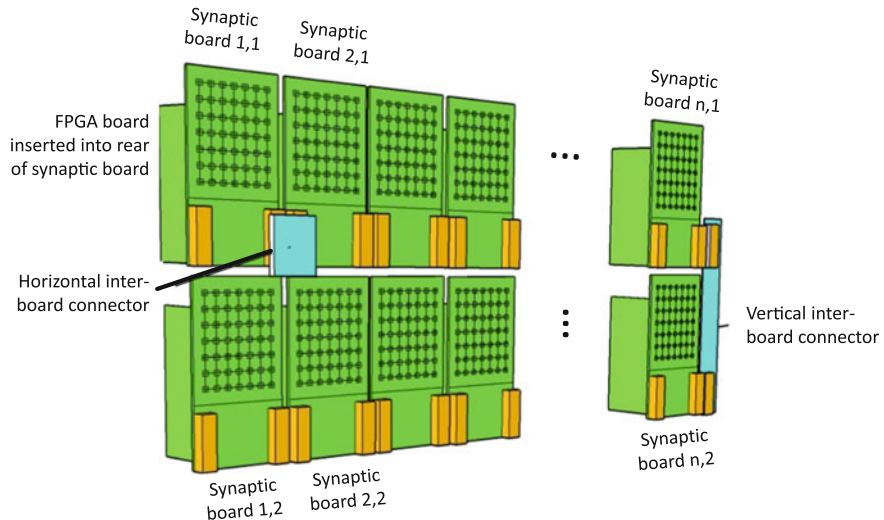


Fig. 14 Schematic of the combined wire-based and optical connectome

Advantages. This setup can be operated either as a parallel wire-based or as an electro-optical connectome by switching between the two modalities. This allows for a direct performance comparison. A purely wire-based data flow is expected to be robust and will not require any alignment. All 302 modules are identical and can be installed in standard 19" racks.

Disadvantages. One of the disadvantages is the reduced area for the photodetectors instalment with the consequence of an increased projection area, which may require high-power light sources. In addition, there is little freedom in aligning the optical receivers with the projection setup. Any malfunctioning in the daisy chain logic of the purely wire-based connection scheme will cause difficult-to-trace errors in the whole system. Furthermore, implementing a reliable switching concept between the two operation modalities will be challenging. Finally, the handling of synaptic input by the neuronal response models on each FPGA has to be changed when switching from one mode to the other.

4 DMD Projector Placement—Comparison of Different Installation Scenarios

Another important aspect is the position of the neural firing modules with respect to the synaptic boards. We consider three possible scenarios.

4.1 Neural Output Module Combined with Synaptic Input Board

Features. The first solution considers the placing of the light source, the DMD array and the projection optics directly onto the synaptic board. Each synaptic board will then be composed of three parts: a connector to the FPGA board and signal conditioning electronics on its back side, a photodetector area on the front side and a neural firing module underneath as depicted in Fig. 15.

The neural firing module is composed of a PCB with the DLP module, an LED or laser source and a dispersion lens. Mounting holes will serve for an easy installation and module replacement. An additional laser may be installed for separate gap junction addressing or for FPGA synchronization. Communication with the FPGA neuron board is established through a connector on the back side. As depicted in Fig. 9, the projection will hit a mirror installed opposite to the

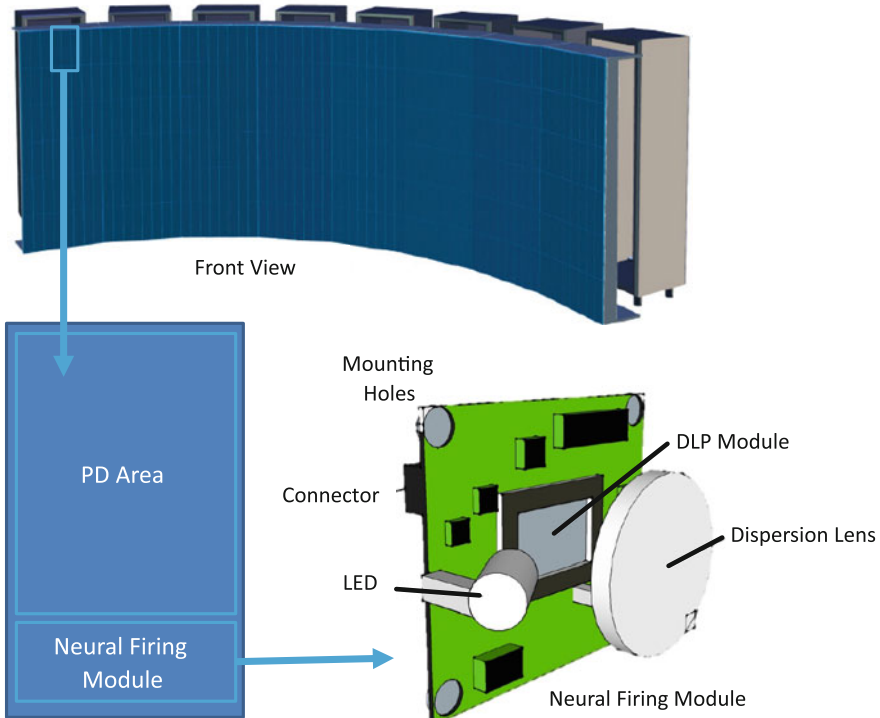


Fig. 15 Example of arranging both the receptive photodiode array and the light patterning module on the same synaptic board. Part of the *front* area will be dedicated to the photodetectors and the remaining area to the neural firing module. The *back side* and part of the *front* area are reserved to connectors and electronics

synaptic board to back-reflect the structured light onto the photodetectors on the synaptic board assembly.

Advantages. Because all components are mounted on the same board, any vibration is coupled, which makes additional vibration sensors obsolete.

Disadvantages. This configuration requires additional space on each synaptic board to accommodate the neural firing module. This results in a bigger synaptic screen, which leads to bigger pixel dimensions and a lower optical power density. Addressing the mirror on the opposite wall also requires the light to travel twice the distance. While this may help in enlarging the projected pixel pattern to cover the synaptic panel, a more powerful light source is required to trigger the photodetectors. Finally, the dispersed distribution of the individual projection modules will require individually adjusted optics to compensate for increasing pixel distortions the farther a module is placed off-center.

4.2 Separate DMD Rack Opposite to FPGA Rack with Synaptic Boards Attached to FPGA Neuron Boards

Features. In this design, the photodetector array is separated from the light source array. One option would be to install the firing neural module depicted in Fig. 15 opposite to the synaptic screen at a distance that allows for the correct addressing of individual photodetectors (Fig. 16).

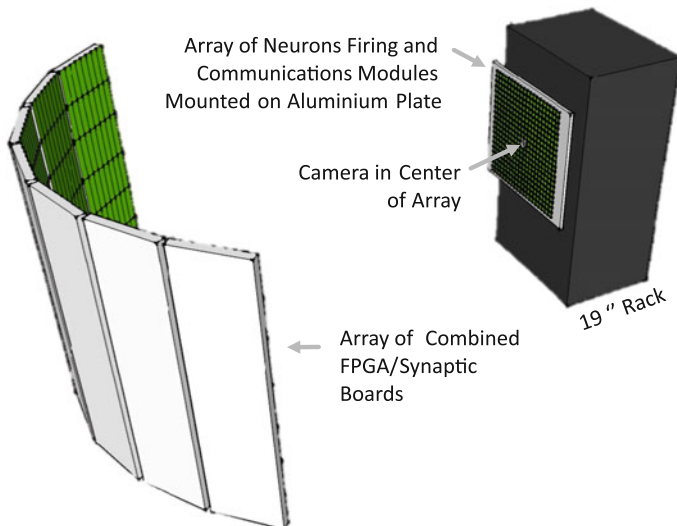


Fig. 16 Schematic of the installation of synaptic boards with photodetectors (*left*) and the opposite firing neural module array on a movable 19" rack (*right*)

The array of individually alignable modules is mounted on a plate on a movable rack that allows for a correction of the projection distance. An optional camera in the center of the DLP array may help in detecting and correcting possible misalignment and other optical distortions.

Advantages. In this configuration, the absence of the firing module frees space on the synaptic board to host more photodetectors. This allows increasing the number of possible connections and reduces the loss of projectable area. Being situated on the opposite side of the room, the direct and shorter light path requires less optical power to trigger the photodetectors. Finally, the more compact arrangement will reduce the need for correcting optical distortions.

Disadvantages. Vibration may cause the constant and uncontrollable misalignment between the synaptic rack and the DLP array because they are not coupled anymore. Moreover, the shorter light path could actually demand for a more complex optical design to achieve the expected throw ratio and coverage of the photosensitive field. Being separated from the FPGA modules, each DLP has to be connected individually by means of external cables (e.g. guided along the ceiling), thereby causing additional costs and encumbrance.

4.3 Separate DMD Rack Opposite to the FPGA Rack Projecting onto an Independent Synaptic Board Screen in Front of the FPGA Racks

The third and final case is very similar to the second in that the DLP modules are mounted as an array on the opposite side of the synaptic board screen. The only difference is the free-standing synaptic photodetector screen in front of the FPGA racks as depicted in Fig. 17.

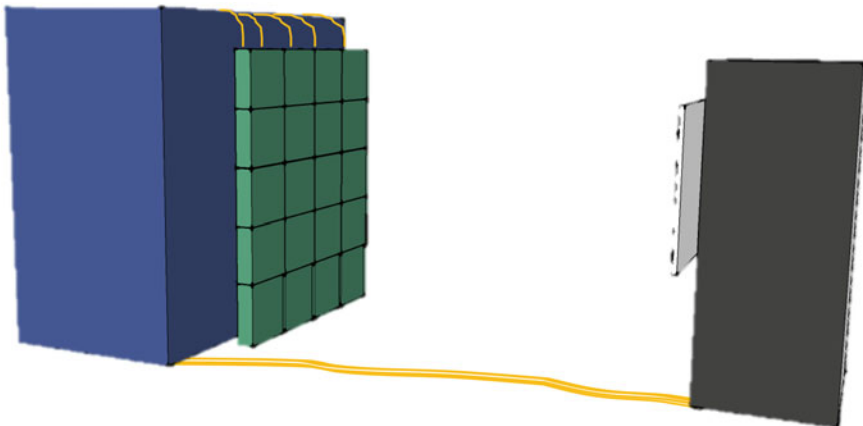


Fig. 17 Schematic sketch of the FPGA rack assembly (*left*), the synaptic screen in front of it and the optical firing module array on a rack (*right*) with the highest cabling demands

Advantages. With respect to the previous arrangement, the separation of the FPGAs from the synaptic screen allows for more freedom in the optical alignment and lower losses in the absence of any rack frames.

Disadvantages. The additional cabling between the synaptic frame and the FPGA boards increases costs and makes the structure less compact.

5 Conclusions

In this chapter, several installation scenarios of an electro-optical connectome with the aim of mimicking parallel information flow between artificial neurons were compared. All of them have to meet a set of geometric boundary conditions dictated by the type, resolution and throw ratio of the chosen micromirror device in the optical engine. Therefore, every solution is a compromise between complexity, flexibility and costs. Although 19" rack-based systems may be most comfortable to work with from an engineer's perspective, their encasings somewhat disturb the placement of stereotypic synaptic boards on their front faces if they were directly connected to the FPGA neuron boards at 90°. In contrast, a custom-made frame carrying an array of synaptic boards would allow their arbitrary arrangement at the cost of an additional design effort. Connecting synaptic boards to their respective FPGA neuron board by cables instead may allow the two entities to be physically separated and installed in the most suitable frameworks. Decoupling the synaptic boards from the FPGA board frames will permit their tiling in a geometry that is more compatible with the micromirror projection engine. However, the required number of cables increases both costs and system complexity and sets limits to system scalability. The same compromise holds for the placing of the optical projection modules. Therefore, the distribution of mated FPGA-synaptic boards on a dedicated custom-made frame that allows for their individual alignment with the optical projection engine placed in front of it may be the most opportune solution.

Acknowledgments The *Si elegans* project 601215 is funded by the 7th Framework Programme (FP7) of the European Union under FET Proactive, call ICT-2011.9.11: Neuro-Bio-Inspired Systems (NBIS). We would like to thank David Evans and Duncan Turner from EBV as well as Noel Nevin, Rahiv Bhateja, Anisha Nanda and Stef Niewiadomski from Altera for fruitful discussions and sponsorship.

References

1. Bhatla, N.: An Interactive Visualization of the *C. elegans* Neural Network (2009)
2. Chen, B.L., Hall, D.H., Chklovskii, D.B.: Wiring optimization can relate neuronal structure and function. Proc. Natl. Acad. Sci. USA **103**, 4723–4728 (2006)
3. Gütig, R.: To spike, or when to spike? Curr. Opin. Neurobiol. **25**, 134–139 (2014)
4. Kloppenburg, P., Nawrot Martin, P.: Neural coding: sparse but on time. Curr. Biol. **24**, R957–R959 (2014)

5. Oshio, K., Iwasaki, Y., Morita, S., et al.: Database of synaptic connectivity of *C. elegans* for computation. Technical Report of CCeP, Keio Future. Keio University (2003)
6. Petrushin, A., Ferrara, L., Liberale, C., et al.: Towards an electro-optical emulation of the *C. elegans* connectome. In: Proceedings of the 2nd International Congress on Neurotechnology, Electronics and Informatics (NEUROTECHNIX). Rome, Italy, pp. 184–188 (2014)
7. Qian, J., Hintze, A., Adami, C.: Colored motifs reveal computational building blocks in the *C. elegans* brain. *PLoS ONE* **6**, e17013 (2011)
8. Ruvkun, G.: Patterning the nervous system, Chapter 20. In: Riddle, D., Blumenthal, T., Meyer, B. (eds.) *C. elegans II*. Cold Spring Harbor Laboratory Press, New York, pp. 543–581 (1997)
9. Stein, R.B., Gossen, E.R., Jones, K.E.: Neuronal variability: noise or part of the signal? *Nat. Rev. Neurosci.* **6**, 389–397 (2005)
10. Vanrullen, R., Guyonneau, R., Thorpe, S.J.: Spike times make sense. *Trends Neurosci.* **28**, 1–4 (2005)
11. Varshney, L.R., Chen, B.L., Paniagua, E., et al.: Structural properties of the *Caenorhabditis elegans* neuronal network. *PLoS Comput. Biol.* **7**, e1001066 (2011)

Supervised EEG Ocular Artefact Correction Through Eye-Tracking

P. Rente Lourenço, W.W. Abbott and A. Aldo Faisal

Abstract Electroencephalography (EEG) is a widely used brain signal recording technique with many uses. The information conveyed in these recordings is a useful tool in the diagnosis of some diseases and disturbances, basic science, as well as in the development of non-invasive Brain-Machine Interfaces (BMI). However, the electrical recording setup comes with two major downsides, a. poor signal-to-noise ratio and b. the vulnerability to any external and internal noise sources. One of the main sources of artefacts is eye movements due to the electric dipole between the cornea and the retina. We have previously proposed that monitoring eye-movements provides a complementary signal for BMIs. Here we propose a novel technique to remove eye-related artefacts from the EEG recordings. We coupled Eye Tracking with EEG allowing us to independently measure when ocular artefact events occur through the eye tracker and thus clean them up in a targeted “supervised” manner instead of using a “blind” artefact clean up correction technique. Three standard methods of artefact correction were applied in an event-driven, supervised manner: 1. Independent Components Analysis (ICA), 2. Wiener Filter and 3. Wavelet Decomposition and compared to “blind” unsupervised ICA clean up. These are standard artefact correction approaches implemented in many toolboxes and experimental EEG systems and could easily be applied by their users in an event-driven manner. Already the qualitative inspection of the clean up traces shows that the simple targeted artefact event-driven clean up outperforms the traditional “blind” clean up approaches. We conclude that this justifies the small extra effort of performing simultaneous eye tracking with any EEG recording to enable simple, but targeted, automatic artefact removal that preserves more of the original signal.

P.R. Lourenço · W.W. Abbott · A.A. Faisal (✉)
Brain and Behaviour Lab, Department of Bioengineering, Imperial College London,
Exhibition Road, London, UK
e-mail: aldo.faisal@imperial.ac.uk

A.A. Faisal
Brain and Behaviour Lab, Department of Computing, Imperial College London,
Exhibition Road, London SW7 2AZ, UK

Keywords EEG · Eye-tracking · Ocular artefacts · ICA · Wiener filter · Wavelet decomposition

1 Introduction

Electroencephalogram (EEG) recordings are widely used for different neurological applications, such as diagnosis of epilepsy or sleep disorders, or brain machine interfaces [1, 2, 3]. The EEG trace is known to be highly variable, in part due to transient physiological conditions and state of the brain as well as noise inside the nervous system (e.g. [4, 5, 6], for general overview see [7]) but mainly due to noise and artefacts from any kind of non-neuronal generated electromagnetic fields. Noise artefacts are caused by external (e.g. AC line noise, mobile phones, electric motors) or biological electromagnetic activity from muscle contractions of the face and the eyes, as well as movement of the eye-ball itself. Ocular artefacts are most relevant since the influence of the eye dipole (potential difference between the Retinal Pigment Epithelium and the cornea) in the recording is very high, due to the proximity to the electrodes. The influence of eye blinks specifically is very high as it causes a large change in the signal, both due to the influence of the eye lid and the reflex rotation of the eye ball downwards and inwards [8].

Eye Tracking technology, and mostly the video-based recording of eye gaze, have recently become by a factor of up to 1,000 less costly [9] and rapid “walk-up” calibration [10] is enabling this technology to be more widely used in several applications (e.g. medical diagnostics or robotic control). Moreover, video-based eye tracking is not affected by external electrical fields and as such is independent from EEG noise sources.

Most of the current approaches to Ocular Artefact removal are “blind” and include removal of blink regions [11], wavelet decomposition [12], Independent Components Analysis [13] or use Electrooculogram recordings (EOG) to then subtract this from the EEG [14]. “Blind” approaches have the downfall of the artefact removal being performed generically to the whole signal, so there is a step in identifying what is and what is not an artefact, which is prone to error. By having an eye tracking recording we eliminate this error and are sure of when an artefact is occurring. Moreover, it enables the specific ocular artefacts to be characterised for use in other removal approaches, such as the Wiener filter.

In this study we use the Eye Tracking information to detect regions of Ocular Artefacts and use that to perform local correction, thus minimizing the influence of the corrective measures in the rest of the signal. This will provide a non corrupted but clean signal, that can then be used in EEG applications such as Brain Machine Interfaces or Medical Diagnosis.

2 Methods

A simple gaze fixation protocol was used to record EEG and Eye-tracking signals simultaneously. Subjects were instructed to stare at a white dot presented on a screen without moving their head. No instructions were given regarding blinking, allowing the subjects to blink freely. Figure 1 represents the experimental setup.

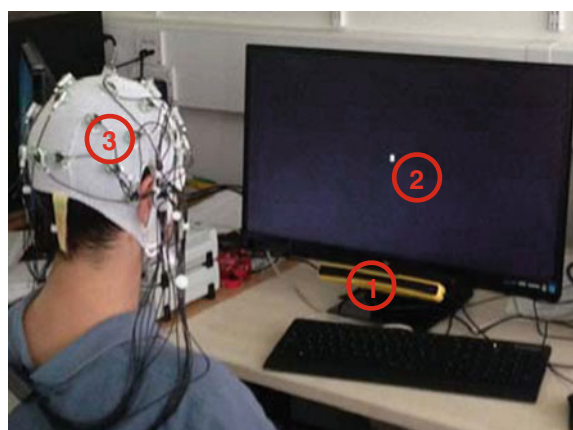
Eye Tracking was performed with an SMI Red-m Eye Tracker (SensoMotoric Instruments GmbH, Teltow, Germany), a binocular, remotely mounted Eye Tracker. EEG data was collected with a BrainProducts ActiChamp amplifier and a 32 active-electrode set with an ActiCap (Brain Products GmbH, Gilching, Germany). Eye Tracking was performed at 120 Hz and EEG recordings were sampled at 500 Hz. Impedance of Electrodes against the skin was reduced to levels always below 15 k Ω , to ensure EEG signal quality. Eye Tracking was performed at a distance of 50–70 cm from the cameras.

The EEG data was then pre-processed by a bandpass filter between 0.1–50 Hz, resampled to 120 Hz and Common Average Re-referenced. Eye Gaze data (retrieved from the Eye Tracker) was used to find blink regions and extract blink markers.

2.1 Experimental Setup

The task was set up in Matlab with the help of the PsychoPhysics Toolbox [15]. Participants were asked to sit at a distance of 50–70 cm from the Eye Tracker and Monitor, to ensure tracking (as per the Eye Tracker's technical information sheet). Time to relax was given to patients while performing the setup of the EEG

Fig. 1 Experimental Setup. 1 is the eye tracker, 2 is the stimuli screen and 3 is the electrode cap



apparatus and participants were instructed to sit comfortably and focus only on the screen. External interference was minimized to avoid distractions that could result in inadvertent saccadic movements.

Data was collected from 12 subjects with an average age of 25 years.

2.2 Analysis Methods

Several popular methods were evaluated in order to find the most suitable for ocular artefact correction and 3 were selected for assessment: 1. Independent Components Analysis (ICA), 2. Wavelet Decomposition and 3. Wiener Filtering. The traces resulting from these methods were then analysed and compared.

3 Independent Components Analysis

ICA is an algorithm that maximizes the independence of different components of a signal by finding a linear coordinate system that creates signals that are statistically independent [16]. ICA is used for Blind Source Separation. As ocular artefacts do not correspond to neural activity (i.e. they have a different source), ICA seemed a suitable approach to ocular artefact correction in EEG signals.

The ICA algorithm used is present in the EEGLAB toolbox for Matlab and uses the *infomax* learning rule [1]. This rule minimizes the mutual information in the components in the output, thus maximizing their statistical independence.

The original *infomax* condition fails to separate sub-Gaussian sources due to the sigmoid function used; a solution to this problem was proposed by Bell and Sejnowski and consisted of a flexible sigmoid function [1], but empirical results have shown that sometimes it is not possible to find independent components with this approach, alongside it being highly demanding in terms of computational load.

To evaluate the Gaussianity of a distribution, a measure of its kurtosis can be used. Kurtosis is defined as the 4th order cumulant and gives a measure of the shape of a distribution. A cumulant is used to describe and in some cases approximate a normal distribution; these are similar to moments in the sense that two distributions with identical moments will also have identical cumulants.

To overcome the problems of the original rule proposed by Bell and Sejnowski, an extended version of their algorithm was created: in this version the algorithm switches according to the kurtosis of the distribution of the data points. This means that according to the sign of the kurtosis, the learning rule is updated and this way it is possible to overcome the original problem. Simulations run on datasets with multiple sources and a variety of sub- and super-Gaussian distributions show that this extended version of the *infomax* algorithm is able to separate the sources [17].

The original learning rule with a natural gradient is defined as [1]:

$$\Delta W \propto (I - \tanh(u) \times u') \times W \quad (1)$$

where u represents the estimated sources, I denotes the identity matrix and $u = W \times x$, x being the mixed components signals. The extended learning rule, proposed in [17] is defined as:

$$\Delta W \propto [I - K \tanh(u)u' - uu'] \quad (2)$$

where k_i are elements of the N-dimensional diagonal matrix K . This matrix is related to the kurtosis of the data, so if $k_i = -1$ the data is sub-Gaussian and if $k_i = 1$ the data is super-Gaussian.

3.1 Wiener Filter

The Wiener Filter approach creates an optimal linear filter based on the signal and noise power spectra, as stated in the equation:

$$y(n) = x(n) + \omega(n) \quad (3)$$

where $x(n)$ is the EEG neural signal and $\omega(n)$ is the ocular artefact (both in time domain). Since we can retrieve the artefact positions in the signal through the Eye Tracker, an “average artefact” can be obtained by averaging the signal pieces that contain an artefact, and thus the Wiener Filter kernel can be calculated and applied to the signal.

Let’s assume that $x(n)$ and $\omega(n)$ are stationary and uncorrelated—a valid assumption, considering these signals have different origins and therefore should not have any strong correlation. This can be translated into the fact that the expectation is zero:

$$E[x(n), \omega(n)] = 0 \quad (4)$$

The goal is to find an optimal filter that minimizes the error between the signal $x(n)$ and the estimated signal $\hat{x}(n)$:

$$\min \left(E \left[(x(n) - \hat{x}(n))^2 \right] \right) \quad (5)$$

and

$$\hat{x}(n) = g(n) * y(n) \quad (6)$$

where $g(n)$ denotes the filter and $*$ represents convolution. By using the orthogonality principle [18] it is possible to obtain the filter that minimizes the mean square error:

$$\begin{aligned} E[e(n), y(n)] &= E[(x(n) - \hat{x}(n)), y(n)] \\ &= E[x(n), x(n)] - g(n) * E[y(n), y(n)] = 0 \end{aligned} \quad (7)$$

When converted to Fourier Space, the above equation will turn into an algebraic equation:

$$G(\omega) = \frac{P_x(\omega)}{P_x(\omega) + P_w(\omega)} \quad (8)$$

where $P_x(\omega)$ represents the power spectral density of the signal (with no artefacts), $P_w(\omega)$ is the power spectral density of the artefact extracted and $G(\omega)$ is the filter function. $P_x(\omega)$ and $P_w(\omega)$ were computed by extracting a mean artefact and mean clean signal and then calculating the power spectral density of each.

After the computation of this filter function and in order to apply it to the whole signal, either the filter function has to be inversely transformed to be in a time basis or the signal has to be transformed to be in Fourier space. The signal is then convolved (time) or multiplied (Fourier) with the filter and the noise should be removed.

3.2 Wavelet Decomposition

Wavelets and wavelet decomposition are tools used in signal processing to analyse, correct and characterize signals. Wavelet functions define the basis over which the signal is going to be decomposed.

From the several different types of wavelets in existence in signal processing it is possible to choose some whose properties adjust better to a specific purpose or case. In the case of artefact correction, wavelets that mimic the artefact will be more suitable, since the coefficients of the transform will be higher in the artefact zones.

The Discrete Wavelet Transform (DWT) consists of the decomposition of a signal into a wavelet basis, thus attributing coefficients that relate the signal to the wavelet form. The main equation that describes this process is [12]:

$$\Psi_{j,k}(t) = 2^{j/2} \Psi(2^j t - k) \quad (9)$$

where Ψ represents the wavelet function. The process of obtaining the wavelet coefficients of a signal can be performed at different levels, each one of them defined by the binary decimation factor \mathfrak{D}_0 [19]:

$$(\mathfrak{D}_0 x)_j = x_{2j} \quad (10)$$

where x represents the signal. This implies that \mathfrak{D}_0 chooses every even number of a sequence.

The main issue of the Discrete Wavelet Transform (DWT) is that it is not time-invariant, and thus the translation invariance property is lost, i.e. the translated DWT of a signal is not the same as the DWT of a translated signal.

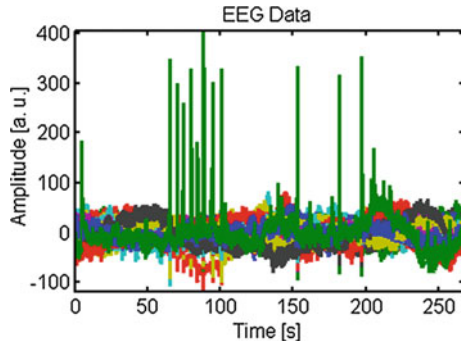
Stationary Wavelet transform is a variation of the usual Discrete Wavelet transform. The advantage relies on the independence of the choice of origin for the wavelets, which is achieved by applying appropriate high and low pass filters to the data at each level, thus producing two sequences at the next level. This way there is no decimation, instead the filters are changing at each level by zero-padding in a well-defined way. The details of the filter adaptation are described in [19]. The Stationary Wavelet Transform (SWT) contains the coefficients of the Discrete Wavelet Transform but shifted according to the choice of the origin of DWT. There is no restriction on the localisation as the stationary wavelet transform fills the gaps between coefficients in decimated DWT [19].

In the case of artefact correction of the EEG, [12] show a simple way to correct the eye blink artefacts from the EEG using Stationary Wavelet Transforms and Symlet Wavelets (part of the Daubechies [20] family) of level 3. In this paper they show a method to correct the artefacts with a simple threshold of the wavelet coefficients.

4 Results

In order to visualize the influence of the artefacts in the signal, all 31 channels of the recording are shown in Fig. 2. The same recording is shown in this paper for the sake of comparison, and it is only illustrative of the data collected.

Fig. 2 EEG recording. Different colours represent different channels; the *spikes* in the signal are blink artefacts



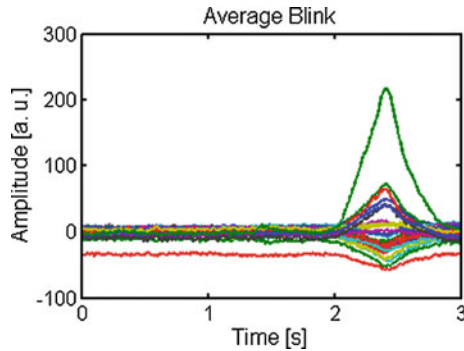


Fig. 3 Average Blink for one subject. The artefact extracted is quite large and thus can influence the use of the data

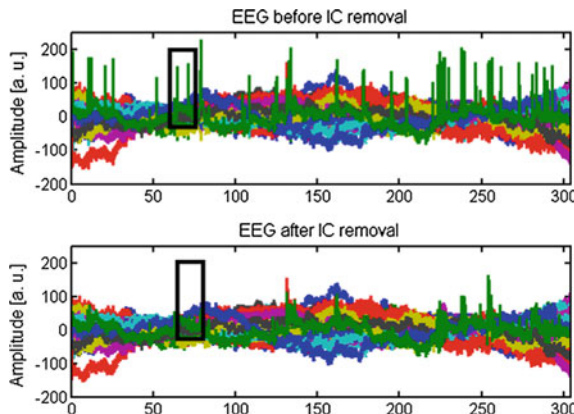


Fig. 4 Top EEG signal before artefact correction. Bottom Same signal after correction of artefacts with ICA. The artefacts that correspond to the *spikes* in the *upper plot* are reduced in the *bottom plot*. The *black window* represents the region that was zoomed for the detail plot in Fig. 5

The Eye Tracker data was aligned with the EEG recording and thresholded to yield a set of artefact markers. The extraction and average of blink artefacts through the use of these markers is represented in Fig. 3.

Event-driven Independent Components Analysis: ICA was applied to 1500 points in the data around the artefact; 30 channels were used to guarantee full-rank data. After projection of Independent Components to the original data space, Artefact components were identified and subtracted from the data. The result is shown in Figs. 4 and 5.

Event-driven Wiener Filtering: To calculate the filter kernel, the EEG signal with the artefacts and without artefacts was separated and averaged; both signals were zero-padded to the length of the signal and the power spectral density was

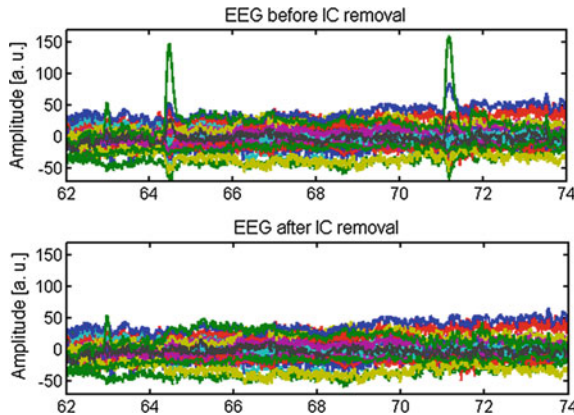


Fig. 5 Detail plot of two blink artefacts. *Top* before correction; *Bottom* after correction with ICA

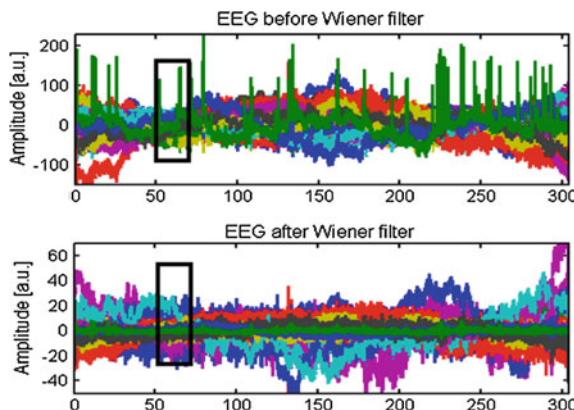


Fig. 6 EEG signal before and after correction of artefacts with Wiener filter. *Top* signal before artefact correction; *Bottom* signal after artefact correction. The black window represents the region of the signal that is zoomed in the detail plot (Fig. 7)

calculated and then used in the filter function calculation [21, 22, 23]. The result of the filtering is shown in Figs. 6 and 7.

Event driven Wavelet Decomposition: Stationary wavelet decomposition was used to correct the artefact; Symlet wavelets were chosen due to their resemblance to the ocular artefact [12] and 8 levels of decomposition were applied to 1500 data points around the ocular artefact. Figures 8 and 9 show the results of this method.

“Blind” Independent Components Analysis: Another method applied to the data in order to prove the pertinence of our methods, was a standard ICA clean up,

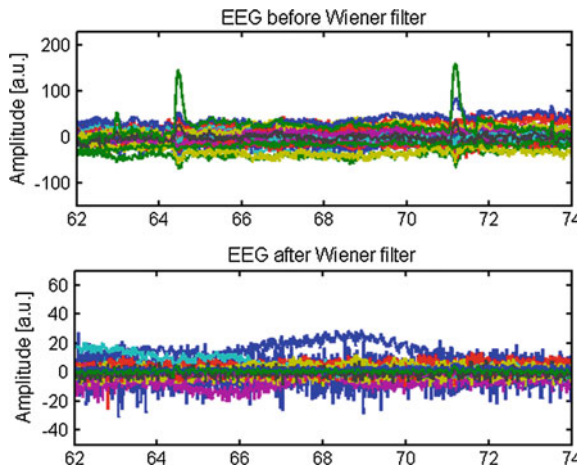


Fig. 7 Detail plot of the EEG signal. *Top* signal before artefact correction; *Bottom* signal after artefact correction with Wiener filter

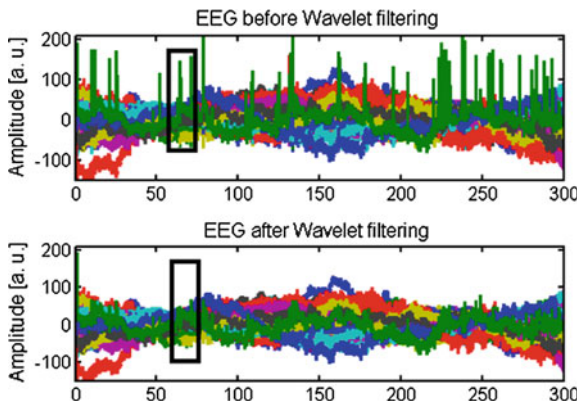


Fig. 8 EEG signal before and after correction of artefacts with Wavelet Decomposition. *Top* signal before artefact correction; *Bottom* signal after artefact correction. The *black window* indicates the region of the signal that is zoomed in the detail plot (Fig. 9)

where we have a sliding window over the data, calculating Independent Components and eliminating those that resemble an artefact. This approach is blind and as such has no knowledge of how a blink artefact looks like or even their locations. Results are shown in Figs. 10 and 11.

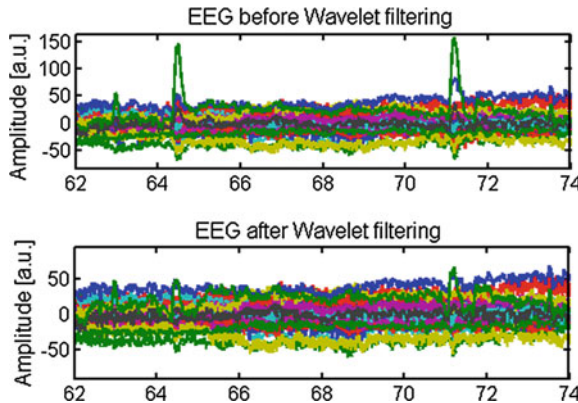


Fig. 9 Detail plot of the EEG signal. *Top* signal before artefact correction; *Bottom* signal after artefact correction with Wavelet Decomposition

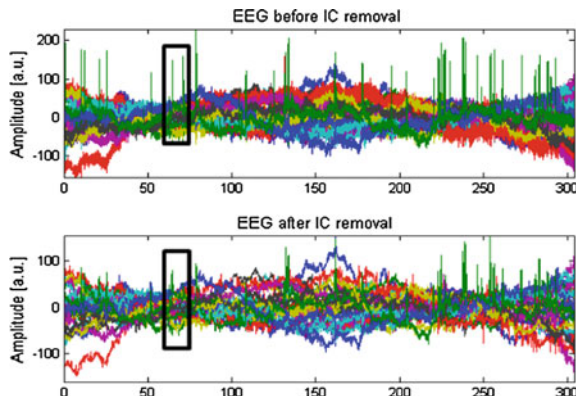
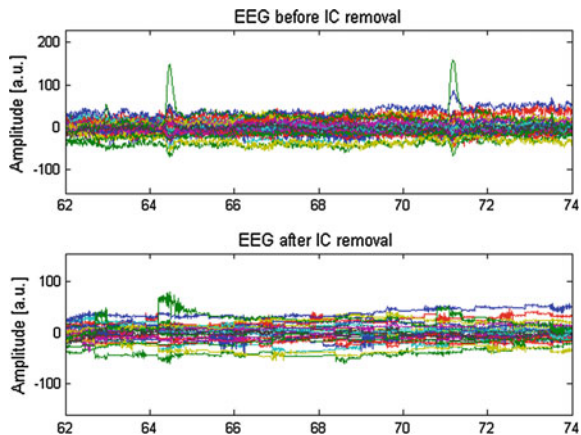


Fig. 10 EEG signal before and after correction of artefacts with Blind ICA. *Top* signal before artefact correction; *Bottom* signal after artefact correction. The *black window* indicates the region of the signal that is zoomed in the detail plot (Fig. 9)

5 Discussion

We studied the benefits of using an Eye-Tracker for the ultimate purpose of real-time, on-line Ocular Artefact correction of EEG data. To this end, we implemented standardised signal processing methods such as ICA or Wavelet Decomposition, as well as a Wiener Filter—a method not generally used in conventional “blind” EEG artefact correction. Eye-tracking provides automatic annotation of eye-movement artefact events. The approach here is pragmatic, we use the event annotation to perform targeted “blind” artefact removal: i.e. we make here as much as possible use of existing EEG processing pipelines, but guide their

Fig. 11 Detail plot of the EEG signal. *Top* signal before artefact correction; *Bottom* signal after artefact correction with Blind ICA



processing only to event-tagged periods of the data. Our results show that all 3 methods are successful in correcting eye movement artefacts, although Event-Driven ICA seems to yield the best signal after correction. This is expected, considering that the origins of the artefact and the signal are different, and thus minimising mutual information between potential sources is going to have significant benefits. When compared to the other methods, Blind ICA clearly is stricter with the data and sometimes leads to an over-correction. In Fig. 11 we can clearly see that the data, although it might preserve most of its frequency spectrum, has been severely affected by the corrective measure.

As expected from EEG data, there is high inter- and intra-subject variability on the EEG recordings; shape of head, changes in electrode impedance or subject behaviour can influence the data recordings, by introducing artefacts and non-linear trends in the signal. Moreover, attention or drowsiness can influence the Eye-Tracking data quality over longer usage times [24]. The Wiener Filter is the method that is most prone to failure, as it relies on an effective extraction of the average artefact. Moreover it will filter out all the frequencies represented in the artefact, which are low (duration of about 200 ms) [25] and thus can eliminate relevant information from the EEG signal [26, 3, 27].

One improvement that could be performed to the Wavelet Decomposition method is the use of a more complex adaptive thresholding technique, since the one used for this analysis combines only the mean and variance of the signal to obtain a threshold; other methods have been tested in “blind” approaches [28, 29] and thus could be implemented in this study. The ICA technique could be implemented as an online correction technique, though it would lead to some delay in the output of results. Wavelet and Wiener filter methods can only be used for post-processing and not for online correction with the approaches described in this work.

As further work we would like to appoint the validation of these techniques and their pertinence in artefact correction. A validation approach was attempted, with a Movement Imagery task and a simple K-Nearest Neighbours classifier. The goal

was to examine the classifier's accuracy for different methods of ocular artefact correction, but in the experiments the number of ocular artefacts was correlated with the Movement Imagery epochs (number of blinks increased in Movement Imagery and lowered in Rest epochs), thus proving this validation method as unable to accurately find the best corrective algorithm. Online implementation is although required for this purpose, but the usage of an eye tracker that is not affected by external electromagnetic fields (unlike, for example, electrooculograms or magnetic search coils [30]). Our work suggests simple steps towards a cleaner EEG signal, hopefully with more usable neural information being conveyed in it and useable in real-time.

The potential benefits of a clean EEG signal that can be expected are among a better understanding of neural signals and better use for these, such as in Brain Machine Interfaces that can be used to help patients suffering from Locked in Syndrome, as an example. The supervised clean-up of EEG data supports current developments in data-efficient EEG decoding algorithms [31] and by reducing spurious variability in a predictable way, the rapid automatic tuning of EEG-based systems in clinical settings where patient time is precious [32, 33]. Integration of EEG and eye tracking for artefact correction is going to become a natural by-product of BCI approaches for assistive devices, such as mind-controlled wheel-chairs [34], becoming multi-modal [35]. Thus, eye-tracking based EEG artefact removal is an *en passant* benefit that should be seized in the future.

Acknowledgments We acknowledge NEUROTECHNIX 2014 (Rome, Italy), where this work was originally contributed for their conference proceedings [36], and we are grateful that the paper was now selected for this publication format.

References

1. Bell, A.J., Sejnowski, T.J.: An information-maximization approach to blind separation and blind deconvolution. *Neural Comput.* **7**(6), 1129–1159 (1995)
2. Giannitrapani, D., Kayton, L.: Schizophrenia and EEG spectral analysis. *Electroencephal Clin. Neurophysiol.* **36**, 377–386 (1974)
3. Iber, C., Ancoli-Israel, S., Chesson., A.L., Quan, S.F.: The AASM Manual for the Scoring of Sleep and Associated Events: Rules, Terminology and Technical Specifications, 1st edn. American Academy of Sleep Medicine, Westchester
4. Faisal, A.A.: Stochastic simulation of neurons, axons and action potentials. *Stochast. Methods Neurosci.* 297–343 (2010)
5. Neishabouri, A., Faisal, A.A.: Axonal noise as a source of synaptic variability. *PLoS Comput. Biol.* **10**(5), e1003615 (2013)
6. Sengupta, B., Faisal, A.A., Laughlin, S.B., Niven, J.E.: The effect of cell size and channel density on neuronal information encoding and energy efficiency. *J. Cereb. Blood Flow Metab.* **33**(9), 1465–1473 (2013)
7. Faisal, A.A., Selen, L.P.J., Wolpert, D.M.: Noise in the nervous system. *Nat. Rev. Neurosci.* **9** (4), 292–303 (2008)

8. Iwasaki, M., Kellinghaus, C., Alexopoulos, A.V., Burgess, R.C., et al.: Effects of eyelid closure, blinks, and eye movements on the electroencephalogram. *Clin. Neurophysiol.* **116**(4), 878–885 (2005)
9. Abbott, W.W., Faisal, A.A.: Ultra-low-cost 3D gaze estimation: an intuitive high information throughput compliment to direct brain-machine interfaces. *J. Neural Eng.* **9**(4), 046016 (2012)
10. Abbott, W.W., Zucconi, A., Faisal, A.A.: Large-field study of ultra low-cost, non-invasive task level BMI: In: 6th International IEEE/EMBS Conference on Neural Engineering (NER), pp. 97–100 (2013)
11. Yoo, K.-S., Basa, T., Lee, W.-H.: Removal of eye blink artifacts from EEG signals based on cross-correlation. In: International Conference on Convergence Information Technology. pp. 2005–2014 (2007)
12. Kumar, P.S., Arumuganathan, R., Sivakumar, K., Vimal, C.: Removal of ocular artifacts in the EEG through wavelet transform without using an EOG reference channel. *Int. J. Open Probl. Compt. Math.* **1**(3), 188–200 (2008)
13. Vigário, R.N.: Extraction of ocular artefacts from EEG using independent component analysis. *Electroencephalogr. Clin. Neurophysiol.* **103**(3), 395–404 (1997)
14. Jervis, B.W., Coelho, M., Morgan, G.W.: Effect on EEG responses of removing ocular artifacts by proportional EOG subtraction. *Med. Biol. Eng. Comput.* **27**(5), 484–490 (1989)
15. Brainard, D.H.: The psychophysics toolbox. *Spat. Vis.* **10**(4), 433–436 (1997)
16. Lee, T.-W.: Independent Component Analysis—Theory and Applications, 1st edn. Springer Science+Business Media, Dordrecht (1998)
17. Lee, T.-W., Girolami, M., Sejnowski, T.J.: Independent component analysis using an extended infomax algorithm for mixed sub-Gaussian and super-Gaussian sources. *Neural Comput.* **11**(2), 417–441 (1999)
18. Papoulis, A., Pillai, U.: Probability, Random Variables and Stochastic Processes, 4th edn. McGraw-Hill, New York (2002)
19. Nason, G.P., Silverman, B.W.: The stationary wavelet transform and some statistical applications. *Lect. Notes Stat.* **103**, 281–299 (1995)
20. Daubechies, I.: The wavelet transform, time-frequency localization and signal analysis. *IEEE Trans. Info. Theory* **36**(5), 961–1005 (1990)
21. Izzetoglu, M., Devaraj, A., Bunce, S., Onaral, B.: Motion artifact cancellation in NIR spectroscopy using wiener filtering. *IEEE Trans. Biomed. Eng.* **52**(5), 934–938 (2005)
22. Chen, J., Benesty, J., Huang, Yiteng, Doclo, S.: New insights into the noise reduction Wiener filter. *IEEE Trans. Audio Speech Lang. Process.* **14**(4), 1218–1234 (2006)
23. Kailath, T., Sayed, A.H., Hassibi, B.: Linear Estimation. Prentice Hall, Upper Saddle River (2000)
24. Di Stasi, L.L., McCamy, M.B., Catena, A., Macknik, S.L., et al.: Microsaccade and drift dynamics reflect mental fatigue. *Eur. J. Neurosci.* **38**(3), 2389–2398 (2013)
25. Caffier, P.P., Erdmann, U., Ullsperger, P.: Experimental evaluation of eye-blink parameters as a drowsiness measure. *Eur. J. App. Physiol.* **89**(3), 319–325 (2003)
26. Harmony, T., Fernández, T., Silva, J., Bosch, J., et al.: Do specific EEG frequencies indicate different processes during mental calculation? *Neurosci. Lett.* **266**(1), 25–28 (1999)
27. Whitham, E.M., Pope, K.J., Fitzgibbon, S.P., Lewis, T., et al.: Scalp electrical recording during paralysis: quantitative evidence that EEG frequencies above 20 Hz are contaminated by EMG. *Clin. Neurophysiol.* **18**(8), 1877–1888 (2007)
28. Stein, C.M.: Estimation of the mean of a multivariate normal distribution. *Ann. Stat.* **9**(6), 1135–1151 (1981)
29. Krishnaveni, V., Jayaraman, S., Anitha, L., Ramadoss, K.: Removal of ocular artifacts from EEG using adaptive thresholding of wavelet coefficients. *J. Neural Eng.* **3**(4), 338–346 (2006)
30. Schlag, J., Merker, B., Schlag-Rey, M.: Comparison of EOG and search coil techniques in long-term measurements of eye position in alert monkey and cat. *Vision. Res.* **23**(10), 1025–1030 (1983)

31. Ferrante, A., Gavriel, C., Faisal, A.: Data-efficient hand motor imagery decoding in EEG-BCI by using Morlet wavelets and common spatial pattern algorithms. In: IEEE/EMBS Neural Engineering (NER), pp. 948–951 (2015)
32. Lowery, C., Faisal, A.: Towards efficient, personalized anesthesia using continuous reinforcement learning for propofol infusion control. In: IEEE/EMBS Neural Engineering (NER), p. 1414–1417 (2013)
33. Ferrante, A., Gavriel, C., Aldo Faisal, A.: Towards a brain-derived neurofeedback framework for unsupervised personalisation of brain-computer interfaces. In: IEEE/EMBS Neural Engineering (NER), pp. 162–165 (2015)
34. Ktena, S.-I., Abbott, W.W., Faisal, A.: A virtual reality platform for safe evaluation and training of natural gaze-based wheelchair driving. In: IEEE/EMBS Neural Engineering (NER), pp. 236–239 (2015)
35. Xiloyannis, M., Gavriel, C., Thomik, A., Faisal, A.: Dynamic forward prediction for prosthetic hand control by integration of EMG, MMG and kinematic signals. In: IEEE/EMBS Neural Engineering (NER), p. 611–614 (2015)
36. Lourenço, P.R., Abbott, W.W., Faisal, A.A.: EEG and eye tracking integration for ocular artefact correction. *Neurotechnix* **2014**, 79–86 (2014)
37. Faisal, A.A., Fislage, M., Pomplun, M., Rae, R., Ritter, H.: Observation of human eye movements to simulate visual exploration of complex scenes. *SFB Rep.* **360**, 1–34 (1998)
38. Saatchi, M.R., Oke, S., Allen, E.M., Jervis, B.W., et al.: Signal processing of the contingent negative variation in schizophrenia using multilayer perceptrons and predictive statistical diagnosis. *IEE Proc. Sci. Meas. Technol.* **142**(4), 269–276 (1995)

An fMRI-Compatible System for 3DOF Motion Tracking of Objects in Haptic Motor Control Studies

M. Rodríguez, A. Sylaidi and A.A. Faisal

Abstract Fusing naturalistic motor psychophysics with neuroimaging remains a key challenge in neuroscience, given that the former requires advanced motion tracking and the latter commonly entails certain technical compatibility constraints. Here we designed and developed fMOVE, a novel 3DOF fMRI-compatible motion tracking system to support realistic object manipulation (haptic) tasks during a neuroimaging session. fMOVE constitutes an ultra-low-cost technology, based on a standardized zoom-lens camera and ARTToolkit, a software library for augmented reality applications. Motion tracking occurs with a 120 Hz frequency, that lies within the range of established fMRI-incompatible motion tracking methods. It captures the real-time movement of a marked hand-held object and provides online feedback of motor performance to subjects, thereby enabling closed-loop motor control and learning experiments. Tracking accuracy was tested against the performance levels of a commercial electromagnetic motion tracker. fMOVE thus constitutes a promising methodological platform to pursue the real-time, closed-loop study of motor behavior in real-world tasks and decipher its underlying neural mechanisms.

Keywords fMRI · Motion tracking · Low cost · Object manipulation

1 Introduction

On a daily basis, humans acquire new motor skills or enhance their performance on already encountered motor tasks. Occasionally, they may also re-acquire skills, which are difficult to perform or cannot be executed because of injury or disease.

M. Rodríguez (✉) · A. Sylaidi · A.A. Faisal
Bioengineering Department, Imperial College London, London, UK
e-mail: marisol.ru@gmail.com

A.A. Faisal
Computing Department, Imperial College London, London, UK
e-mail: a.faisal@imperial.ac.uk

The motor learning experience in all these cases involves a number of different processes, which support motor behaviour through interacting and/or hierarchical roles.

At the level of information extraction, skilled performance is based on the efficient gathering of information from the environment. Humans use task dependent attentional mechanisms to actively select [3, 4] and integrate multisensory stimuli [2]. They uncover the dynamics of a task by learning key properties of their body and the world [1, 11]. Crucially, they determine the necessary motor commands so as to optimize their performance according to task goals [12, 13]. This process ranges from high-level decision making that dictates the structure of an effective control policy to low-level optimization of the execution of the selected policy.

Although motor behaviour has been systematically studied for more than 100 years, the mechanisms that underlie motor learning and the formation of control policies remain unclear. A large body of research has examined motor behaviour through psychophysical experiments, which provide insight into the patterns of adaptive responses in tasks that introduce changes in the target, the workspace or the force-field [9, 10, 15]. Such studies have relied primarily on behavioural data and have inspired a number of computational approaches that describe abstract mechanisms of the interplay between perception and action (e.g. optimal feedback control, reinforcement learning, Bayesian inference).

Despite this substantial progress in computational sensorimotor control, less methodological advancement has been achieved in linking computational models to their underlying neurophysiological correlates. Brain imaging based on fMRI, one of the predominant technological paradigms to access the neural implementation level, has been primarily used in studies that examine purely cognitive tasks. In the less common cases, in which fMRI has been employed in motor neuroscience research, the examined functions refer to simple, lab-constrained movements (e.g. finger-tapping) and the designed experiments instruct non-realistic open-loop tasks, which do not provide any sensory feedback of performance so as to encourage learning. The main reason for this restriction lies in the technical constraints, which are interwoven with the fMRI function and which often set its use as incompatible to most advanced motion tracking systems.

Here we designed and built an fMRI-compatible motion tracking system that allows us to examine how humans learn complex motor tasks. Our proposal, fMOVE, constitutes a system capable of acquiring information about 3D motion inside an fMRI scanner in a 3 degrees-of-freedom context. The designed platform can host closed-loop motion studies by establishing continuous motion tracking and providing human subjects with online virtual feedback of their motor behaviour and performance. fMOVE thus provides an expansion of conventional motion tracking methods used in fMRI, which are commonly used to improve the analysis of fMRI data (compensation for head and body motion) or adjust the block design to the actual motion start and pause.

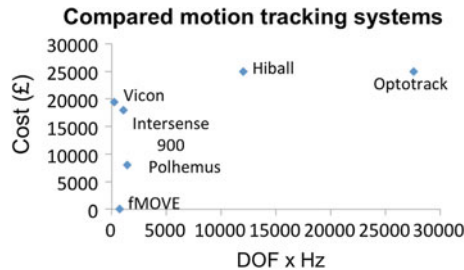


Fig. 1 Comparison of fMOVE and commercial motion tracking systems. fMOVE has the lowest cost and possesses motion tracking performance within the range covered by established motion trackers (e.g. Polhemus, Vicon). The processing power of the displayed systems is estimated as the product of DOF and processing frequency

At the same time fMOVE possesses motion tracking performance in the same range as established fMRI-incompatible motion tracking methods (e.g. Vicon with motion tracking at 1DOF and 250 Hz, Intersense 900 at 6DOF and 180 Hz, Polhemus Liberty at 6DOF and 240 Hz) and is significantly cheaper than other fMRI-incompatible technologies with better information processing features (e.g. Hiball with motion tracking at 6DOF and 2000 Hz, Optotrack at 6DOF and 4600 Hz) (Fig. 1).

The development of the software that supports this platform is based on the use of ARTToolkit, a software library for building Augmented Reality applications. The motion tracking setup was developed inside a simulated fMRI environment to match the fMRI scanner located at the Clinical Imaging Facility at Hammersmith Hospital, London, UK.

2 Materials and Methods

2.1 Hardware Development

Our system consists of the motion tracking installation inside the fMRI environment and the software that runs the experiment by adapting its phases and provided feedback to the subject's captured performance. In particular, subjects lay inside the fMRI-scanner holding the fMOVE object in their dominant hand. The fMOVE adjusted camera is installed at the distal end of the scanner room with its telezoom lens facing the foot-end view of the scanner cylinder with the hand-held object clearly visible (Fig. 2b). Camera images are processed in real-time by laptop-based system which controls the experiment and can present real-time feedback to the patient via the scanner's visual display setup.

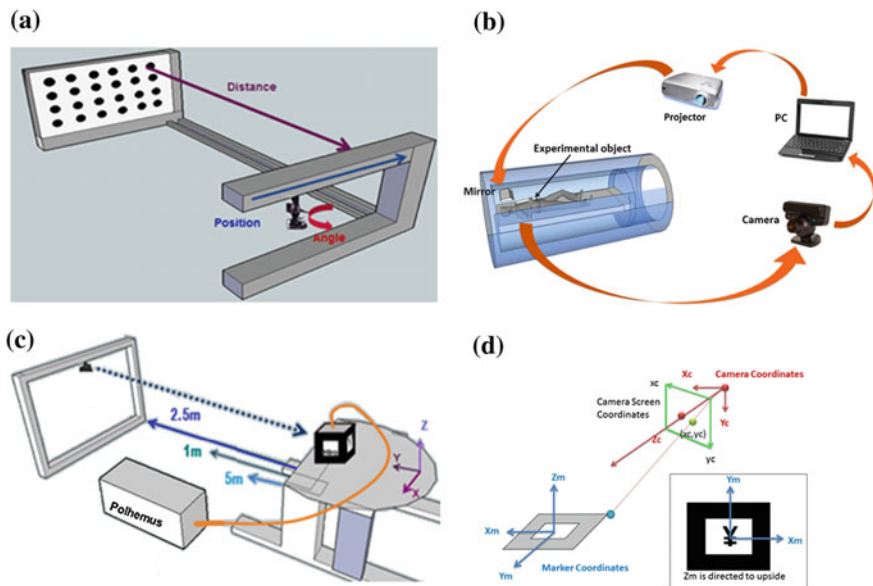


Fig. 2 **a** Setup for the one-time calibration for any camera system to be used with fMOVE system. Rigid aluminium frames allow mounting of camera and target calibration pattern at defined position and orientation. **b** fMOVE system in use: healthy subject lying inside the fMRI-scanner holding the fMOVE object in his right hand. Camera installed at the distal end of the scanner room with its telezoom lens facing the foot-end view of the scanner cylinder with the hand-held object clearly visible. Camera images are processed in real-time by laptop-based system which controls the experiment and can present real-time feedback to the patient via the scanner's visual display setup. **c** Set-up to measure the motion tracking performance of the fMOVE system against a commercial electromagnetic (i.e. non-optical) motion tracking system used as reference gold-standard (LIBERTY polhemus). A reference fMOVE object (*black cube*) which contains the magnetic motion-tracking sensor is moved at defined distances and orientations. See text for details. **d** The coordinate systems used by fMOVE include the camera coordinates (X_c , Y_x —green coordinate arrows), the coordinate system of the camera view (x_c , y_c —green coordinate arrows) and the relative coordinates of the fMOVE object surface(s) (X_m , Y_m , Z_m —blue coordinate arrows)

We used a PlayStation 3 Eye ® camera to track the motion of markers attached to a hand-held object. This camera is able to work with frame rates of 120 Hz at a 320×240 pixel resolution and can also work with frame rates of 60 Hz at 640×480 if more resolution is needed. In addition, this device can be set for close up framing at 56° field of view or 75° for long shot framing. All these features provide the camera a satisfying image acquisition quality for the needs of our motion tracking setup. Its market price of 23€ constitutes the sole cost of fMOVE and therefore establishes the latter as the cheapest 3DOF motion tracking technology amongst a number of commercially available systems (Fig. 1). fMOVE's motion tracking accuracy was tested for 3 different camera lenses in order to examine whether the markers are captured successfully both for smaller and larger

distances to the camera. We selected the variable lens focal lengths taking into account three different distances to the camera (0.5, 1, 2.5 m) based on:

$$f = \frac{w_{CMOS} \cdot D}{FOV} \quad (1)$$

where f denotes the focal length, w_{CMOS} the width of the CMOS sensor (3.98 mm), FOV the Field Of View (400 mm), D the distance between the camera and the tracked marker. The focal lengths for the different distances were estimated as 6.35, 12 and 35 mm.

2.2 Calibration

The camera was calibrated in a setup, which consists of two reference planes; the marker and the camera plane (Fig. 2a). The marker plane remained fixed throughout the calibration whereas the camera plane could be rotated around a reference point and translated away from or closer to the marker plane. The camera was positioned at a fixed height on the camera plane and at variable distances to the camera plane's rotation axis. Altogether in each calibration we tested three different camera positions with regard to the camera plane rotation axis (11.5, 18.5, and 25.5 cm), three different camera plane rotation angles (29° , -17° , 19° or/and 65°) and three different camera plane distances to the marker plane (either 33, 49.5, 41 or 56.5, 45, 37 cm).

2.3 Coordinate Systems

Our motion tracking platform takes three coordinates systems into account: a camera screen based (2D), a camera based (3D) and a marker based (3D) (Fig. 2d). The marker coordinate system is located in the centre of the marker, having X_m and Y_m parallel to the borders of the marker, and Z_m pointing away from the marker. The centre of the marker is defined as $(X_m, Y_m, Z_m) = (0, 0, 0)$. The relationship between the camera and marker coordinate system is determined through rotational and translational operations based on:

$$\begin{pmatrix} X_c \\ Y_c \\ Z_c \\ 1 \end{pmatrix} = \begin{pmatrix} R_{11} & R_{12} & R_{13} & T_1 \\ R_{21} & R_{22} & R_{23} & T_2 \\ R_{31} & R_{32} & R_{33} & T_3 \\ 0 & 0 & 0 & 1 \end{pmatrix} \cdot \begin{pmatrix} 0 \\ 0 \\ -V/2 \\ 1 \end{pmatrix} \quad (2)$$

where R_{ij} and T_i determine the values of rotation and translation matrices respectively [6] and V denotes an edge of the cubic component of the object; it has a negative sign due to the orientation of the axes of the camera based coordinate system.

2.4 Testing the Motion Tracking Accuracy

In order to assess the tracking accuracy of fMOVE, the system was compared with Polhemus Liberty, a commercial electromagnetic motion tracker (Fig. 2c). One Polhemus sensor was positioned exactly in the centre of an exemplary multi-marker object. The designed object was free of metal so as to suit usage inside the fMRI scanner. It consisted of a wooden handle and a plastic cube at the surfaces of which we attached four different ARToolkit compatible markers. These markers can be identified by the image processing algorithm of our system and assigned to a different label according to the pattern they display. Labelling the different patterns enabled the identification of rotational movements.

In this setup, the object's 3D position could be tracked simultaneously by the calibrated camera of fMOVE and the electromagnetic sensor. The two streams of motion data were subsequently compared after their respective reference coordinate systems were aligned. The estimated error between them was used as a performance measure for fMOVE's motion tracking accuracy in translational and rotational movements of the object.

Translational movements were constrained between the borders of a specified workspace. During translation, the camera was always tracking the same face and consequently the same marker on the object. On the other hand, during rotational movements within the same workspace borders, the system's motion tracking switched between the different markers positioned on the object surfaces.

3 Results

We assessed the tracking accuracy of fMOVE by testing its position measurements against a widely used electromagnetic motion tracker (Polhemus Liberty). The comparison was performed for three different distances between camera and object plane (0.5, 1 and 2.5 m). For each of these three cases we completed 15 trials of movements. In 10 of these the object was translated and in the remaining 5 it was rotated.

After temporally and spatially aligning the position measurements of the marker-based fMOVE and the sensor-based Polhemus Liberty, we noticed that our motion tracking system acquires data streams that accurately match our ground truth. This matching is evident in the overlaid position plots for both translational

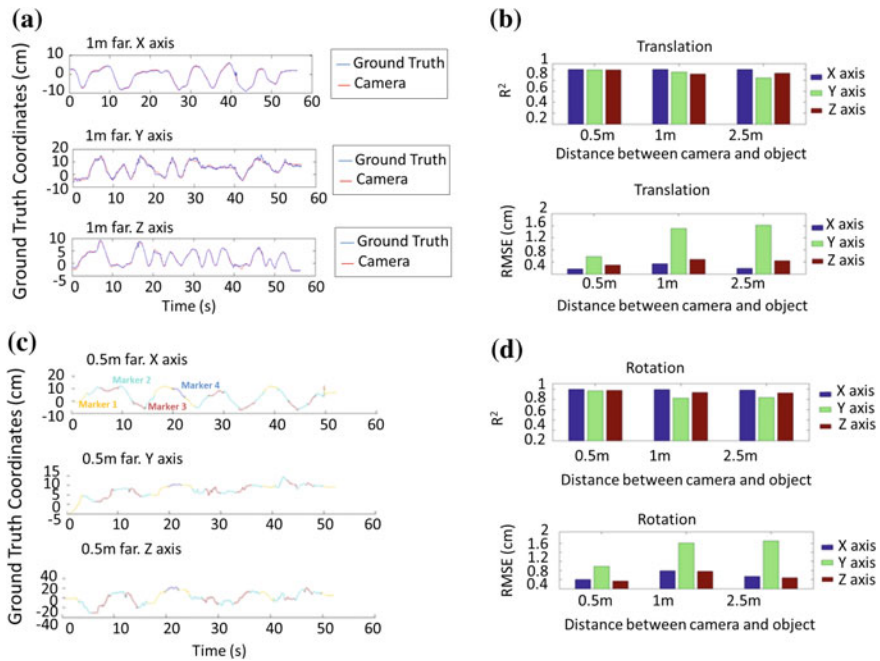


Fig. 3 **a** Spatial and temporal alignment of fMOVE and Polhemus data during translational movements in X, Y and Z axis. **b** fMOVE and ground truth comparison based on R^2 and Root Mean Squared Error (RMSE) for translational movements in X, Y and Z axis. **c** Spatial and temporal alignment of fMOVE and Polhemus data during rotational movements in X, Y and Z axis. **d** fMOVE and ground truth comparison based on R^2 and RMSE for rotational movements in X, Y and Z axis

and rotational trials (Fig. 3a, c). In fact, during rotational movements fMOVE manages to efficiently avoid tracking omissions, by switching from one marker to another (as is evident in the color-coding of Fig. 3).

Two measures of comparison of the acquired data streams (R^2 and RMSE) verify the efficiency of fMOVE in motion tracking (Fig. 3b, d). In translational movements R^2 reflects over 84 % accuracy for all tested distances between camera and tracked object. The lowest R^2 level ($R^2 = 0.846$) is estimated for the largest distance (2.5 m) in the y-dimension. The same case produces the highest RMSE (RMSE = 1.6181 cm). Throughout all cases, the y-dimension produces the highest error levels, which reflects the fact that fMOVE is mostly sensitive along the axis that connects the camera centre with the marker centre. Even these instances however, do not significantly affect the R^2 levels as displayed in Fig. 3b.

Similarly, in rotational movements our assessment verifies a matching between the measurements of our system and the ground truth. The lowest R^2 level ($R^2 = 0.8214$) is estimated again for the largest distance (2.5 m) in the y-dimension (Fig. 3c) for which the corresponding RMSE = 1.6181 cm (Fig. 3d). As in the

translational movements, the largest tracking errors here are noted again in the y-dimension. It is thus evident that fMOVE displays its highest sensitivity in the y-direction for a broader range of movements.

4 Conclusions

We designed and built fMOVE, an fMRI-compatible marker-based motion tracking system capable of capturing 3 DOF movement. The system acquires behavioral data from subjects, while they manipulate a marked object inside an fMRI scanner and it provides to them online visual feedback of motion and task performance.

We tested the efficiency of the system against Polhemus Liberty, a commercial electromagnetic motion tracker, which operates with high accuracy at 240 updates per second. We found that fMOVE achieves high tracking accuracy for both translational and rotational movements of the markers and preserves this accuracy for variable distances of the camera to the moving object.

fMOVE poses technical advantages since it allows high frequency data acquisition inside the fMRI environment which is commonly incompatible to all widely used motion tracking technologies, due to the applied magnetic field. Our system is amenable to further customization depending on the needs of the experimental study, designed to be carried out inside the scanner. Such customization can include developing a multiple-marker tracking algorithm, so as to increase the motion tracking accuracy, avoid false marker detections and cover the motion of multiple body parts or more complex behavioural tasks.

Importantly, apart from its compatibility to the fMRI environment, fMOVE constitutes an ultra-low-cost motion tracking technology, that limits expenses to the price of the used camera. At the same time, the methodological platform it supports, offers promising advantages for future studies of motor behaviour [5, 7, 14]. It namely enables a tight integration of psychophysical and functional imaging [7] studies and can thereby guide investigations of the still unknown neural foundation of cortical action selection and motor learning rules.

Acknowledgments We acknowledge NEUROTECHNIX 2014 (Rome, Italy), where this work was originally contributed for their conference proceedings [8], and we are grateful that the paper was now selected for this publication format.

References

- Brayanov, J.B., Press, D.Z., Smith, M.A.: Motor memory is encoded as a gain-field combination of intrinsic and extrinsic action representations. *J. Neurosci.* (2012). doi:[10.1523/JNEUROSCI.1928-12.2012](https://doi.org/10.1523/JNEUROSCI.1928-12.2012)
- Faisal, A.A., Wolpert, D.M.: Near optimal combination of sensory and motor uncertainty in time during a naturalistic perception-action task. *J. Neurophysiol.* **101**(4), 1901–1912 (2009)

3. Friston, K.: The free-energy principle: a unified brain theory? *Nat. Rev. Neurosci.* **11**(2), 127–138 (2010)
4. Friston, K.J., Daunizeau, J., Kiebel, S.J.: Reinforcement learning or active inference? *PLoS. ONE.* **4**, (2009). doi:[10.1371/journal.pone.0006421](https://doi.org/10.1371/journal.pone.0006421)
5. Hecht, E.E., Gutman, D.A., Khreichesh, N., Taylor, S.V., Kilner, J., Faisal, A.A., Bradley, B. A., Chaminade, T., Stoud, D.: Acquisition of paleolithic toolmaking abilities involves structural remodeling to inferior frontoparietal regions. *Brain. Struct. Funct.*, 1–17 (2014)
6. Kato, H., Billinghamurst, M.: Marker tracking and HMD calibration for a video-based augmented reality conferencing system. In: Proceedings. 2nd IEEE and ACM International Workshop on Augmented Reality. (IWAR'99) , pp. 85–94. (1999)
7. Lorenz, R., Monti, R., Violante, R., Anagnostopoulos, C., Faisal, A., Montana, G., Leech, R.: *Bioarxiv* (2015)
8. Rodriguez, M., Sylaidi, A., Faisal, A.A.: Developing a novel fMRI-compatible motion tracking system for haptic motor control experiments. *Neurotechnix* **2014**, 25–30 (2014)
9. Shadmehr, R., Moussavi, Z.M.: Spatial generalization from learning dynamics of reaching movements. *J Neurosci. : J. Soc. Neurosci.* **20**, 7807–7815 (2000)
10. Shadmehr, R., Mussa-Ivaldi, F. A.: Adaptive representation of dynamics during learning of a motor task. *J Neurosci. : J. Soc. Neurosci.* **14**, 3208–3224 (1994)
11. Sylaidi, A., Faisal A.A.: What is the hierarchical representation of tasks involving objects with complex internal dynamics? *Front. Comput. Neurosci.* (2012). doi:[10.3389/conf.fncm.2012.55.00129](https://doi.org/10.3389/conf.fncm.2012.55.00129)
12. Todorov, E. Optimality principles in sensorimotor control. *Nat. Neurosci.* **7**, 907–915 (2004). doi:[10.1038/nn1309](https://doi.org/10.1038/nn1309)
13. Todorov, E., Jordan, M.I.: Optimal feedback control as a theory of motor coordination. *Nat. Neurosci.* **5**, 1226–1235 (2002). doi:[10.1038/nn963](https://doi.org/10.1038/nn963)
14. Wolpert, D.M., Flanagan, J.R.: Motor learning. *Curr. Biol.*, 467–472 (2010)
15. Wolpert, D.M., Diedrichsen, J., Flanagan, J.R.: Principles of sensorimotor learning. *Nat. Rev. Neurosci.* **12**(12), 739–751 (2011). doi:[10.1038/nrn3112](https://doi.org/10.1038/nrn3112)

Comparing Methods for Decoding Movement Trajectory from ECoG in Chronic Stroke Patients

Martin Spüler, Florian Grimm, Alireza Gharabaghi, Martin Bogdan and Wolfgang Rosenstiel

Abstract Decoding the neural activity based on ECoG signals is widely used in the field of Brain-Computer Interfaces (BCIs) to predict movement trajectories or control a prosthetic device. However, there are only few reports of using ECoG in stroke patients. In this paper, we compare different methods for predicting contralateral movement trajectories from epidural ECoG signals recorded over the lesioned hemisphere in three chronic stroke patients. The results show that movement trajectories can be predicted with correlation coefficients ranging from 0.24 to 0.64. Depending on the intended application, either the use of Support Vector Regression (SVR) or Canonical Correlation Analysis (CCA) obtained the best results. By investigating how ECoG based decoding performs in comparison with EMG based decoding it becomes visible that abnormal muscle activation patterns affect the prediction and that using activity of only the forearm muscles, there is no significant difference between ECoG and EMG for predicting wrist movement trajectory.

M. Spüler (✉) · W. Rosenstiel

Department of Computer Engineering, Wilhelm Schickard Institute for Computer Science,
University of Tübingen, Sand 13, 72076 Tübingen, Germany
e-mail: spueler@informatik.uni-tuebingen.de

W. Rosenstiel

e-mail: Wolfgang.Rosenstiel@uni-tuebingen.de

F. Grimm · A. Gharabaghi

Functional and Restorative Neurosurgery Unit, Department of Neurosurgery,
University Clinic Tübingen, Tübingen, Germany
e-mail: florian.grimme@cin.uni-tuebingen.de

A. Gharabaghi

e-mail: alireza.gharabaghi@uni-tuebingen.de

M. Bogdan

Department of Computer Engineering, University of Leipzig, Augustusplatz 10,
04109 Leipzig, Germany
e-mail: bogdan@informatik.uni-leipzig.de

1 Introduction

In the last decade, Brain-Computer Interfaces (BCIs) or Brain-Machine Interfaces (BMIs) have become increasingly popular as a tool that translates brain activity into output signals to control a computer, a robot or an assistive device. This technology might be useful for people suffering from paresis due to neurodegenerative diseases, traumatic brain injuries or stroke. More than 80 % of the patients surviving a stroke are affected by hemiparesis [1] and in 30 to 66 % of those hemiparetic stroke patients the paretic arm remains without function when measured 6 months after stroke [2]. While BCIs might help those patients as an assistive device to compensate the missing motor function [3], they can also be used as tool for rehabilitation.

The use of BCI for stroke rehabilitation has been particularly prominent in the last time [4–9]. In this neurorehabilitation approach, the patients' intention to move is coupled with haptic feedback given through an orthosis moving the paretic limb [4]. Since the connection between the sensorimotor cortex and the peripheral muscles is disrupted by stroke, a coincident activation of the primary motor cortex and the sensory feedback loop may induce Hebbian plasticity and thus support functional recovery [10].

Stroke patients tend to perform compensatory movements [11], which can be a problem when using BCI feedback for stroke rehabilitation, since compensatory movements produce brain activity which is unrelated to the intended movement [12] but inadvertently influences BCI feedback. Therefore it would be beneficial if brain activity related to compensatory movements could be separated from the activity related to the intended movement and only activity related to the intended movement is feedbacked by the BCI.

In this paper we evaluate different methods for the prediction of wrist movement trajectory based on ipsilesional Electrocorticography (ECoG) data in chronic stroke patients. A special emphasis is given on the use of Canonical Correlation Analysis (CCA) for this purpose. While CCA has been previously used for SSVEP BCIs [13], c-VEP BCIs [14], as well as general spatial filtering method for classification of evoked or event-related potentials [15], we show in this paper how it can also be used for trajectory prediction and extraction of movement components from the trajectory data, which may help to feedback brain activity related to the true movement intention.

2 Methods

In this section we describe the methods we evaluated for the prediction of the movement trajectory, the evaluation process itself, as well as the ECoG (and EMG) data used for evaluation.

Since the use of Canonical Correlation Analysis yields some particularly interesting results, we will explain the CCA method and its application in more detail.

2.1 Canonical Correlation Analysis (CCA)

CCA is a multivariate statistical method developed by Hotelling [16]. When having two datasets, which may have some underlying correlations, CCA can be used to find linear transformations for these two datasets, which maximize the correlation between the transformed datasets. Assuming there are two multidimensional datasets X and Y with p variables in $X = (X_1, X_2, \dots, X_p)^T$ and $q \leq p$ variables in $Y = (Y_1, Y_2, \dots, Y_q)^T$ and their transformed datasets $U = W_x^T X = (U_1, U_2, \dots, U_q)^T$ and $V = W_y^T Y = (V_1, V_2, \dots, V_q)^T$. CCA can be used to find the two transformations W_x and W_y , which maximize the canonical correlation ρ_i^* between the canonical variables U_i and V_i .

$$\rho_i^* = \frac{\text{cov}(U_i, V_i)}{\sqrt{\text{var}(U_i)\text{var}(V_i)}} \quad (1)$$

The linear transformations W_x and W_y are selected so that their variance equals one, while they are uncorrelated to all other canonical variables.

$$\text{var}(U_i) = \text{var}(V_i) = 1 \quad (2)$$

$$\text{cov}(U_i, V_j) = \text{cov}(U_j, V_i) = 0, \forall i \neq j \quad (3)$$

2.1.1 CCA and Linear Regression

A traditional regression can be formulated as having a multidimensional dataset X with dimensions $n \times p$ containing n observations of p variables and another dataset Y with dimensions $n \times 1$ containing the dependent variable. A linear regression tries to model the relationship between X and Y by finding a weight vector W with dimensions $p \times 1$ so that

$$Y_i = X_i W + \varepsilon_i \quad (4)$$

with ε_i being the error term which should be minimal. Thereby one can use W to predict Y' based on the observations contained in X .

$$Y' = XW \quad (5)$$

In the case of an ordinary least squares regression, this problem is solved by finding a W that minimizes the sum of the squared differences between the predicted Y' and the observed Y . With $\|\cdot\|$ being the euclidean distance, the problem can be written as:

$$\min \|Y - Y'\|^2 = \|XW - Y'\|^2 \quad (6)$$

CCA can also be used to solve a regression problem. Applying CCA to X and Y , the method tries to find a transformation W_x that maximized the correlation

$$\rho = \frac{W_x^T X Y^T W_y}{\sqrt{(W_x^T X X^T W_x)(W_y^T Y Y^T W_y)}} \quad (7)$$

The results is W_x being a weight vector with dimensions $p \times 1$ and W_y being a scalar, which can be used to predict Y with

$$Y' = XW \cdot W_y^{-1} \quad (8)$$

Since CCA only maximizes the correlation, CCA can only be used for regression methods under the condition that X and Y have a mean of 0. If this condition holds, CCA delivers results similar to other linear regression methods. Relationships between least squares and CCA have been established earlier in the literature. Hastie et al. [17] found CCA to be equivalent to Fisher Linear Discriment Analysis in a binary-class case, which in turn was found to be equivalent to least squares problems in this case [18]. Sun et al. [19] showed that CCA can be formulated as least squares problem which can be used to introduce regularized CCA and sparse CCA (using L1-norm regularization).

2.1.2 CCA and Component Analysis

While we have outlined the relationship between CCA and linear (least squares) regression, there is also a distinct relationship between CCA and methods for component analysis like independent component analysis (ICA) and principal component analysis (PCA).

If CCA is used with a multidimensional dataset Y , the resulting transformation matrix W_y can be used as transformation matrix that separates the dataset Y in different components (called canonical variables in the context of CCA). Due to the constraints how CCA selects W_y (see Eqs. 2 and 3), the resulting components are uncorrelated, which is also the case for ICA and PCA. Therefore, CCA can be seen as a method that extracts components V from Y , with the components V being maximally correlated to $U = W_x^T X$.

Table 1 Demographic data for the three chronic stroke patients

Patient	Age	Sex	FMA	FMB	FMC	TSI
P1	63	f	9	0	0	71
P2	56	m	19	3	1	80
P3	52	m	13	6	2	159

Age, Sex, Fugl-Meyer Score for upper extremity (FMA, max 30), wrist (FMB, max 10), hand (FMC, max 14) and the time since insult (TSI) in month

2.2 Data

2.2.1 Patient Description

The ECoG and EMG data used in this study was recorded from 3 patients who suffered from left-sided chronic handparesis due to stroke. The patients took part in a long-term investigational study for motor cortex stimulation with epidural implants concurrent to rehabilitation training to improve upper limb motor function after stroke. The study protocol was approved by the local ethics committee (Faculty of Medicine, University Hospital Tübingen) and included an initial 4 week evaluation period immediately after implantation of the ECoG grids to investigate patients individual cortical physiology for optimization of stimulation location and paradigms. Data recorded during that evaluation period was used for the evaluation of the method presented in this paper. An overview of the patients' demographic data and the Fugl-Meyer scores [21] for wrist movement (FMB) are shown in Table 1.

Each of the 3 patients was epidurally implanted with 16 platinum disk electrodes (Medtronic, Inc.) with a diameter of 4 mm, which were arranged in 4 strips with 4 electrodes each. The strips were placed in a grid-like fashion with a center-to-center distance of 1 cm. Although technically these are 4 strips, we will refer to it as one grid. These grids were placed above the hand area of the ipsilesional motor cortex and also covered premotor and sensory areas. The location of the grids are shown in Fig. 1. More detailed information about the patients can be found in a previous publication [20].

2.2.2 Task Description

During the aforementioned evaluation period, the patients also participated in a robot-assisted stroke rehabilitation program and ECoG data was recorded during the performed exercises. Each of the patients participated in 10 to 20 sessions performed on different days in which they had to repeat wrist extension and wrist flexion several times using their paretic arm. On average 8 min of wrist extension/flexion were recorded per session.

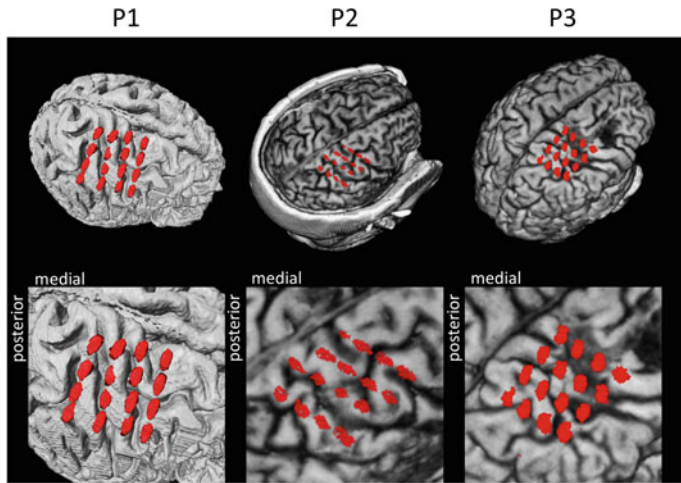


Fig. 1 Locations of the epidurally implanted ECoG electrodes. Patients were implanted with 4 strips with 4 electrodes each. MRI images are reproduced from a previous publication [20]

The degree to which the patients were able to perform extension/flexion varied, but movement was supported by an upper limb rehabilitation robot (Hocoma Armeo Spring), which removed gravitational effects. Further, the robot allowed movement along 7 degrees of freedom (DOF) with the angle of the 7 joints being constantly recorded.

Although the patients were instructed to do a wrist extension/flexion (needing only 1 DOF), movement along several DOF was visible due to coactivation and compensatory movements resulting from stroke. Therefore, the performed (and recorded) trajectory does not match the actual intended movement trajectory and also there is a movement trajectory present for the other DOF, where no movement was intended.

2.3 ECoG Data Processing and Feature Extraction

ECoG signals were recorded with Brainamp DC (Brain Products GmbH, Munich, Germany) amplifiers at a sampling rate of 1000 Hz and a high-pass filter at 0.16 Hz. After recording, the signal was re-referenced to the common average and a notch filter at 50 Hz was applied to filter out power line noise. To estimate the power spectrum we used the maximum entropy method [22] with a model order of 50. The power spectrum was estimated for each channel in the range from 1 to 500 Hz with a bin width of 4 Hz and the logarithm function was applied to each value.

To reduce dimensionality of the input space, we performed a feature selection based on R^2 values [23] and selected the 50 features which had the highest values. In the end, those features served as input to train a model (using either a regression method or CCA) to predict movement trajectory.

2.4 EMG Data Processing and Feature Extraction

The EMG data was recorded with a Brainamp-EXG (Brain Products GmbH, Munich, Germany) amplifier at a sampling rate of 1000 Hz and a high-pass filter at 0.16 Hz. Seven bipolar electrodes were placed at the left (paretic) side of the body over the following muscles: Extensor Digitorum (ED), Flexor Digitorum (FD), Biceps Brachii (BI), Triceps Brachii (TR), Deltoid Anterior (DA), Deltoid Medial (DM), Deltoid Posterior (DP).

For predicting the movement trajectory we extracted different features. One feature was the waveform length (WL) [24], which is the cumulative length of the waveform over the time segment. If x_t is the amplitude of the EMG channel at time t , the waveform length can be calculated with the following equation:

$$WL = \sum_{n=1}^{N-1} |x_{n+1} - x_n| \quad (9)$$

In addition, we calculated the coefficients of an autoregressive model with a model order of 4 estimated by the Burg method and used these 4 coefficients as additional features for EMG-based trajectory prediction.

2.5 Trajectory Prediction on ECoG Data

To evaluate which method is suited best for prediction of movement trajectory, we used the following five methods:

1. **(L1 reg)** Lasso regression: Linear regression with L1 Norm regularisation using the regularisation parameter $\lambda = 0.1$.
2. **(L2 reg)** Ridge regression: Linear regression with L2 Norm regularisation using the regularisation parameter $\lambda = 0.1$.
3. **(SVR)** Support Vector Regression with a linear kernel or a radial basis function (RBF) kernel. For implementation we used LibSVM [25] with default kernel parameters and the hyperparameter $C = 1$.
4. **(CCA)** Canonical Correlation Analysis for the prediction of movement components. A more detailed explanation how we applied CCA will be presented later (see Sect. 2.5.1).

5. (**PCA + L2 reg**) Since CCA was not used to predict the actual wrist movement trajectory, but to predict movement components identified by CCA, we also used Principal Component Analysis (PCA) [26] on the recorded movement data (7 degrees of freedom) to obtain movement components that better match the movement intention of the stroke patients. The principal components with the highest variance was used for trajectory prediction by using a ridge regression as explained previously.

2.5.1 CCA to Predict Movement Components Based on ECoG Data

We have previously shown that the calculation of W_x can be seen as a linear regression, where W_x is used to predict a variable. We have also shown that the calculation of W_y can be seen as a form of component analysis, where CCA transforms the dataset Y into uncorrelated components. When both datasets X and Y are multidimensional both aspects have to be considered and the application of CCA can be seen as an extraction of components and a regression to predict those components. Both is done by CCA in one step.

When applying CCA to the ECoG data (as X) and movement trajectory data (as Y), we can use CCA to find movement components in the trajectory data and do a regression to predict those movement components based on the ECoG data. The reasoning behind this approach is that the performed (and recorded) trajectory differs from intended movement trajectory due to compensatory movements and the stroke patients not being able to properly perform the intended movement. With the extraction of trajectory components, we hope to find components which are closer to the actual intended movement trajectory. In this work we always used the first component extracted by CCA.

2.6 Trajectory Prediction on EMG Data

Since the focus on this paper lies on trajectory prediction using ECoG data, we did not want to repeat the comparison of different prediction methods for EMG data. Instead we used the regression method that was best suited for ECoG data and applied it to the EMG signals, which allows for a direct comparison between ECoG and EMG regarding their potential for predicting movement trajectory in stroke patients.

We tested two different approaches for trajectory prediction: either using only features from the EMG electrodes placed over the ED and FD muscles (where one would expect activity for healthy subjects for the given task) or using features from all 7 electrodes (including 5 electrodes over muscles that should not participate in this task in healthy subjects).

2.7 Performance Evaluation

To evaluate the performance of the different methods for trajectory prediction, we used a 5-fold cross-validation procedure to make sure that training and test data do not overlap. To quantify the performance of the methods, we used Pearson's correlation coefficient (CC) and the normalized root mean squared error (NRMSE), which we defined as

$$\text{NRMSE} = \sqrt{\frac{\sum_{t=1}^n (\hat{y}_t - y_t)^2}{n}} \cdot \text{var}(y)^{-1} \quad (10)$$

with y_t being the actual and \hat{y}_t being the predicted value. $\text{var}(y)$ denotes the variance of the actual trajectory. Since the trajectory values are different depending if PCA or CCA are used, the normalization is important to compare the RMSE between the methods.

3 Results

3.1 Performance of Trajectory Prediction

On average, CCA performed best with an average $CC = 0.41$ and an average $NRMSE = 1.15$. While CCA performs consistently better than the other linear methods, a Support Vector Regression (SVR) with a RBF-kernel has a significantly ($p < 0.01$) higher CC for subject P3. The results are shown in Fig. 2 in more detail. For each subject and method, the results are averaged over all session with the standard deviation being indicated by error bars and the significance between each of the methods and CCA being assessed by a two-sided Wilcoxon ranksum test.

A comparison of the prediction performance using SVR with RBF kernel on ECoG and EMG signals is shown in Fig. 3. Using EMG signals only from ED and FD muscle achieved an average $CC = 0.43$ and an average $NRMSE = 1.19$, which is not significantly different ($p > 0.05$) than the results obtained with ECoG ($CC = 0.40$, $NRMSE = 1.17$). However, EMG using all 7 electrodes performed significantly better ($p < 0.0001$) with an average $CC = 0.77$ and an average $NRMSE = 0.79$.

3.2 Interpretation of CCA Transformation Matrices

Due to the nature of CCA, the transformation matrices W_x and W_y could be used for some neurophysiological interpretation of the data. While W_x is used to predict the

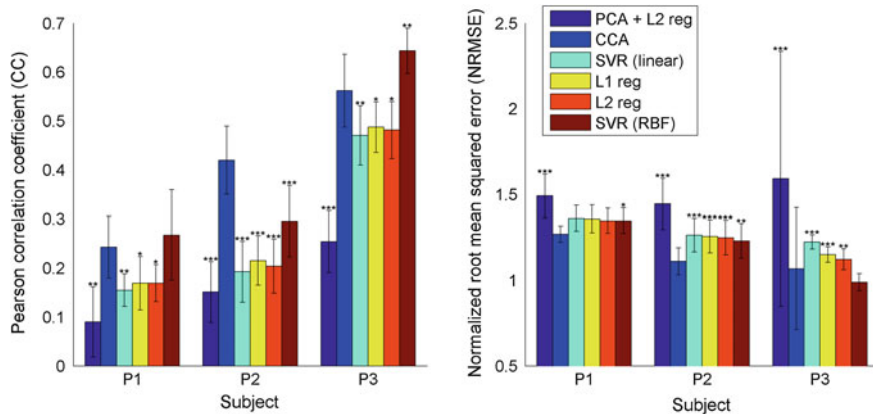


Fig. 2 Performance (NRMSE and CC) for different methods for trajectory prediction averaged over all sessions for one subject. The error bars indicate the standard deviation. Asterisk denote if there is a significant difference between the method and CCA, with * $p < 0.05$, ** $p < 0.01$, *** $p < 0.001$ (Wilcoxon ranksum test)

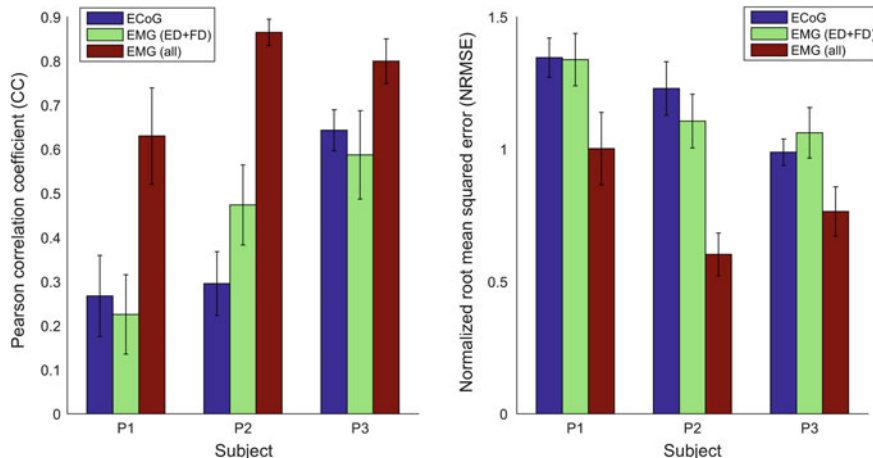


Fig. 3 Performance (NRMSE and CC) using Support Vector Regression (SVR) with RBF kernel on ECoG and EMG data. For the EMG-based prediction two different sets of electrodes were used. One set containing only two EMG electrodes over the Extensor Digitorum (ED) and Flexor Digitorum (FD) muscles on the forearm, and one set containing all 7 EMG electrodes placed at the forearm, upper arm and shoulder

movement trajectory, it shows which electrodes and which frequency ranges are important for the prediction. Thereby one can infer where (location and frequency) movement-related activity is present. W_y is used to calculate the movement components and in turn can be used to infer which joints (represented by the DOFs in

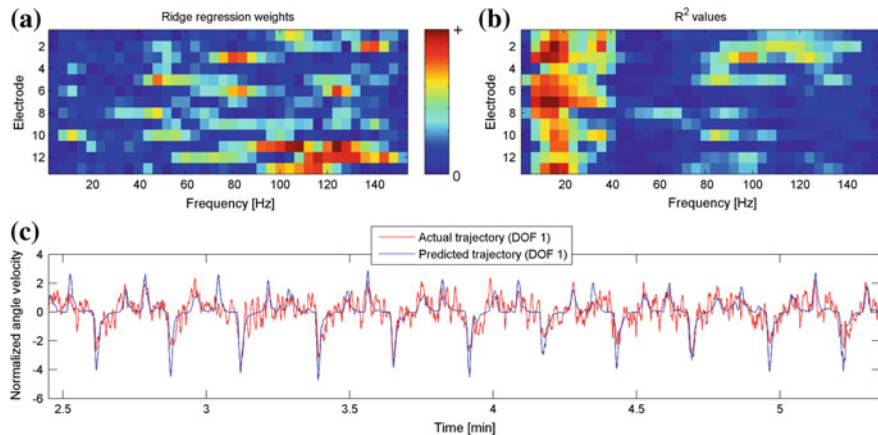


Fig. 4 **a** Absolute weights from ridge regression for each feature (frequency \times electrode) used in trajectory prediction. **b** R^2 values indicating high correlation between each feature and the trajectory. **c** Actual and predicted trajectory of the movement component calculated by ridge regression

our data) are active during an intended wrist movement. This could be used to gain more knowledge regarding the compensatory movement patterns of stroke patients.

Figure 4 shows the weights using a linear regression to visualize which electrodes and frequencies are used to predict the recorded wrist movement trajectory, as well as the recorded and predicted wrist movement trajectory for one exemplary session. Figure 4 also shows the R^2 -values [27] indicating which features (electrode \times frequency) correlate best with the trajectory.

Figure 5 shows the weights of the W_x and W_y (for the first movement component) when using CCA on one exemplary session. As well as the actual and predicted movement trajectory.

When comparing both figures, the activity pattern obtained by CCA (Fig. 5a) is more localized than the one obtained by a linear regression (Fig. 4a). Furthermore, the weights of W_y (Fig. 5b) yield information, which DOFs are affected by the intended wrist movement, thereby showing the coactivation pattern present during the intended wrist movement.

Figure 4c shows the actual and the predicted wrist movement trajectory using linear regression, while Fig. 5c shows the predicted and actual movement trajectory obtained by CCA. When comparing the results from CCA with the results using a linear regression, the trajectory obtained by CCA seems more noisy but more natural and more representative of the true intended movement.

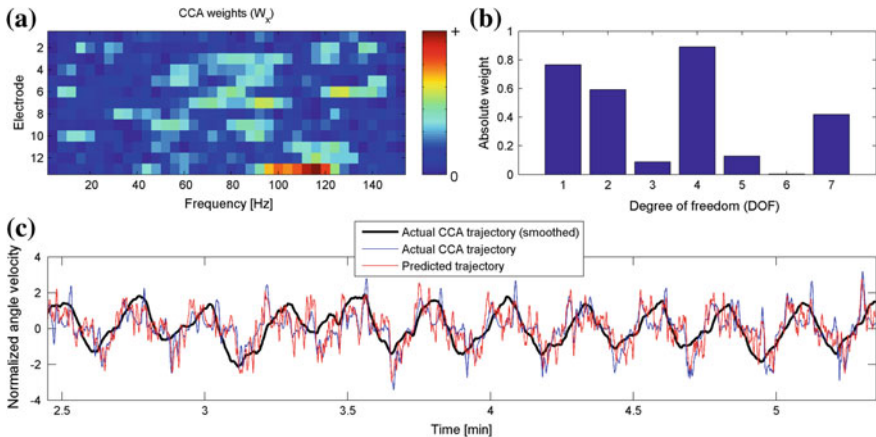


Fig. 5 **a** Absolute weights from CCA for each feature (frequency \times electrode) used in trajectory prediction of the first movement component. **b** Absolute weights for each DOF to calculate the movement component. **c** Actual and predicted trajectory of the movement component calculated by CCA. The smoothed trajectory is only shown for better display purposes and was not used for trajectory prediction or performance evaluation

4 Discussion

In this paper we have compared different methods for the trajectory prediction from ECoG in stroke patients. The fact that ECoG can be used for trajectory prediction was shown in several studies for subjects with an intact sensorimotor system [28, 29]. In [30] average CCs were approximately between 0.22 and 0.71, in [31] CCs between 0.3 and 0.6 were reached and performance in later studies yielded CCs in a similar range. Nakanishi et al. [32] have shown that it is also possible to predict movement trajectory in stroke patients from ipsilesional ECoG. With an average CC ranging between 0.44 and 0.73 the performance obtained by Nakanishi et al. is similar to the results obtained in earlier studies with subjects without motor dysfunction. We could reproduce this finding in our work and were able to decode the trajectory with an average CC between 0.24 and 0.64 depending on the subject, which is similar to the results by [32].

It should be noted that there seems to be a negative correlation between the Fugl-Meyer (FM) Score regarding wrist movement and the accuracy of wrist trajectory prediction, since the patient with the lowest FM score (indicating a high wrist motor dysfunction) had the lowest CC and vice versa. Although it seems reasonable to assume that wrist movement trajectory is harder to decode for patients whose motor system is more damaged by stroke, the current dataset (with only three patients measured) is too small to draw any significant conclusions.

When comparing the results obtained on ECoG data with the results obtained from EMG, we find no significant difference in performance when only the activity of forearm muscles (which are used for wrist movement in healthy subjects) are recorded. However, using activity from muscles in the upper arm and shoulder drastically improved prediction performance. This results can be explained by the patients having abnormal muscle coactivation [33] or by performing compensatory movements, since they have trouble to actually move their wrist. Although this abnormal EMG activity might be useful for control of an assistive device, in terms of rehabilitation it should not be used, and neurofeedback should concentrate only on brain activity or on forearm muscles.

Regarding the comparison of different prediction methods for wrist trajectory prediction, we found CCA and Support Vector Regression (SVR) with an RBF kernel to perform best. While CCA performed on average slightly better than SVR, the use of CCA has either advantages or disadvantages compared to SVR, depending on the point of view. While SVR predicts the trajectory of a specific joint, CCA predicts the trajectory of a component. So CCA should not be used when the aim is the prediction of a certain joint or a certain movement direction. But in case of stroke rehabilitation or orthotic control, one could also use the components predicted by CCA to give the user feedback using multiple joints at once (individual DOFs weighted by W_y), which would allow for a more natural feedback. This gets clearer when looking at the movement trajectories. The performed (and recorded) wrist movement trajectory looks unnatural and choppy, which is likely caused by abnormal muscle coactivations and compensatory movements. The movement trajectory obtained by CCA, although being more noisy, seems to resemble the intended wrist extension and flexion trajectory much better. Thereby we argue that CCA might be better suited for trajectory decoding if the aim is to predict the real movement intention of the patient instead of the performed and impaired movement of the stroke patient. When interpreting the transformation matrices obtained by CCA, the movement related activity is more localized to one electrode and a specific frequency band, which agrees with findings regarding the decoding of different hand movement intentions from ECoG in stroke patients [7]. While one can further interpret the transformation matrices to infer knowledge regarding the participation of different joints, CCA might also be useful to investigate compensatory movements or muscle coactivation patterns, and which parts of the brain signal yield information regarding both.

In conclusion, we have shown that we are able to decode wrist movement trajectory from hemiparetic chronic stroke patients based on ipsilesional ECoG recordings over their contralateral sensorimotor cortex and compared it to results obtained on EMG data. We have further compared different methods for trajectory prediction and could show that either SVR (with RBF kernel) or CCA are the best methods for trajectory prediction, depending on the intended application. Further, we have outlined that CCA seems to be a potential tool in this field with possible applications beyond the use for trajectory prediction, and should be further investigated in future research.

Acknowledgments This manuscript is an extended version of a paper presented at the *2nd International Congress on Neurotechnology, Electronics and Informatics* [34]. The work was supported by the European Research Council (ERC 227632-BCCI) and the *Baden-Württemberg Stiftung* (GRUENS).

References

1. Cramer, S., Nelles, G., Benson, R., Kaplan, J., Parker, R., Kwong, K., Kennedy, D., Finklestein, S., Rosen, B.: A functional MRI study of subjects recovered from hemiparetic stroke. *Stroke* **28**, 2518–2527 (1997)
2. Kwakkel, G., Kollen, B.J., van der Ground, J., Prevo, A.J.: Probability of regaining dexterity in the flaccid upper limb: impact of severity of paresis and time since onset in acute stroke. *Stroke* **34**, 2181–2186 (2003)
3. Yanagisawa, T., Hirata, M., Saitoh, Y., Goto, T., Kishima, H., Fukuma, R., Yokoi, H., Kamitani, Y., Yoshimine, T.: Real-time control of a prosthetic hand using human electrocorticography signals: technical note. *J. Neurosurg.* **114**, 1715–1722 (2011)
4. Buch, E., Weber, C., Cohen, L., Braun, C., Dimyan, M., Ard, T., Mellinger, J., Caria, A., Soekadar, S., Fourkas, A., Birbaumer, N.: Think to move: a neuromagnetic brain-computer interface (BCI) system for chronic stroke. *Stroke* **39**, 910–917 (2008)
5. Broetz, D., Braun, C., Weber, C., Soekadar, S., Caria, A., Birbaumer, N.: Combination of brain-computer interface training and goal-directed physical therapy in chronic stroke: a case report. *Neurorehabil. Neural Repair* **24**, 674–679 (2010)
6. Ramos-Murguialday, A., Broetz, D., Rea, M., Läer, L., Yilmaz, Ö., Brasil, F.L., Liberati, G., Curado, M.R., Garcia-Cossio, E., Vyziotis, A., et al.: Brain-machine interface in chronic stroke rehabilitation: a controlled study. *Ann. Neurol.* **74**, 100–108 (2013)
7. Spüler, M., Walter, A., Ramos-Murguialday, A., Naros, G., Birbaumer, N., Gharabaghi, A., Rosenstiel, W., Bogdan, M.: Decoding of motor intentions from epidural ECoG recordings in severely paralyzed chronic stroke patients. *J. Neural Eng.* **11**, 066008 (2014)
8. Gharabaghi, A., Kraus, D., Leao, M.T., Spüler, M., Walter, A., Bogdan, M., Rosenstiel, W., Naros, G., Ziemann, U.: Coupling brain-machine interfaces with cortical stimulation for brain-state dependent stimulation: enhancing motor cortex excitability for neurorehabilitation. *Front. Hum. Neurosci.* **8** (2014)
9. Gharabaghi, A., Naros, G., Khademi, F., Jesser, J., Spüler, M., Walter, A., Bogdan, M., Rosenstiel, W., Birbaumer, N.: Learned self-regulation of the lesioned brain with epidural electrocorticography. *Front. Behav. Neurosci.* **8** (2014)
10. Silvoni, S., Ramos-Murguialday, A., Cavinato, M., Volpato, C., Cisotto, G., Turolla, A., Piccione, F., Birbaumer, N.: Brain-computer interface in stroke: a review of progress. *Clin. EEG Neurosci.* **42**, 245–252 (2011)
11. Cirstea, M., Levin, M.F.: Compensatory strategies for reaching in stroke. *Brain* **123**, 940–953 (2000)
12. Lee, M.Y., Park, J.W., Park, R.J., Hong, J.H., Son, S.M., Ahn, S.H., Cho, Y.W., Jang, S.H.: Cortical activation pattern of compensatory movement in stroke patients. *NeuroRehabilitation* **25**, 255–260 (2009)
13. Bin, G., Gao, X., Yan, Z., Hong, B., Gao, S.: An online multi-channel SSVEP-based brain-computer interface using a canonical correlation analysis method. *J. Neural Eng.* **6**, 046002 (2009)
14. Spüler, M., Rosenstiel, W., Bogdan, M.: Online adaptation of a c-VEP Brain-Computer Interface (BCI) based on Error-related potentials and unsupervised learning. *PLoS ONE* **7**, e51077 (2012)

15. Spüler, M., Walter, A., Rosenstiel, W., Bogdan, M.: Spatial filtering based on canonical correlation analysis for classification of evoked or event-related potentials in EEG data. *IEEE Trans. Neural Syst. Rehabil. Eng.* **22**, 1097–1103 (2014)
16. Hotelling, H.: Relations between two sets of variates. *Biometrika* **28**, 321–377 (1936)
17. Hastie, T., Buja, A., Tibshirani, R.: Penalized discriminant analysis. *Ann. Stat.* **73**–102 (1995)
18. Bishop, C.M., et al.: Pattern recognition and machine learning, vol. 1. Springer, New York (2006)
19. Sun, L., Ji, S., Ye, J.: A least squares formulation for canonical correlation analysis. In: Proceedings of the 25th International Conference on Machine Learning. ACM, pp. 1024–1031 (2008)
20. Walter, A., Murguialday, A.R., Spüler, M., Naros, G., Leão, M.T., Gharabaghi, A., Rosenstiel, W., Birbaumer, N., Bogdan, M.: Coupling BCI and cortical stimulation for brain-state-dependent stimulation: methods for spectral estimation in the presence of stimulation after-effects. *Front. Neural Circuits* **6** (2012)
21. Fugl-Meyer, A., Jääskö, L., Leyman, I., Olsson, S., Steglind, S.: The post-stroke hemiplegic patient. a method for evaluation of physical performance. *Scand. J. Rehabil. Med.* **7**, 13–31 (1975)
22. Burg, J.P.: Maximum entropy spectral analysis. In: 37th Annual International Meeting., Society of Exploration Geophysics (1967)
23. Spüler, M., Rosenstiel, W., Bogdan, M.: A fast feature selection method for high-dimensional MEG BCI data. In: Proceedings of the 5th International Brain-Computer Interface Conference, pp. 24–27. Graz (2011)
24. Phinyomark, A., Chujit, G., Phukpattaranont, P., Limsakul, C., Hu, H.: A preliminary study assessing time-domain EMG features of classifying exercises in preventing falls in the elderly. In: 2012 9th International Conference on Electrical Engineering/Electronics, Computer, Telecommunications and Information Technology (ECTI-CON), pp. 1–4 (2012)
25. Chang, C.C., Lin, C.J.: LIBSVM: a library for support vector machines. *ACM Trans. Intell. Syst. Technol. (TIST)* **2**, 27 (2011)
26. Duntzman, G.H.: Principal components analysis. No. 69. Sage, Newbury Park (1989)
27. Sheikh, H., McFarland, D.J., Sarnacki, W.A., Wolpaw, J.R.: Electroencephalographic (EEG)-based communication: EEG control versus system performance in humans. *Neurosci. Lett.* **345**, 89–92 (2003)
28. Schalk, G., Kubanek, J., Miller, K., Anderson, N., Leuthardt, E., Ojemann, J., Limbrick, D., Moran, D., Gerhardt, L., Wolpaw, J.: Decoding two-dimensional movement trajectories using electrocorticographic signals in humans. *J. Neural Eng.* **4**, 264 (2007)
29. Waldert, S., Pistohl, T., Braun, C., Ball, T., Aertsen, A., Mehring, C.: A review on directional information in neural signals for brain-machine interfaces. *J. Physiol. Paris* **103**, 244–254 (2009)
30. Schalk, G., Miller, K., Anderson, N., Wilson, J., Smyth, M., Ojemann, J., Moran, D., Wolpaw, J., Leuthardt, E.: Two-dimensional movement control using electrocorticographic signals in humans. *J. Neural Eng.* **5**, 75–84 (2008)
31. Pistohl, T., Ball, T., Schulze-Bonhage, A., Aertsen, A., Mehring, C.: Prediction of arm movement trajectories from ECoG-recordings in humans. *J. Neurosci. Methods* **167**, 105–114 (2008)
32. Nakanishi, Y., Yanagisawa, T., Shin, D., Fukuma, R., Chen, C., Kambara, H., Yoshimura, N., Hirata, M., Yoshimine, T., Koike, Y.: Prediction of three-dimensional arm trajectories based on ECoG signals recorded from human sensorimotor cortex. *PLoS ONE* **8**, e72085 (2013)
33. Wright, Z.A., Rymer, W.Z., Slutsky, M.W.: Reducing abnormal muscle coactivation after stroke using a myoelectric-computer interface a pilot study. *Neurorehabil. Neural Repair* **28**, 443–451 (2014)
34. Spüler, M., Rosenstiel, W., Bogdan, M.: Predicting wrist movement trajectory from ipsilesional ECoG in chronic stroke patients. In: Proceedings of 2nd International Congress on Neurotechnology, Electronics and Informatics (NEUROTECHNIX), pp. 38–45 (2014)

Detection of Gait Initiation Through a ERD-Based Brain-Computer Interface

E. Hortal, D. Planelles, E. Iáñez, A. Costa, A. Úbeda and J.M. Azorín

Abstract In this paper, an experiment designed to detect the will to perform several steps forward (as gait initiation) before it occurs using the electroencephalographic (EEG) signals collected from the scalp is presented. In order to detect this movement intention, the Event-Related Desynchronization phenomenon is detected using a SVM-based classifier. The preliminary results from seven users have been presented. In this work, the results obtained in a previous paper are enhanced obtaining similar true positive rates (around 66 % in average) but reducing the false positive rates (with an average around 20 %). In the future, this improved Brain-Computer Interface will be used as part of the control system of an exoskeleton attached to the lower limb of people with incomplete and complete spinal cord injury to initiate their gait cycle.

E. Hortal (✉) · D. Planelles · E. Iáñez · A. Costa · A. Úbeda · J.M. Azorín
Brain-Machine Interface Systems Lab, Miguel Hernández University of Elche,
Avda. Universidad, Elche (Alicante), Spain
e-mail: ehortal@umh.es

D. Planelles
e-mail: dplanelles@umh.es

E. Iáñez
e-mail: eianez@umh.es

A. Costa
e-mail: acosta@umh.es

A. Úbeda
e-mail: aubeda@umh.es

J.M. Azorín
e-mail: jm.azorin@umh.es

1 Introduction

There is a range of longer-term problems that a person who has suffered a stroke might continue to face after they have left hospital. Patients with stroke normally have communication, cognitive, emotional, physical or visual problems so they need attendance or even rehabilitation. However, there are other disabilities as people with spinal cord injury or multiple sclerosis that involve lost of voluntary mobility. Therefore, the research community has to do a huge effort to find solutions to restore their capacities or, at least, to facilitate new technology with the aim of improving their lives.

For this reason, Brain-Computer Interfaces (BCIs) have seen a rapid development during the last years as an assistive technology. BCIs are an alternative communication method for people with a severe motor disability as they allow generating control commands with the only help of the thoughts [1, 2]. Therefore, BCIs could increase their independence and also could improve their quality of life.

Current technology allows collecting and processing EEG signals that occur just before performing an action and thus we can know the intention to perform a movement [3]. It can be used to assist subject movements whenever he/she wishes which is one of the great practical advantages of this approach. In a motor rehabilitation process, it can make a big improvement since it would be possible to share efforts between the subject and, for example, an exoskeleton attached to the lower limb [4]. This coordination between the will to execute a movement and the performance of the action itself increases the likelihood of the brain to create new communication channels due to neuronal plasticity [5]. Through this, the effects of rehabilitation increase a greater extent in a much shorter time frame.

This paper has been developed under the BioMot project—Smart Wearable Robots with Bioinspired Sensory-Motor Skills (FP7-ICT-2013-10) funded by the Commission of the European Union, which pretends to control an exoskeleton attached to the lower limb of the disabled user capturing and processing their electroencephalographic (EEG) signals. As part of this challenge, our purpose is to activate the controlled gait cycle of the exoskeleton using the intention to walk of the user. Therefore, the EEG signals will be analysed in order to detect the intention of the gait initiation and this will be turn into an activation command of the exoskeletons engines or a stimulus over the leg muscles with Functional Electrical Stimulation (FES). At the moment, the focus is on the system to detect the intention to start walking and initially, only healthy subjects have performed the test.

To our knowledge, there are several phenomena extensively used in BCI related to the motor intention such as a kind of Movement-Related Cortical Potential (MRCP) which is a slow potential called Bereitschaftspotential or readiness potential [6] or the event-related desynchronization (ERD). This phenomenon is characterized by a decrease in the spectral power of EEG signals in mu and beta frequency bands [7]. ERD starts up to 2 s before the movement onset and it ends more or less when the movement is finished. After that, the spectral power recovers its magnitude generating the event-related synchronization (ERS).

Taking into account the results obtained in a previous work [8], a new analysis based again in the ERD phenomenon is performed. In this work, a Laplacian filter is applied to enhance the quality of the signals obtained from the 32 electrodes. Furthermore, a new feature extractor based on the Fast Fourier Transform is applied instead of the linear regression used previously. Moreover, the number of user has been extended to seven.

2 Materials and Methods

2.1 Test Description

Seven healthy subjects between 24 and 29 years old (27.6 ± 2.4) performed one session. All volunteers had normal vision and hearing and no history of neurological or psychiatric disorders. Each subject was instructed to remain at rest on their two legs during at least 5 s to have enough information to be used as resting time (or baseline) and then to perform several steps forward. However, the user could begin the movement whenever they want after the restricted period (limited to 5 s). Finally, user stands between 3 and 5 s before the next repetition of the tasks starts. No interface guides the subject but they know when a task starts through an advice from the experimenter. In Fig. 1 this protocol is shown.

Eight runs with ten repetitions each have been performed. Between each run there is 1 or 2 min of break time. The user has to wear several measurement equipments to register the EEG signals and the kinematic of the user. A cap with EEG electrodes and seven Inertial Measurement Units (IMUs) distributed over the lower limb are used to measure EEG signals and kinematics information. These devices are connected to a laptop which is over a cart managed by the experimenter. In this cart, the electronic devices that register the EEG signals are also placed. Therefore, the experimenter pushes the cart while the user is moving forward to keep around 1.5 m between the user and the cart. Figure 2 shows an example of the test environment.

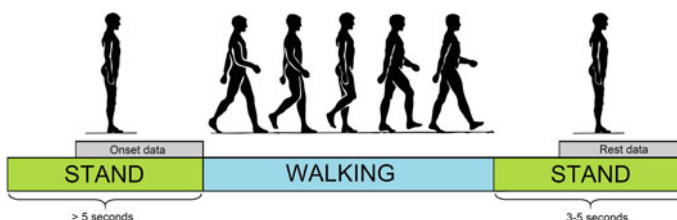


Fig. 1 Protocol followed during the experimental tests. The data used for the onset and rest classification is shown in gray

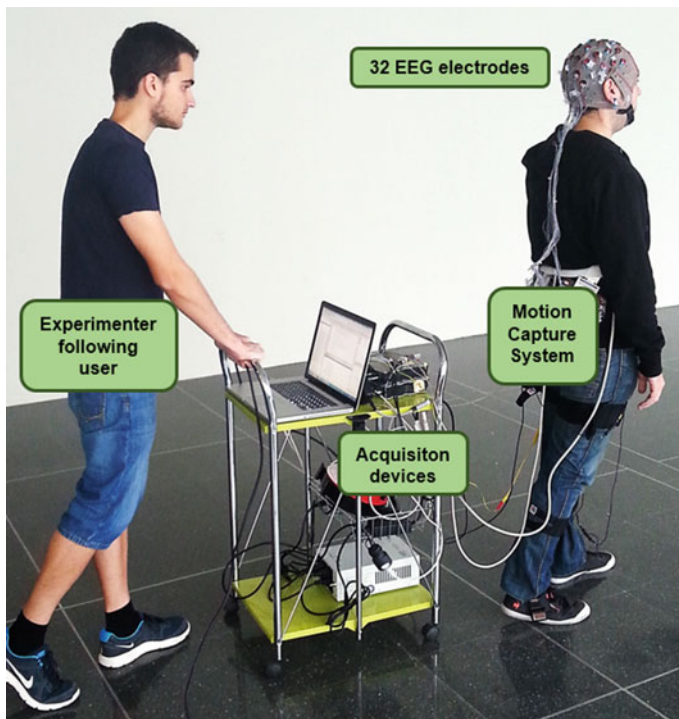


Fig. 2 The user is wearing the cap and the Motion Capture System while the experimenter follows him with the cart and the computer

2.2 Experimental Set-up

The system architecture is composed by a Brain-Computer Interface (BCI) that will capture and process EEG signals to command, in the future, an exoskeleton attached to the lower limb and seven Inertial Measurement Units (IMUs) managed by the Motion Capture System (Technaid S.L.), which are distributed over the lower body to register kinematics. Both acquisition systems are synchronized.

2.2.1 Brain-Machine Interface

The EEG signals are registered through 32 active electrodes. These electrodes are placed using a cap (g.GAMMAcap, g.tec medical engineering, GmbH, Austria). This cap is very useful as it allows an easy placement of the electrodes. The 32 electrodes are distributed following a uniform distribution over the scalp. According to the International 10–10 System, the position of the electrodes is the following: Fz, FC5, FC3, FC1, FCz, FC2, FC4, FC6, C5, C3, C1, Cz, C2, C4,

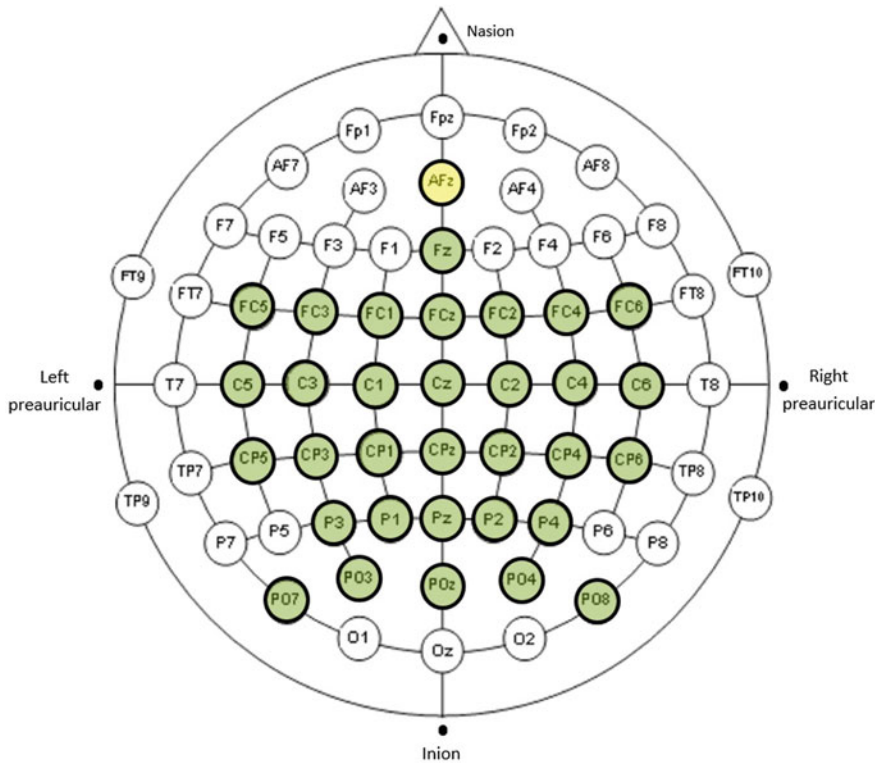


Fig. 3 Placement of the 32 electrodes over frontal and parietal lobes according to the International 10–10 System

C6, CP5, CP3, CP1, CPz, CP2, CP4, CP6, P3, P1, Pz, P2, P4, PO7, PO3, POz, PO4 and PO8. This distribution of the electrodes is shown in Fig. 3.

These electrodes are the g.LADYbird model, sintered Ag/AgCl crown with a 2-pin safety connector. These electrodes need a conductive gel that comes in contact the scalp with the sensor. The ground sensor is located in AFz and the reference is placed on the earlobe. The signals of the 32 electrodes are acquired through two commercial g.USBamp devices from g.tec synchronized by using g.INTERsync device and they have two preamplifiers g.GAMMAbox. Each amplifier has 16 channels and the sampling frequency used to register the signals is 1200 Hz.

2.2.2 Motion Capture System

The motion capture system Tech MCS is a complete wireless motion analysis system. It manages the seven IMUs of the company Technaid which are used in our experiments and they are placed as Fig. 4 shows. The sampling frequency used is 30 Hz. Each Tech IMU integrates three different types of sensors as an

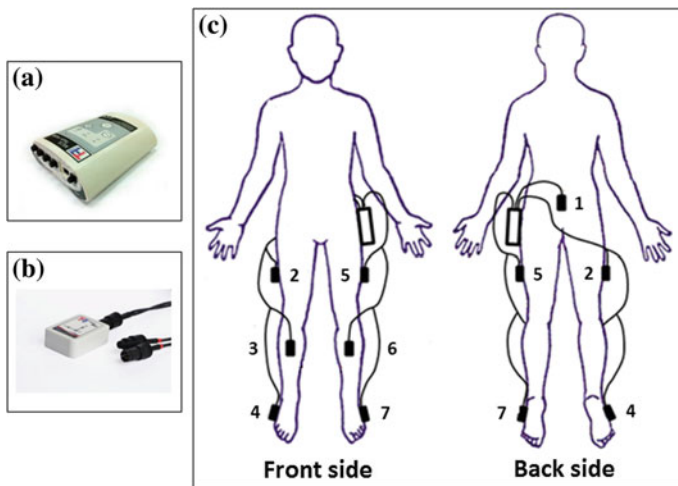


Fig. 4 **a** Tech Hub that manages all the IMUs. **b** An Inertial Measurement Units. **c** IMUs distribution. 1 Lumbar, 2 Right quadriceps, 3 Right biceps, 4 Right foot, 5 Left quadriceps, 6 Left biceps, 7 Left foot

accelerometer, a gyroscope and a magnetometer. A sophisticated and robust algorithm, calibrated also taking into account changes in temperature, results in a very precise and robust estimation of 3D orientation, even during changing environmental conditions.

2.3 Data Selection Procedure

ERD phenomenon appears approximately 2 s before the movement initiation. In this work, EEG data are segmented in windows of 3 s. The 3 s prior to each movement onset sample are used as premovement data. The last 3 s subsequent to the walking period are used as resting data. These data are analyzed in order to know where the users are starting a walking cycle compared to the rest state (baseline).

To know the starting sample, the data acquired from the IMUs are used. An automatic searching method based on the first change in the curve obtained from IMUs is implemented.

2.4 Signal Processing

The EEG signals voltage is around a few microvolts, consequently the signals are easily affected by other sources of voltage that are not the cerebral activity as ocular

or muscular movements. Therefore, it is necessary to reduce the undesirable contribution of each electrode using some temporal and frequency filters. In this sense, the EEG data is filtered with two frequency filters that eliminate the power line interference, the DC component and some artifacts. Then, a 50 Hz Notch filter and a 4th order Butterworth from 1 to 100 Hz filter are used. Thus, the information of mu and beta (8–30 Hz) and surrounding frequencies are isolated. Moreover, due to the proximity of the EEG electrodes and the numerous neural connections, the signal acquired per each electrode is partially affected by the potential produced in other location of the scalp. Hence, in this paper a spatial filters (Laplacian algorithm [9]) is used to reduce that neighbor contribution.

The Laplacian algorithm is applied for all electrodes. This algorithm uses the information received from all the remaining electrodes and their distances from them. The visual result is a smoother time signal which should contain only the contribution coming from the particular position of the electrode. The Laplacian is computed according to the formula:

$$Vi^{LAP} = Vi^{CR} - \sum_{j \in Si} g_{ij} Vj^{CR} \quad (1)$$

where Vi^{LAP} is the result of applying this algorithm to the electrode i , Vi^{CR} is the electrode i signal before the transformation and,

$$g_{ij} = \frac{\frac{1}{d_{ij}}}{\sum_{j \in Si} \frac{1}{d_{ij}}} \quad (2)$$

where Si contains all the electrodes except from the electrode i and d_{ij} is the distance between i and j electrodes.

2.5 Features Extraction and Classifier

The data groups obtained in Sect. 2.3 are segmented in windows of 1 s each 200 ms. Each window is processed separately to extract the features which represent the task. Selected EEG data are processed with a Fast Fourier Transform (FFT) to know the spectral power [10]. The features used are the sums of three frequency bands, 8–12, 13–24 and 25–30 Hz per each electrode which represents mu and beta bands, so 96 features define each class (32 electrodes, 3 features per electrode).

Therefore, these coefficients are used to train a Support Vector Machine (SVM) classifier. SVM is an approach where the objective is to find the best separation hyperplane, which provides the highest margin distance between the nearest points of the two classes to separate them [11].

3 Results and Discussion

The system is tested using an eightfold cross validation with each run as a fold. This statistic analysis performs all combinations of seven runs to train the SVM classifier and uses the other one to test it. The following three statistical indices are calculated:

$$TPR = \frac{\text{Premovement data correctly detected}}{\text{Number of premovement data}} * 100 \quad (3)$$

$$FPR = \frac{\text{Resting data incorrectly detected}}{\text{Number of resting data}} * 100 \quad (4)$$

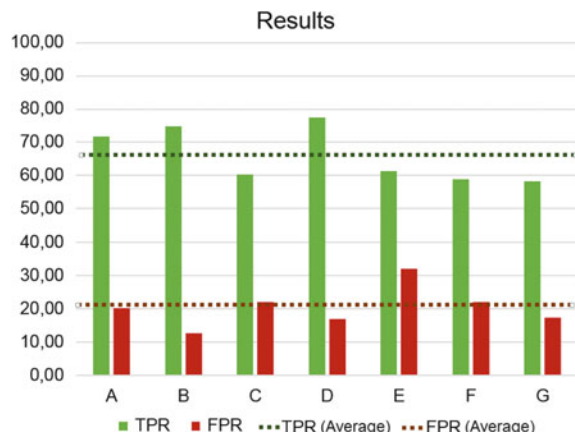
$$ACC = \frac{\text{Tasks correctly detected}}{\text{Number of tasks performed}} * 100 \quad (5)$$

The results obtained per session are summarized in Table 1 and represented graphically in Fig. 5. In average, the system reaches a 66.09 % in the TPR. Therefore, most of the premovement data is correctly classified. On the other hand, it is necessary to obtain a reduced FPR since these errors provoke a wrong detection of the user movement intention. In this work, the average of the FPR is around 20 %. This value is better than the results obtained in the previous work (between 20 % and 30 %).

Table 1 Results of the eightfold cross validation

Session	A	B	C	D	E	F	G	Average
TPR	71.70	74.89	60.23	77.39	61.25	58.86	58.30	66.09
FPR	20.31	12.73	22.19	17.03	32.19	22.19	17.50	20.59
ACC	76.44	82.22	70.65	80.69	65.14	70.09	72.64	73.98

Fig. 5 True Positive (*TP*) and False Positive (*FP*) rates and their average values for all the users



33 and 45 depending on the method applied) [8]. Individually, users A, B and D obtained better results for both TPR and FPR. These users achieved TPR around 70–75 % with low FPR (lower than 20 %). Users C, F and G obtained worse results, with TPR near to 60 %. However, their FPR are similar to the best users. Finally, user E obtained the worst results, with a high FPR (more than the 30 %) and a similar TPR than users C, F and G. This behavior is more clearly represented in the ACC value which shows an accuracy around the 80 % for the best users (A, B and D) and higher than 70 % for the rest of the users except from the worst session (user E) who obtained a 65.14 %.

This work presents an improvement compared to the previous study [8], obtaining similar right detections (TPR) but reducing the wrong detection of the gait initiation. Moreover, the behavior of the system has been tested in a bigger group of users.

4 Conclusions and Future Works

In this paper a system to detect the intention of gait initiation has been presented. According to the results obtained from seven healthy users, the system has to be improved to achieve better TPR and FPR. The system has been improved in relation to the previous work, obtaining similar TPR but with a reduced FPR (from 33–45 to 20.59 % in average). If the system is able to predict each movement with a really low FP rate, the classifier output could serve as a command to activate the engines of an exoskeleton or a FES system to help in the start walking. Therefore, in a rehabilitation process an exoskeleton could be used to support the lower limbs while the user carries out mentally walking intentions. The relationship between the cognitive process to perform such movement and the real movement could improve the rehabilitation due to cerebral plasticity [5].

Therefore, other methods to characterize the EEG signals before the movement onset will be studied. For example, a comprehensive study of every frequency band used in this work could help in the improvement of the results. The frequency bands used in the classification could be personalized depending on the user. Moreover, other methods which show the movement intention of the users as the Bereitschaftspotential or the MRCP (Movement-Related Cortical Potential) can be analyzed in future works.

The population of this experiment and also the number of sessions will be increased. Furthermore, patients with complete and incomplete spinal cord injury will perform the experiment in order to test the system and to evaluate the performance in final users. It is expected that some patients keep their brain procedures related to the intention of movement as healthy people although they could be weaker or allocated in other brain areas [12]. Then, a real-time test with a better system could be performed for both healthy as spinal cord injured users.

Acknowledgments This research has been funded by the Commission of the European Union under the BioMot project—Smart Wearable Robots with Bioinspired Sensory-Motor Skills (Grant Agreement number IFP7-ICT-2013-10-611695) and by Conselleria d'Educació, Cultura i Esport of Generalitat Valenciana of Spain through grant VALi+d ACIF/2012/135.

References

1. Dornhege, G., Millán, J., del, R., Hinterberger, T., MacFarland, D.J., Muller, K.R.: Towards Brain-Computer Interfacing. The MIT Press (2007)
2. Nicolelis, M.A.L.: Actions from thoughts. *Nature* **409**, 403–407 (2001)
3. Bai, O., Rathi, V., Lin, P., Huang, D., Battapady, H., Fei, D.Y., Schneider, L., Houdayer, E., Chen, X., Hallett, M.: Prediction of human voluntary movement before it occurs. *Clin. Neurophysiol.* **122**(2), 364–372 (2011)
4. Moreno, J.C., Ama, A.J., Reyes-Guzmán, A., Gil-Agudo, N., Ceres, R., Pons, J.L.: Neurorobotic and hybrid management of lower limb motor disorders: a review. *Med. Biol. Eng. Comput.* **49**(10), 1119–1130 (2011)
5. Kolb, B., Muhammad, A., Gibb, R.: Searching for factors underlying cerebral plasticity in the normal and injured brain. *J. Commun. Disord.* **44**, 503–514 (2011)
6. Shibasaki, H., Hallett, M.: What is the Bereitschaftspotential? *Clin. Neurophysiol.* **117**, 2341–2356 (2006)
7. Pfurtscheller, G., da Silva, F.H.L.: Event-related EEG/MEG synchronization and desynchronization: basic principles. *Clin. Neurophysiol.* **110**, 1842–1857 (1999)
8. Planelles, D., Hortal, E., Costa, A., Iáñez, E., Azorín, J.M.: First steps in the development of an EEG-based system to detect intention of gait initiation. In: 8th Annual IEEE International Systems Conference, Ottawa, Canada, pp. 167–171 (2014)
9. McFarland, D.J., McCane, L.M., David, S.V., Wolpaw, J.R.: Spatial filter selection for EEG-based communication. *Electroencephalogr. Clin. Neurophysiol.* **103**, 386–394 (1999)
10. Bracewell, R.N.: The Fourier Transform and Its Applications. McGraw-Hill Electrical and Electronic Engineering Series (1978)
11. Hsu, C.W., Chang, C.C., Lin, C.J.: A practical guide to support vector classification. <http://www.csie.ntu.edu.tw/cjlin/libsvm/>
12. Wei, L., Yue, H., Jiang, X., He, J.: Brain activity during walking in patient with spinal cord injury. In: International Symposium on Bioelectronics and Bioinformatics, pp. 96–99 (2011)

Author Index

A

- Abbott, W., 99
Alexandre, F., 1
Azorín, J., 141

B

- Belloso, A., 63
Blau, A., 79
Bogdan, M., 125
Brannick, D., 79

C

- Carrere, M., 1
Connolly, B., 79
Costa, A., 141

D

- Denoyelle, N., 1

E

- Epelde, G., 19

F

- Faisal, A., 99, 115
Ferrara, L., 79

G

- Gharabaghi, A., 125
Grimm, F., 125

H

- Hortal, E., 141

I

- Iáñez, E., 141

K

- Keller, T., 63

L

- Leškovský, P., 19
Liberale, C., 79
Lourenço, P., 99

M

- Machado, P., 31
McGinnity, T., 31
Mitchell, P., 79
Mujika, A., 19

O

- Oyarzun, D., 19

P

- Perry, J., 63
Petrushin, A., 79
Planelles, D., 141
Popović, M., 63
Pouget, F., 1

R

- Rodríguez, M., 115
Rodríguez-de-Pablo, C., 63
Rosenstiel, W., 125

S

- Savić, A., 63
Silva, A., 47
Spüler, M., 125
Sylaidi, A., 115

T

Tomić, T., [63](#)

U

Úbeda, A., [141](#)

V

Viéville, T., [1](#)

W

Wade, J., [31](#)